DESIGN AND IMPLEMENTATION OF WIDEBAND STRIPLINE CIRCULATORS

A THESIS SUBMITTED TO
THE GRADUATE SCHOOL OF NATURAL AND APPLIED SCIENCES
OF
MIDDLE EAST TECHNICAL UNIVERSITY

BY

GÖKÇEN YILMAZ DAYANIKLI

IN PARTIAL FULFILLMENT OF THE REQUIREMENTS
FOR
THE DEGREE OF MASTER OF SCIENCE
IN
ELECTRICAL AND ELECTRONICS ENGINEERING

DECEMBER 2012

Approval of the thesis:

DESIGN AND IMPLEMENTATION OF WIDEBAND STRIPLINE CIRCULATORS

submitted by **GÖKÇEN YILMAZ DAYANIKLI** in partial fulfillment of the requirements for the degree of **Master of Science in Electrical and Electronics Engineering Department, Middle East Technical University** by,

Prof. Dr. Canan Özgen _____
Dean, Graduate School of **Natural and Applied Sciences**

Prof. Dr. İsmet Erkmen _____
Head of Department, **Electrical and Electronics Engineering**

Assoc. Prof. Dr. Şimşek Demir _____
Supervisor, **Electrical and Electronics Engineering Dept., METU**

Examining Committee Members:

Prof. Dr. Canan Toker _____
Electrical and Electronics Engineering Dept., METU

Assoc. Prof. Dr. Şimşek Demir _____
Electrical and Electronics Engineering Dept., METU

Prof. Dr. Özlem Aydın Çivi _____
Electrical and Electronics Engineering Dept., METU

Prof. Dr. Altunkan Hızal _____
Electrical and Electronics Engineering Dept., METU

Eyüp Töngel, M.Sc. _____
ASELSAN Inc.

Date: 25.12.2012

I hereby declare that all information in this document has been obtained and presented in accordance with academic rules and ethical conduct. I also declare that, as required by these rules and conduct, I have fully cited and referenced all material and results that are not original to this work.

Name, Last name : Gökçen Yılmaz DAYANIKLI

Signature :

ABSTRACT

DESIGN AND IMPLEMENTATION OF WIDEBAND STRIPLINE CIRCULATORS

Dayanıklı, Gökçen Yılmaz
M.S., Department of Electrical and Electronics Engineering
Supervisor: Assoc. Prof. Dr. Şimşek Demir

December 2012, 123 pages

Ferrite circulators are crucial elements for T/R modules of RADAR systems. Unlike many other mature devices, ferrite circulators have not been replaced by IC devices and have been used in T/R modules since 60s because of two main reasons. Firstly, they do not require environmental elements like capacitors or inductors unlike IC devices. Secondly, their performance is superior in terms of insertion loss, matching and isolation. Basically, they are used for the aim of the discrimination of the incoming and outgoing signals of a single antenna. Thus, the design of wideband circulators is an important issue for the frequency band of RADAR systems.

In this thesis, it is aimed to give the details of the design, simulation, fabrication and measurement procedure of a *one octave* and a *more than one octave* circulator. Firstly, a *one octave* circulator is designed by using continuous tracking technique. Then, the designed circulator is fabricated and observed that it performs an insertion loss of 1dB and an isolation and a return loss of better than 13 dB in the frequency band of 8.75-18.75 GHz. In the following part of the thesis, a *more than one octave* circulator is designed, fabricated and measured to prove that it is possible to achieve

wider band circulator applications by using composite substrates. Moreover, measurement results show that an insertion loss of 1 dB and an isolation and a return loss of better than 13 dB have been achieved in the frequency band of 7.7-18.7 GHz.

Keywords: Ferrite circulator, continuous tracking technique, wideband circulator, composite substrate

ÖZ

GENİŞBANT ŞERİTHAT SİRKÜLATÖRLERIN TASARIMI VE GERÇEKLENMESİ

Dayanıklı, Gökçen Yılmaz
Yüksek Lisans, Elektrik ve Elektronik Mühendisliği Bölümü
Tez Yöneticisi: Doç. Dr. Şimşek Demir

Aralık 2012, 123 sayfa

Ferit sirkülatörler radar sistemlerinin almaç göndermeç modülleri için vazgeçilmez elemanlardır. Diğer olgunlaşmış teknolojilerin tersine, ferit sirkülatörler entegre devreler tarafından yerlerinden edilememiş ve 60lardan bu yana almaç göndermeç modüllerinde kullanılmıştır. Bunun iki ana sebebi vardır. Birincisi, ferit sirkülatörler entegre devrelerin tersine, kapasitor ve bobin gibi çevresel elemanlara ihtiyaç duymazlar. İkinci olarak da, giriş kaybı, uyum ve izolasyon açısından performansları daha iyidir. Temel olarak, tek bir antene giden ve antenden gelen sinyallerin ayırımı için kullanılırlar. Dolayısıyla, RADAR sistemlerinin frekans bandını belirlerler, bu da geniş bant sirkülatör tasarımını geniş bant RADAR sistem tasarımları için önemli bir konu haline getirir.

Bu tez çalışmasında, biri *bir oktav* ve biri *bir oktavdan geniş bantlı* olmak üzere 2 farklı sirkülatörün tasarım, benzetim, üretim ve ölçüm süreçlerinin detaylarının verilmesi amaçlanmıştır. İlk olarak, bir *bir oktav* sirkülatör sürekli izlem tekniği kullanılarak tasarlanmıştır. Daha sonra tasarlanan sirkülatör gerçeklenmiş ve bu sirkülatörün 8.75-18.75 GHz bandında 1dB giriş kaybı ve 13 dBden iyi izolasyon ve

geri dönüş kayıplarına sahip olduğu gözlemlenmiştir. Tez çalışmasının bir sonraki kısmında, kompozit tabanlar kullanılarak daha geniş bantlı sirkülatör uygulamalarının olası olduğunu kanıtlamak için *bir oktavdan geniş bantlı* bir sirkülatör tasarlanmış, üretilmiş ve ölçülmüştür. Ayrıca, ölçümler bu sirkülatörün 7.7-18.7 GHz bandında 1dB giriş kaybı ve 13 dBden iyi izolasyon ve geri dönüş kayıplarına sahip olduğunu göstermiştir.

Anahtar Kelimeler: Ferit sirkülatör, sürekli izlem tekniği, geniş-bant sirkülatör, kompozit taban

To *my lovely family*

ACKNOWLEDGMENTS

I would like to express my gratitude to my supervisor Assoc.Prof. Şimşek Demir for his guidance and support throughout this thesis study.

I would like to thank to Şebnem Saygıner, Eyüp Töngel and Hakkı İlhan Altan for their valuable suggestions and support throughout this study. Moreover, I wish to express my appreciation to Zeynep Eymür for her great effort during the design of mechanical structures. Finally, I want to thank Murat Mutluol for his help during the assembly of the structures.

I would like to thank ASELSAN for allowing me to use their facilities for design, fabrication and measurement processes.

I would also like to thank TUBITAK for their financial support during my graduate study.

Finally, I want to express my deepest gratitude to my lovely family for supporting and encouraging me and I sincerely thank to Yasemin Yorgun for standing by me and giving me strength in every second of the process.

TABLE OF CONTENTS

LIST OF TABLES

TABLES

LIST OF FIGURES

FIGURES

LIST OF ABBREVIATIONS

$4\pi M_s$	: Saturation Magnetization
ΔH	: Resonance Linewidth
AL	: Aluminum Garnet
CHG	: Cobalt and Holmium Garnet
CoA	: Certificate of Analysis
EM	: Electromagnetic
G	: Gauss
GA	: Gadolinium Aluminum Garnet
GD	: Gadolinium Garnet
HF	: High Frequency
HG	: Holmium Garnet
MF	: Magnesium Ferrite
NF	: Nickel Ferrite
NL	: Narrow Line Width Garnet
Oe	: Oersted
SMA	: Subminiature Version A (Connector)
T	: Tesla
TCI	: TRAK Ceramics, Inc. (Ferrite Producer)
T/R	: Transmit and Receiver
VCM	: Vibrating Coil Method
VSM	: Vibrating Sample Method
YIG	: Yttrium Iron Garnet

CHAPTER 1

INTRODUCTION

A circulator is a non-reciprocal and symmetrical device, the ports of which are arranged in such a manner that signal entering a port is coupled to an adjacent port, but not coupled to the others. Thus, this operation can be thought as the circulation of inputted signal in a cyclic manner which explains the name of the device. In this thesis, our main focus will be the three port stripline circulators, which are frequently used at the front end of RADAR T/R modules to discriminate the incoming signal from antenna and outgoing signal from transmitter.

1.1 The Wideband Circulator Design in The Literature

Microwave circulators firstly appeared in the early 1950s. They were basically Faraday rotation circulators, which are bulky waveguide circulators with 4 ports. In the modern systems, Faraday rotation circulators are not used any more due to their complexity and size. However, they started a new era for the research of ferrite materials [1]. For example, Polder mathematically describes the permeability characteristics of the ferrite materials in terms of magnetization, microwave frequency and *saturation magnetization* [2]. The determination of permeability tensor is a milestone for circulator designers, because it reveals the behavior of ferrite materials used in circulators [3,4].

After Polder had clarified the permeability tensor of the ferrite materials, researchers tried to explain the electromagnetic circulation mechanism in the y junction circulators. Auld explained the circulator operation by considering the scattering matrix of the device [5]. However, two different explanation of circulator operation have been widely accepted by the researchers. One of them is the Green's function approach proposed by H.Bosma, which is revealed in 1964. In this approach, Bosma

explained the circulator operation by solving boundary-value problem of the ferrite disk by defining a Green's function, which relates the high frequency (HF) magnetic field to the HF electric field [3,18]. In 1965 Fay and Comstock provides a new approach and explained the circulation by using "counter-rotating propagation modes" [6].

With the help of the defined approaches, it was possible to design narrowband circulators. However, these approaches cannot provide a wideband operation for circulators. In 1974, Wu and Rosenbaum presented the *continuous tracking technique*, which is based on the Green's function approach and provided for the design of one *octave band* circulators [4]. Wu and Rosenbaum's *continuous tracking technique* has been widely accepted by researchers as a reliable method to realize *one octave* circulators. However, this approach is insufficient for more than *one octave* frequency band circulations, because it does not take precautions for gyromagnetic losses. Schloemann and Blight suggest that the gyromagnetic losses are to be eliminated, a circulation performance for *more than one octave* is possible [7]. Moreover, they suggested 2 methods to decrease the effect of demagnetization [7,8]. In the design of the *more than one octave* circulator, one of these methods is applied to widen the frequency band.

Although our main focus is on wideband stripline circulator design, some other properties of the circulators can also be improved in terms of the operation requirements. For instance, Davis and Borjak provide a method to eliminate impedance transformers for smaller size circulator designs [9].

Since Japanese researcher Yoshihiro Konishi [10] presented the lumped element circulator in 1964, circulators are irreplaceable elements of the RADAR transceiver modules. Although ferrite technology is a relatively "old" technology, the technologically advanced active devices cannot achieve the simplicity and high performance of the ferrite circulators, so the ferrite circulators seem to continue being irreplaceable for the near future for microwave devices.

1.2 Outline of The Thesis

In this thesis, the aim is to provide a reliable guide for the design of wideband stripline circulators. If related sources for circulator design are analyzed, it can be said that there is not a complete source which explains design, simulation and production procedures together. In this thesis, it is aimed to explain all these procedures in one source.

In Chapter 2, the aim is to provide the theoretical basis of ferrimagnetic material properties and wideband circulator design. This chapter consists of 2 parts. In the first part, an overview of the magnetic materials and some important properties of ferrimagnetic materials are given. In the second part of the Chapter, the theoretical basis of *one octave* circulators is provided. In this part, firstly the Green's function approach is clarified and then an approach which is called *continuous tracking technique* for *one octave* circulator design is explained in detail.

In Chapter 3, our main focus is on the 9-18 GHz *one octave* circulator. In the first part of the chapter, analytical design approach of 9-18 GHz *one octave* circulator is described with the help of given information in Chapter 2. And then, by using analytically found *one octave* circulator parameters, a model is structured in CST. The simulation results of the structured model are presented. The details of the simulation procedure in CST EM and CST MICROWAVE STUDIO are also explained in Chapter 3. With the help of optimization tools in CST, 3 different structures are optimized for 9-18 GHz circulation. Moreover, the 3 optimized structures are produced and measured, the details of which are given in the following parts of the chapter. In the final part of the chapter, the measurement results and simulation results are provided to comment on the reliability of the design method and simulation tools.

In Chapter 4, the aim is to analyze the design, simulation, realization and measurement procedure of the *more than one octave* circulator. In the first part of Chapter 4, the phenomena called demagnetization effect, which is the main reason for limited band performance of circulators, is explained in detail. In the following

part of the chapter, two methods for widening the band are provided. Finally, a method is preferred for frequency band widening and the *more than one octave* circulator is fabricated by following this method. At the end of the chapter, the measurement results are provided and some comments are made whether the method is efficient in widening the band performance of the circulators.

CHAPTER 2

FERRITE MATERIALS AND WIDEBAND CIRCULATOR DESIGN

2.1 An Overview of Ferrimagnetic Materials

Circulator structures are very interesting structures, because they have the property of non-reciprocity unlike many other microwave devices. This property is resulted by the excited ferrimagnetic materials used in the structure. Ferrimagnetic materials are a subgroup of magnetic materials, and they are ceramic materials which makes them very suitable for low-loss high frequency applications. In the following parts, general properties of magnetic materials are given. Moreover, some details of ferrimagnetic materials is provided which are crucial to understand wideband circulator design procedure.

2.1.1 Types of Magnetism

Magnetic materials can be divided into five subgroups which is due to the different orientation of the magnetic domains in the material. These subgroups are named as diamagnetic, paramagnetic, ferromagnetic, antiferromagnetic and ferrimagnetic [11]. In the following paragraphs, some properties of them are explained.

Electrons have a magnetic momentum due to their spin. If an external static magnetic field (H_{ext}) is applied on the electrons, due to the magnetic momentum, a torque reveals and this results the magnetic momentum of each electron aligns through the applied field. The overall affect of the aligned electrons results an effect, which is called magnetization. The response of magnetic materials to the applied field can be

evaluated with a term called, susceptibility. In 2.1, susceptibility (χ), magnetic field intensity (H) relation can be observed [11]. Susceptibility of a magnetic material gives a clue about the magnetism type of the material.

$$M = \chi H \tag{2.1}$$

Diamagnetism: When a magnetic field is applied to a solid which has free electrons, the electrons are aligned due to this magnetic force and generate opposing magnetic fields in terms of the applied magnetic field. The induced magnetic field is weak and negative, and the susceptibility of the material is very small and negative [11].

Paramagnetism: For the materials in which there exist unpaired electrons, the main contributor for the magnetic material is the spin of the electrons. If there is no external static field excitation (H_{ext}), the magnetic moments associated to each molecule are randomly aligned due to thermal agitation. If an excitation is implemented, these magnetic dipoles are aligned through the direction of applied field and this results a net field induced through the direction of excitation field. Because of the explained mechanism, the susceptibility of the paramagnetic materials are small and positive [11,12].

Ferromagnetism: In ferromagnetic materials, the unpaired spin of one electron is largely affected by the magnetic moments of the neighboring electrons due to "Weiss field" and this creates magnetic domains. Thus, the magnetism in the ferromagnetic material is expected to be much larger than the other subgroups. Elements like Fe (iron), Ni (nickel), Co (cobalt) are well-known examples of this class of magnetism [11,12].

Antiferromagnetism: Unlike the ferromagnetic materials, in the antiferromagnetic materials, the interaction of the neighboring atoms causes the moments of magnetic domains align anti-parallel. This results a cancellation of the magnetic domains and a zero magnetization of the material [11,12].

Ferrimagnetism: This magnetism type is very important especially in terms of circulator design. Because of their ceramic form, ferrimagnetic materials are insulators which allows very low-loss operations in microwave applications. A ferrimagnetic material is simply an anti-ferromagnetic material in which parallel and anti-parallel magnetic moments are unequal. Thus, they contain 2 different sublattices in which magnetic domains are opposite and unequal and generally these are called as domain A and domain B. The behavior of the 2 domains can be extremely different. For instance, their response to temperature increase can result a cancellation of the overall magnetization of the material which will be explained in Part 2.1.3.3.

Another important property of ferrimagnetic materials is that they require an external static magnetic field to behave as a magnetic material[16]. If they are not externally excited, the behave as simple ceramics with unity permeability (μ). Due to this property, circulator structures require a static field sources like magnets.

Ferrimagnetic ceramics are called as "ferrites". Garnets and spinels are the two main classes of ferrite materials which are dominantly used in circulator applications [11,12]. An overview of different ferrimagnetic material classes is provided in Part 2.1.4. Besides, garnet and spinel ferrites, provided by well-known ceramic producers TRANS-TECH and TCI, can be found in Appendix A.In Figure 2.1, arrangements of magnetic domains in different magnetic material types can be observed.

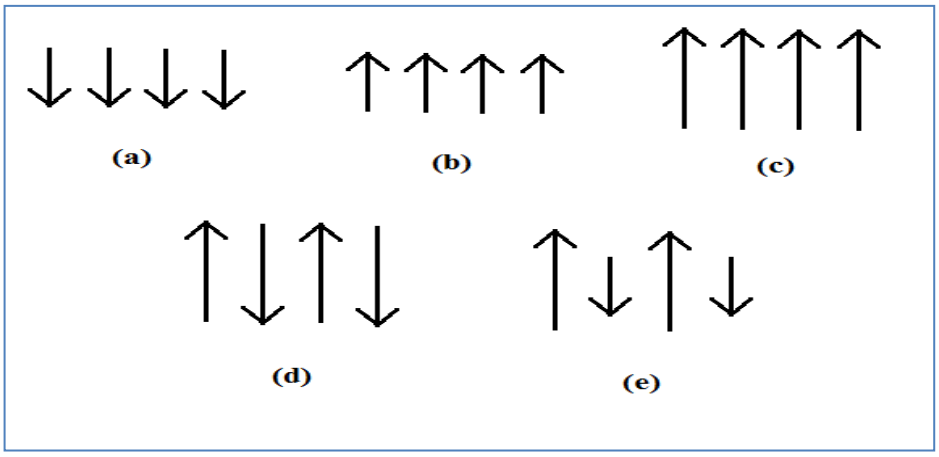

Figure 2.1 Arrangements of magnetic moments in magnetic materials, (a)Diamagnetism, (b)Paramagnetism, (c)Ferromagnetism, (d)Anti-ferromagnetism, (e)Ferrimagnetism

2.1.2 Permeability Tensor of Ferrite Materials

In the previous part, it is explained that ferrites require static magnetic field (H_{ext}) to have a non-zero magnetic anisotropy [3,18]. In other words, if a ferrite material is excited, then it behaves as a gyrotropic material. Thus, the permeability tensor is a property of an excited ferrite material. The given tensor in (2.3) belongs to a ferrite which is excited through z direction. However, this tensor can be modified for the cases where H_{ext} is through x or y direction. Although tensor is given with cylindrical coordinates, the same tensor elements can be used for Cartesian coordinates [19].

$$\vec{B}=\bar{\bar{\mu}}\,\vec{H} \tag{2.2}$$

$$\begin{matrix} B_\Phi \\ B_\rho = \\ B_z \end{matrix} \begin{bmatrix} \mu & j\kappa & 0 \\ -j\kappa & \mu & 0 \\ 0 & 0 & \mu_o \end{bmatrix} \begin{matrix} H_\Phi \\ H_\rho \\ H_z \end{matrix} \tag{2.3}$$

The permeability tensor elements are μ , κ and μ_o. $j\kappa$ and $-j\kappa$ elements have opposite signs, and this is the main reason for the non-reciprocal character of the circulator structures. μ_o is the free space permeability.

Permeability tensor elements κ and μ depend on radian frequencies ω, ω_m and ω_o [19].

$$\kappa=\mu_o \frac{\omega\omega_m}{{\omega_o}^2-\omega^2} \tag{2.4}$$

$$\mu = \mu_o \left(1+\frac{\omega_o\omega_m}{{\omega_o}^2-\omega^2}\right) \tag{2.5}$$

Firstly, ω in equations (2.4) and (2.5) is the radian frequency value of the microwave signal applied to the ferrite material. Secondly, ω_m is the radian magnetization frequency of the ferrite material given in (2.6). Thirdly, ω_o is the internal static field radian frequency, which is given in 2.7. The term ϒ in (2.6) and (2.7) is the gyromagnetic ratio with a value of 2.8 MHz/Oe and it relates the magnetic field values to frequency values.

$$\omega_m = 2\pi (f_m) = 2\pi (4\pi M_s \Upsilon) \quad \textbf{(2.6)}$$

$$\omega_o = 2\pi (f_o) = 2\pi (\overrightarrow{H_i} \Upsilon) \quad \textbf{(2.7)}$$

In (2.6), it is clear that ω_o depends on internal static magnetic field of the ferrite material which shows that internal static field H_i is one of the main factors that determine tensor elements μ and κ. On top of this, the main contributors of internal static magnetic field (H_i) are the external static magnetic field applied (H_{ext}) to the ferrite and the demagnetization effect. In circulator applications, as the shape of the ferrite material is generally a disk, the demagnetization effect results inhomogeneous internal static magnetic fields, the details of which is given in Part 4.1.1. Thus, the inhomogeneous field distribution creates different permeability tensors for each magnetic domain in the ferrite disks which makes the electromagnetic field solution of these structures complicated. Note that, $|\kappa/\mu|$ ratio is called *anisotropic splitting* of the ferrite material, and this term is frequently used during the circulator design.

2.1.3 Parameters That Define Ferrite Materials

In circulator design, the properties of ferrite material have a great influence on the performance and frequency band of operation. In order to gain a high performance circulation, some parameters of the ferrimagnetic materials should be chosen carefully. In the following parts, three parameters of the ferrites which are significant in terms of circulator design are explained in detail. The mentioned parameters are *saturation magnetization (*$\mathbf{4\pi M_s}$), *resonance linewidth (*$\mathbf{\Delta H}$) and compensation temperature ($\boldsymbol{T_N}$).

2.1.3.1 Saturation Magnetization ($4\pi M_s$)

If an external static magnetic field (H_{ext}) is applied to a ferrite, the magnetization increases in proportion of the applied static magnetic field; however, at an exact H_{ext} value, all the magnetic domains inside the ferrite material is aligned and the magnetization does not increase any more. The mentioned maximum magnetization value is called *saturation magnetization* ($\mathbf{4\pi M_s}$) and it is a measure of the magnetic strength of the ferrite material. In Figure 2.2, H_{ext} vs. B characteristics of a ferrite material is displayed. The saturation magnetization of the material can be approximated as 2150 Gauss (0.215 Tesla) by the figure.

Saturation magnetization value refers to frequency value f_m (2.6), which is theoretically the beginning of the band in *one octave* circulator operations. Thus, the *Saturation magnetization* of the chosen ferrite is very critical for circulator design, because it determines frequency band of circulation, the details of which is explained in Chapter 2 [4]. For instance, if a 9-18 GHz one octave circulator operation is desired, a ferrite with an f_m=9GHz should be chosen [4]. Below the f_m value, gyromagnetic resonance losses begin to be dominant in the loss mechanism, and this results a much worse response of the circulator [7,14].

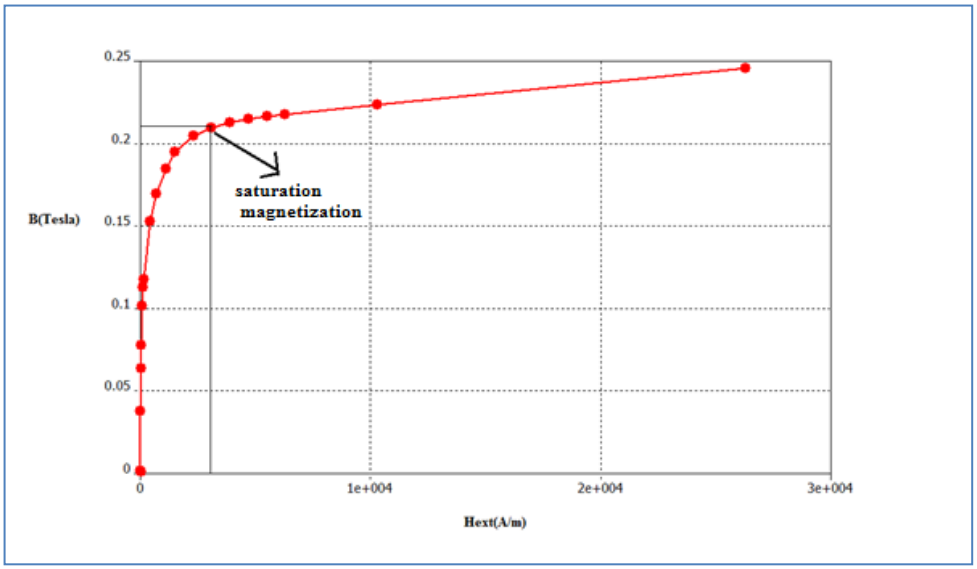

Figure 2.2 Hext(applied field) vs. B (magnetization) characteristics of a ferrite material

Saturation magnetization of the ferrites can be measured by two methods VSM (Vibrating Sample Method) and VCM (Vibrating Coil Method). VSM is a more complicated and more reliable method than VCM [15]. In this method, simply a calibrated ferrite sphere is used to measure the *saturation magnetization* of the ferrite tested. The *saturation magnetization* value of the ferrite materials can vary from very low values up to 5000-6000G (Appendix A). The upper boundary (5000-6000 G) puts a limit for high frequency one octave circulators which will be explained in Chapter 3. The details of these methods are given in Appendix C.

2.1.3.2 Resonance Linewidth (ΔH)

Resonance linewidth is a quantity which gives the width of internal static magnetic field range between the half points of maximum loss . Thus the explanation of the loss mechanism in ferrites is necessary to understand the meaning of Resonance Linewidth. The loss of the ferrite material is resulted by three main contributors, which are internal static magnetic field (H_i), frequency of the microwave signal (f) and the *resonance linewidth* (ΔH) of the ferrite material [16,17,21,28].

Firstly, the internal static magnetic field of the ferrite has an effect on the operation region of the ferrite material. In Figure 2.3, the losses in terms of varying internal static magnetic field of two different frequency signal can be observed. If the loss curves are considered, it is clear that there is a low loss region for internal static magnetic field between low field losses and gyromagnetic resonance losses. This region can be called as below resonance region. If the internal static magnetic field is increased, and the operation point shifts to the right of the gyromagnetic resonance region, the operation region has become above-resonance region. So, the internal static magnetic field affects the losses of the ferrite materials and defines the operation region of the ferrite material. Secondly, increasing the frequency of the microwave signal shifts the loss curve to the right. In Figure 2.3, it can be said that as the frequency increases, there is a larger internal static field range for below resonance region for low-losses. So, for low frequency applications, a narrower range exists for below resonance operation [17].

In our application, below resonance region is clearly more useful, because the starting point of the frequency band (9GHz) is relatively high which offers a wider range for internal static magnetic fields for low losses. On top of this, below resonance operation allows to use lower size magnets due to low static magnetic field requirement. Thus, due to the mentioned reasons, below resonance operation is preferred in circulator structures.

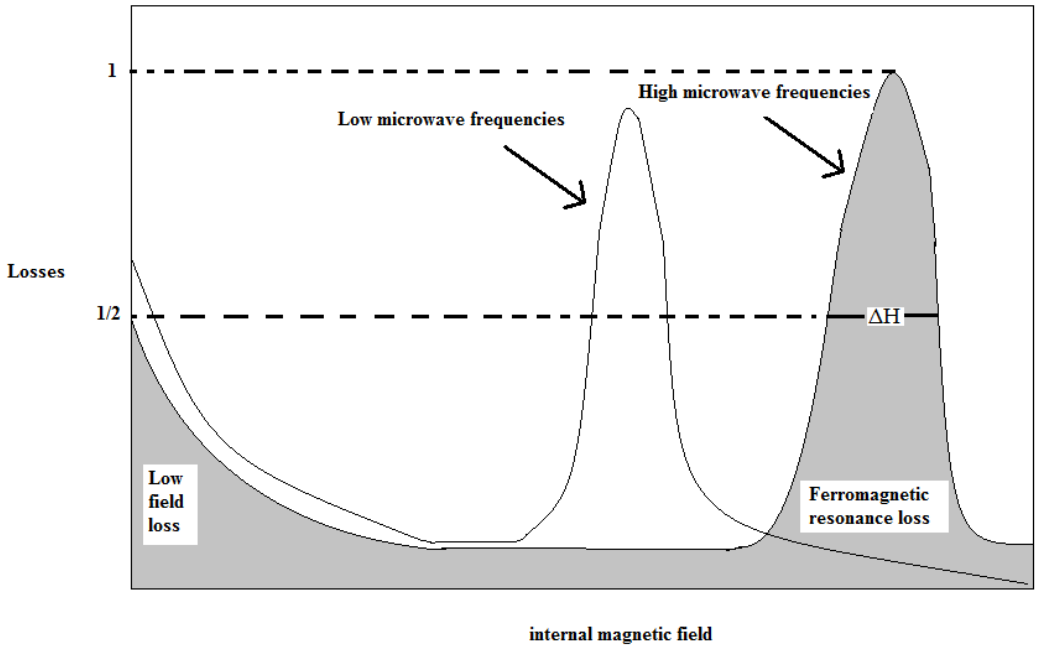

Figure 2.3 Losses in the ferrite materials in terms of varying magnetic field

At the beginning, it is explained that *resonance linewidth (ΔH*) of the ferrite structure is a factor for the loss mechanism of ferrite materials. As can be observed in Figure 2.3, *resonance linewidth (ΔH*) value simply gives the width of internal static magnetic field range between the half points of maximum loss. So, an increase in *resonance linewidth (ΔH*) simply contributes to a narrower low loss range for below resonance operation which is an unwanted effect[37].

Finally, the *resonance linewidth (ΔH*) value gives the shape of the ferromagnetic resonance loss [36]. Thus, choosing a lower *resonance linewidth (ΔH* ferrite results a wider low-loss region which means that kind of such choice is logical.

2.1.3.3 Compensation Temperature (T_N)

It can be said that the magnetization of a ferromagnetic material can be reduced to zero by increasing the temperature above its Curie temperature [12]. A similar temperature definition can be made for ferrimagnetic materials, but the mechanism is much more complicated in this case. The difference between ferromagnetic and ferrimagnetic materials is the alignment of the magnetic domains, shown in Figure 2.1. In ferrimagnetic materials, the magnetic domains are aligned into two opposite directions unlike ferromagnetic materials. If we consider that these domains have different behaviors with increasing temperature, there should be an exact temperature at which these magnetic domains cancel each other. In Figure 2.4, variation of magnetization in terms of changing temperature for ferrties can be observed. M_A and M_B are the two opposite magnetic domains inside the ferrimagnetic material and when they have equal magnitude magnetizations with opposite directions, the net magnetization becomes zero. This exact point is called the magnetic compensation of the ferrite material and the temperature value at this point is $\boldsymbol{T_N}$**.** However there is another temperature term, T_C , which is the curie temperature at which the both M_A and M_B become zero. As there is only one magnetization direction in ferromagnetic material, the net magnetization becomes zero at $\boldsymbol{T_C}$ for ferromagnetic materials [12].

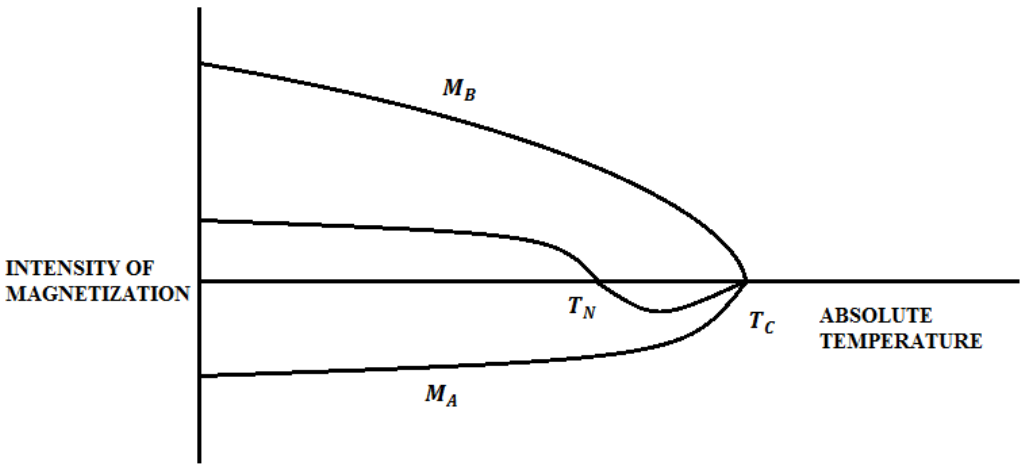

Figure 2.4 Variation of magnetization with temperature

2.1.4 Chemical Properties of Ferrite Materials

Ferrimagnetic materials have been found in the nature in the form of magnetites. For nearly one century, people have the capability of forming artificial ferrimagnetic materials, which can be called ferrites also. Magnetite, in fact, is an iron spinel, which has a chemical formula FeO. Fe_2O_3 [11,21].

There are 3 main classes of the ferrites. These classes are named in terms of the crystal structure of the ferrite materials. The names of the classes are: the *spinels*, the *garnets* and the *hexagonals*. In the following parts, hexagonal ferrites are not explained, because they are out of our interests due to their irrelevant properties. However, *garnets* or *spinels* are useful in terms of the frequency band and losses required in circulators. All the ferrites are in the form of ionic crystals, so they are bonded by ionic bonds. Although it is possible to form single crystal ferrite materials, the microwave ferrites have generally polycrystalline structures, which means that the ferrite has a non-uniform orientation of crystal lattice [21].

2.1.4.1 Garnets

The general formula of *garnets* is $5Fe_2O_3 3M_2O_3$ [1,21]. The M in the formula is a rare earth magnet like yttrium. A pure YIG has a *saturation magnetization (*$\mathbf{4\pi M_s}$) around 1780G. Although *saturation magnetization* values above this value cannot be reached using YIG ferrites, lower values can be achieved by replacing some portion of the iron by aluminum, gadolinium, holmium and calcium [11,12]. For instance aluminum deposition is preferred for narrower *resonance linewidth*, while Vanadium deposition is used for stable $4\pi M_s$ in terms of temperature. However, the deposition of both of the materials decreases $4\pi M_s$of the garnets lower than 1780G.

Our aim is to design a 9-18 GHz *one octave* circulator, the design of which requires a ferrite material with a $4\pi M_s$ value of around 3000 G. The details of the stated fact are explained in Chapter 3. Due to relatively high *saturation magnetization* requirement, garnets are not proper materials for our design. However, if the frequency band was between 5 to10 GHz, they can be used efficiently due to their

low *resonance linewidth* (ΔH) values. Properties of microwave garnets provided by TRANS-TECH and TCI can be observed in Appendix A [13,24].

2.1.4.2 Spinels

The general formula of a microwave *spinel* is $(MOFe_2O_3)_8$, "M" in the formula is a divalent metal like iron, manganese, nickel, zinc, cadmium, cobalt, copper, or a mixture of these [12,21]. The *spinel* ions are structured in the form of *face-centered cubic* (FCC). In *one octave* circulator design, we prefer to use nickel *spinels* and magnesium *spinels* because of their proper *saturation magnetization* values for 9-18 GHz operation. If the datasheets of ferrite manufacturers like TRANS-TECH or TCI [13,24] are investigated, it can be seen that nickel and magnesium *spinel* compositions have very wide *saturation magnetization* range, which is approximately between 500G to 4000G [11,12]. This wide range is resulted by substitution of nickels or magnesium with non-magnetic materials.

Nickel ferrites have been extensively used in below resonance devices from about 10 GHz to approaching 100 GHz [21]. Generally, pure Ni ferrites are not preffered for junction devices due to their wide *resonance linewidth*s (ΔH). However, NiZn ferrites have relatively lower losses and larger $4\pi M_s$ which makes them useful for wideband circulator designs. NiAl ferrites have also lower losses than pure Ni ferrites, but their $4\pi M_s$ is also lower than pure Ni ferrites unlike NiZn. The power handling of the nickel ferrites is increased by Co (cobalt) deposition to material [21].

Magnesium ferrites have useful magnetizations between 700 to 3000G. Their unsubstituted saturation magnetization value of 2200G can be raised by Zn deposition and can be lowered by Al deposition. However, both of them reduce T_N and ΔH. The most important property of magnesium ferrites is their low magnetic losses away from resonance. However, their variable magnetization and broad ΔH values allow them to be used in a few applications.

2.2 The Wideband Circulator Design

In this part, it is aimed to establish the theoretical design methodology for wideband stripline circulators.

2.2.1 The Structure of a Stripline Circulator

In Figure 2.5, the structure of a 3 port stripline circulator can be seen [3]. Firstly, the 3 port stripline circulator is symmetrical around z=0 plane. If the structure of a stripline circulator is explained from the bottom to the top, the first structure at the bottom is the ground plane, which is numbered as *1* in Figure 2.5. The next structure from the bottom is the ferrite disk, which is numbered as *4*. The ferrite disks are covered by the ground plane, which is similar to a stripline structure. Generally, ferrite disks are surrounded radially by a dielectric material. However, in some suspended circulator designs, air is used as the dielectric material. If we come to the explanation of the structure, in the middle the y-junction conductor is located, which is numbered as *3*. The thickness and conductivity of the y-junction is important for the operation of the circulator. In fact, the thickness of the y-junction also defines the thickness of the air remaining between ferrite disks, which is important in terms of performance. Moreover, the conductivity of the y junction affects the insertion loss performance of the circulator. In Figure 2.5, H_i shows the internal static field generated in the ferrite which is compulsory for the circulation operation, because the ferrite materials gain permeability tensor characteristics, if and only if an external static magnetic field is applied.

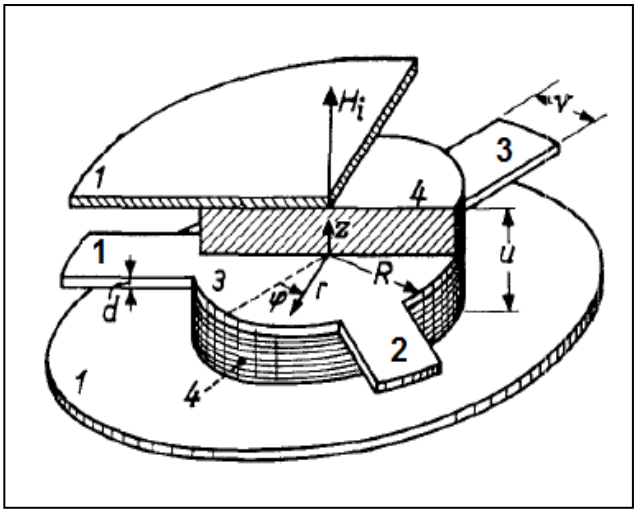

Figure 2.5 The 3-D structure of a stripline circulator[3]

2.2.2 The Theoretical Basis of Wideband Circulator Design

Circulator design theory is based on defining the high frequency (HF) E and H fields and their relations in the ferrite disks. If these relations are revealed, it is possible to optimize design parameters for circulation operation. In the following parts, the Green's function approach is given, which aims to find HF E and H field relations in the ferrite disks and provide circulation conditions [3]. Then, an approach, called *continuous tracking technique*, for *one octave* circulator design is clarified [4].

2.2.2.1 The Green's Function Approach

The design of a circulator highly depends on finding the HF E and H field inside the ferrite disk resonators. Although these fields can be related to each other by using methods like contrarotating surface waves [6], the most accurate results have been gained by using the Green's function approach [3]. Bosma provides Green's function that relates the internal HF E and H fields. Adding to that, 2 perfect circulation graphs are derived by using the Green's function. With the help of perfect circulation graphs, it is possible to design a circulator analytically for the desired center frequency. In the following part of the derivation, mainly Bosma's Green's function approach is provided with some additions [3].

For 3 port stripline circulator design, the ferrite disks and the center conductor can be chosen to have the same radius: however, the central conductor can have different shapes like triangular or clover leaves. The important point about the shape of the central conductor is that it should have 3 fold cyclic symmetry. During the design process, we use a circular junction with the same radius of the central ferrite disk. In all designs, 3 conductor lines are connected to the center conductor with 120 degree apart displacement. The centers of these connections are at –π/3, 0 and π/3 which can be seen in Figure 2.6.

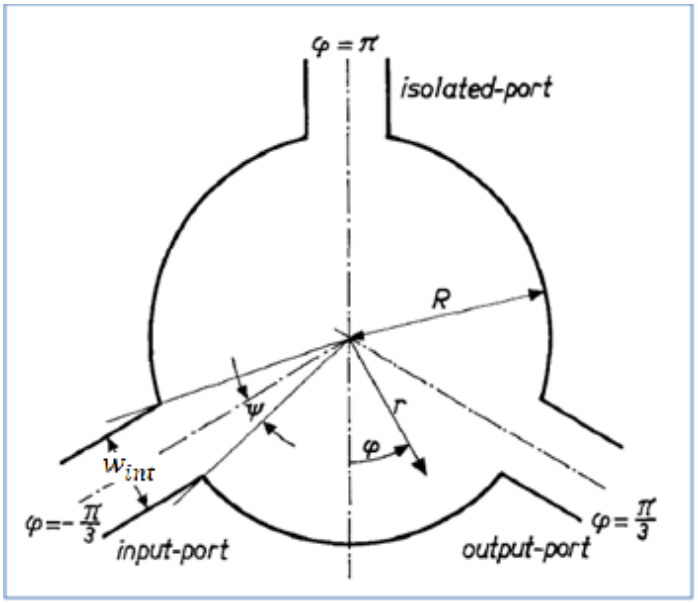

Figure 2.6 The central conductor and the placement of 3 ports

One of the important design parameters of the circulator is the width of the stripline connections (w_{int}) which contributes to a radian angle called *coupling angle*, Ψ in Figure 2.6.

$$\Psi = sin^{-1}\,(w_{int}/2R) \tag{2.8}$$

In this part, the aim is to define the Green's function which relates HF E and H field of the circulator. Before the determination of the Green's function, some assumptions

have been made to ease the problem. Firstly, there is only TEM mode in the strip-transmission lines, and there are ground planes at the top and at the bottom of the structure. Thus, HF E field is through z direction and the HF H field is through the ϕ direction. [3] Secondly, thickness of ferrite disks are assumed to be small enough for field intensities not to vary over the width of the ferrite, so the problem can be considered as a two dimensional problem. In other words, neither E_z nor H_ϕ depend on position through z. Finally, as there is no radial current flow from the edge of the conductor disk except the strip-transmission line and conductor disk connections, there is no H_ϕ distribution at the edge except mentioned connections. In Figure 2.7, E_z and H_ϕ values at the intersections are shown. Moreover, a constant H_ϕ at the boundary between the central conductor and the strip-transmission lines can be assumed to ease the calculations which is given in (2.9).

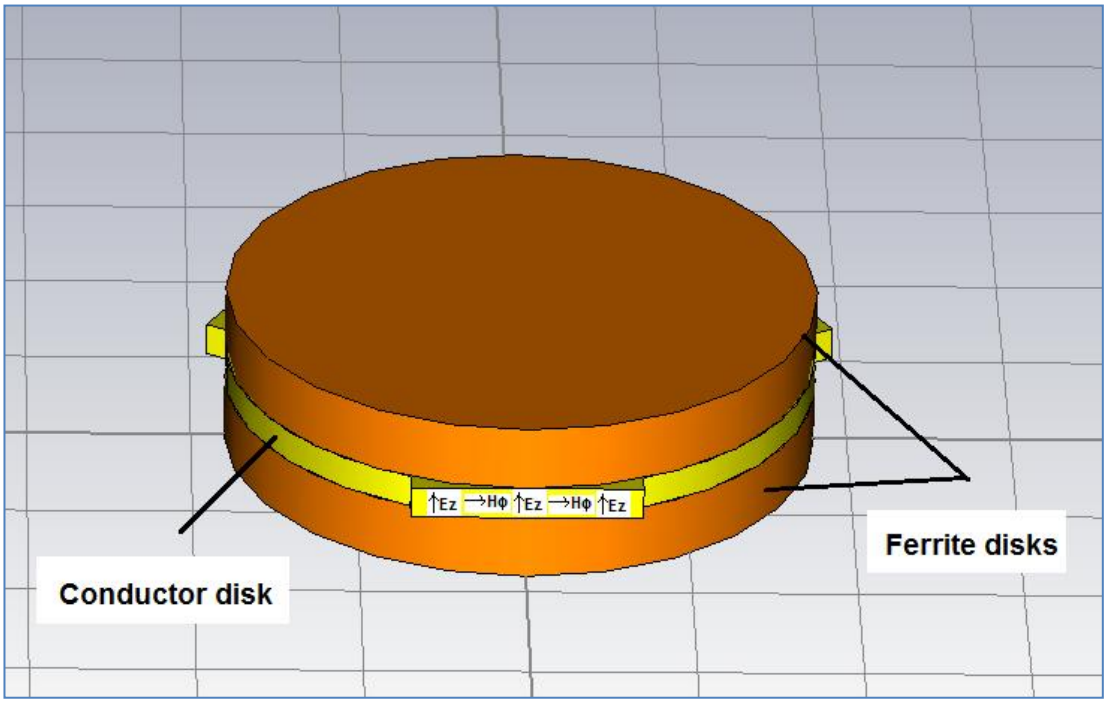

Figure 2.7 Assumed HF-Ez and HF-Hϕ distribution at the intersections

The tangential H field at the intersection of strip-line and central conductor should be equal due to boundary conditions. So, the solution can be initiated by defining constant HF- H_ϕ values at the intersection between conductor disk and the strip-

transmission lines. Constant HF-H_ϕ field can be defined as below, by assigning constant a, b, c magnetic fields at 3 ports in Figure 2.6 [3].

$$H_\Phi(R,\phi) = \begin{cases} a & \text{for } -\pi/3-\psi < \Phi < -\pi/3+\psi \\ b & \text{for } \pi/3-\psi < \Phi < \pi/3+\psi \\ c & \text{for } \pi-\psi < \Phi < \pi+\psi \\ 0 & \text{elsewhere} \end{cases} \quad \textbf{(2.9)}$$

As H_ϕ is known at the edge of central conductor (r=R), it is possible to find E_z field by assigning the Green's function with a superposition integral. The explicit form of the Green's function can be found in (2.38).

$$E_z(r,\Phi) = \int_{-\pi}^{\pi} G(r,\phi;R,\phi')\ H_\Phi(\Phi')\, d\phi' \quad \textbf{(2.10)}$$

As E_z (r, Φ) fields are required only at the boundaries of the conductor, the Green's function can be simplified to a form in which radial position is fixed to r=R. In this new form, only circumferential (r=R) E_z and H_ϕ are related, so it is possible to write the Green's function without r dependence [3].

$$G(R,\phi;R,\phi') = G(\phi;\phi') \quad \textbf{(2.11)}$$

$G(\phi;\phi')$ defines the relation between the HF fields at the boundary of the circular conductor and it is enough for our aim. For the small values of coupling angle(Ψ), it is possible to find the $E_z$values as below, by simplifying integrals given in (2.10) and the Green's function given in (2.11). As Ψ value is very small, the width of the ports can be simplified directly to the radian value of Ψ, and also as H_Φ values are

assumed to be constant, the integral is simplified to a multiplication of fields, port widths and the Green's function values at these points [3].

$$E_z\ (\mathrm{R},-\pi/3)=\mathrm{A}=2\Psi\ [\mathrm{G}\ (-\pi/3;-\pi/3)\mathrm{a}+\mathrm{G}\ (-\pi/3;\pi/3)\mathrm{b}+\mathrm{G}\ (-\pi/3;\pi)\mathrm{c}] \quad \textbf{(2.12)}$$

$$E_z\ (\mathrm{R},\pi/3)=\mathrm{B}=2\Psi\ [\mathrm{G}\ (\pi/3;-\pi/3)\mathrm{a}+\mathrm{G}\ (\pi/3;\pi/3)\mathrm{b}+\mathrm{G}\ (\pi/3;\pi)\mathrm{c}] \quad \textbf{(2.13)}$$

$$E_z\ (\mathrm{R},\pi)=\mathrm{C}=2\Psi\ [\mathrm{G}\ (\pi;-\pi/3)\mathrm{a}+\mathrm{G}\ (\pi;\pi/3)\mathrm{b}+\mathrm{G}\ (\pi;\pi)\mathrm{c}] \quad \textbf{(2.14)}$$

A, B, C given in (2.12), (2.13) and (2.14) are the boundary E_z values at $\phi=-\pi/3, \pi/3, ,\pi$. As we assume that the circulator is a lossless one, the Green's function has the property,

$$\mathrm{G}\ (\phi';\phi)=\text{-}G^*\ (\phi;\phi') \quad \textbf{(2.15)}$$

And also due to the cyclic symmetry for 120 degree,

$$\mathrm{G}\ (\phi+2\pi/3;\phi'+2\pi/3)=\mathrm{G}\ (\phi;\phi') \quad \textbf{(2.16)}$$

We introduce 2 new quantities ξ and ϕ to simplify equations,

$$\acute{\imath}\xi=2\Psi\mathrm{G}\ (-\pi/3;-\pi/3) \quad \textbf{(2.17)}$$

$$\phi=2\Psi\mathrm{G}\ (-\pi/3;\pi/3) \quad \textbf{(2.18)}$$

Due lossless condition is assumed, ξ is real and ϕ is complex. By using the conditions (2.12)- (2.14) with the help of (2.15) and (2.16),

$$A= íξa+ ϕ\ b+ϕ^{*}c \tag{2.19}$$

$$B=-ϕ^{*}a+íξb+ ϕc \tag{2.20}$$

$$C=ϕa-ϕ^{*}b+íξc \tag{2.21}$$

Now the HF-E_z field at the ports (A,B,C) are determined in terms of constant $H_ϕ$ and the Green's function values at the ports. The ratio of the electric and magnetic fields gives the characteristic impedance of the medium, Zo.

$$B/b=C/c=-Zo \tag{2.22}$$

For simplicity, a new quantity Θ is introduced,

$$Θ=Zo+íξ \tag{2.23}$$

By using (2.19)- (2.21),

$$A= (i\xi + \frac{\phi^3-\phi^{*3}+2\phi\phi^*\Theta}{\phi\phi^*+\Theta^2})a \quad \textbf{(2.24)}$$

$$b=\frac{\phi^2+\phi^*\Theta}{\phi\phi^*+\Theta^2}\, a \quad \textbf{(2.25)}$$

$$c=\frac{\phi^{*2}+\phi\Theta}{\phi\phi^*+\Theta^2}\, a \quad \textbf{(2.26)}$$

By using (2.24)- (2.26), it is possible to find the $H_\phi$values at the ports if one of the $H_\phi$value is known at one port. If the input port $H_\phi$value is assumed to be a constant value "a", it is possible to find the $H_\phi$values "b" and "c" at the other ports. Also by using the constant "a", it is possible to find the $E_z$value at the same port which is named as A.

Now, the required relations between E_z and $H_\phi$values are determined to find the scattering matrix of a lossless, cyclic symmetric 3 port circulator. By considering the properties of the circulator, we introduce the scattering matrix below.

$$S = \begin{bmatrix} \alpha & \gamma & \beta \\ \beta & \alpha & \gamma \\ \gamma & \beta & \alpha \end{bmatrix} \quad \textbf{(2.27)}$$

The following relations are valid, if the A_i and a_i are the wave incident to the input port, respectively [3].

$$A_i = \mathrm{Zo} a_i \tag{2.28}$$

$$\mathrm{A} = (1+\alpha)\, A_i \tag{2.29}$$

$$a = (1-\alpha)\, a_i \tag{2.30}$$

$$\beta = \mathrm{B}/A_i \tag{2.31}$$

$$\gamma = \mathrm{C}/A_i \tag{2.32}$$

By using the equations (2.24)- (2.26) with equations (2.28)- (2.32), the scattering parameters α, β and γ can be found as below [3].

$$\alpha = \frac{\phi^3 - \phi^{*3} + \phi\phi^*(2\Theta - {}^*) - {}^{2*}}{\phi^3 - \phi^{*3} + 3\phi\phi^* + {}^3} \tag{2.33}$$

$$\beta = -\frac{(\phi^2 + \phi^*)\,(\Theta + {}^*)}{\phi^3 - \phi^{*3} + 3\phi\phi^* + {}^3} \tag{2.34}$$

$$\gamma = -\frac{(\phi^{*2} + \phi)\,(\Theta + {}^*)}{\phi^3 - \phi^{*3} + 3\phi\phi^* + {}^3} \tag{2.35}$$

Now, the scattering parameters α, β and γ are defined in terms of the Green's function and the properties of the medium.

If the circulator is assumed to perform clockwise circulator operation ideally, the matrix elements (2.27) becomes

$$|\beta|=1 \tag{2.36}$$

$$\alpha=\gamma=0 \tag{2.37}$$

If we assume that the signal is inputted from port 1 , then (2.36) and (2.37) show that the circulator is perfectly matched and port 3 is perfectly isolated from port 1. In other words, the incoming signal is not reflected and all of it goes totally to port 2. If the R (radius of the ferrite) and $\boldsymbol{4\pi M_s}$ of the ferrite are determined, the circulation conditions above can be fulfilled only for some values of ω and H_i. In order to design a circulator for given central frequency, the geometry and the material property of the ferrite should be chosen accordingly. By assuming a 3 port lossless circulator, after some algebraic manipulation, the Green's function can be derived as below.

$$G(r,\phi;R,\phi') = -\frac{j\,Zeff\,J_o(Sr)}{2\,\pi\,J_o'(Sr)} + \frac{Zeff}{\pi}\sum_{n=1}^{\infty}\frac{\left(\frac{\kappa}{\mu}\right)\left(n\frac{J_n(SR)}{SR}\right)\sin n(\phi-\phi') - jJ_n'(SR)\cos n(\phi-\phi')}{(J_n'(SR))^2-\left[\left(\frac{\kappa}{\mu}\right)\left(n\frac{Jn(SR)}{SR}\right)\right]^2}\,J_n(Sr) \tag{2.38}$$

where,

μ, κ	:Polder tensor elements of the ferrite
$J_n(Sr)$	:Bessel function of the first kind with order n
$J_n'(Sr)$	:First derivative $J_n(Sr)$ with respect to its argument
$\left(\frac{\kappa}{\mu}\right)$	:Anisotropic splitting value of the ferrite
$\mu_{eff}=(\mu^2-\kappa^2)/\mu$	:Effective permeability of ferrite
$S=(\omega/c)\,(\mu_{eff}\varepsilon_f)^{1/2}$	:Radial wave propogation constant
$Z_{eff}=(\frac{\mu_o\mu_{eff}}{\varepsilon_o\varepsilon_f})^{1/2}$	:Intrinsic wave impedance of ferrite
ε_f	:Relative dielectric constant of ferrite
r	:Radial coordinate
R	:Ferrite disk radius

2.2.2.2 The Design of One Octave Frequency Band Circulator

Although perfect circulation graphs provide circulator parameters for desired center frequency, using them without a special approach would result very narrowband circulator operations. Wu and Rosenbaum propose a way to design *one octave* frequency band circulators by using special curves in the perfect circulation graphs [4]. Their design approach is called as *continuous tracking technique*, and in this technique, the scattering parameters α, β and γ are defined again by considering higher order modes, unlike the case in the Bosma's Green's function approach. In the following equations, the characteristic impedance of the dielectric around ferrite materials is Z_d, and the n_{th} Bessel function and their first derivatives are named as B_n and A_n , respectively.

$$Z_d = 120\pi / (\varepsilon_d)^{1/2} \tag{2.39}$$

$$A_n = J_n{}' \text{ (SR)} \tag{2.40}$$

$$B_n = J_n \text{ (SR)} \tag{2.41}$$

For simplicity, new quantities C_1, C_2 and C_3 to define α, β and γ in (2.27) are introduced [4]. C_i values depend on variables which are Ψ, Z_d, Z_{eff} and $\frac{\kappa}{\mu}$. Ψ is the coupling angle given in (2.8), Z_d is the characteristic impedance of the dielectric around the ferrite material, Z_{eff} is the intrinsic wave impedance of the ferrite given in (2.38), $\frac{\kappa}{\mu}$ is the anisotropic splitting of the ferrite material. κ and μ are the elements of the permeability tensor and their values have already been given in (2.4) and (2.5).

$$C_1=\frac{\Psi B_o}{2A_o}+\sum_{n=1}^{\infty}\left(\frac{sin^2 n\Psi}{n^2\Psi}\right)\frac{A_nB_n}{{A_n}^2-\left(\frac{n\kappa}{\mu SR}\right)^2{B_n}^2}-\frac{\pi Z_d}{j2Z_{eff}} \quad \textbf{(2.42)}$$

$$C_2=\frac{\Psi B_o}{2A_o}+\sum_{n=1}^{\infty}\left(\frac{sin^2 n\Psi}{n^2\Psi}\right)\frac{A_nB_n\cos\left(\frac{2n\pi}{3}\right)-\left(\frac{jn\kappa}{\mu SR}\right){B_n}^2\sin\left(\frac{2n\pi}{3}\right)}{{A_n}^2-\left(\frac{n\kappa}{\mu SR}\right)^2{B_n}^2} \quad \textbf{(2.43)}$$

$$C_3=\frac{\Psi B_o}{2A_o}+\sum_{n=1}^{\infty}\left(\frac{sin^2 n\Psi}{n^2\Psi}\right)\frac{A_nB_n\cos\left(\frac{2n\pi}{3}\right)+\left(\frac{jn\kappa}{\mu SR}\right){B_n}^2\sin\left(\frac{2n\pi}{3}\right)}{{A_n}^2-\left(\frac{n\kappa}{\mu SR}\right)^2{B_n}^2} \quad \textbf{(2.44)}$$

α, β and γ can again be found by using C_1, C_2 and C_3 [4].

$$\alpha=1+\frac{\pi Z_d\left({C_1}^2-C_2C_3\right)}{jZ_{eff}\left({C_1}^3+{C_2}^3+{C_3}^3-3C_1C_2C_3\right)} \quad \textbf{(2.45)}$$

$$\beta=\frac{\pi Z_d\left({C_2}^2-C_1C_3\right)}{jZ_{eff}\left({C_1}^3+{C_2}^3+{C_3}^3-3C_1C_2C_3\right)} \quad \textbf{(2.46)}$$

$$\gamma=\frac{\pi Z_d\left({C_3}^2-C_1C_2\right)}{jZ_{eff}\left({C_1}^3+{C_2}^3+{C_3}^3-3C_1C_2C_3\right)} \quad \textbf{(2.47)}$$

Input impedance of the circulator can be found in terms of C_1, C_2 and C_3.

$$Z_{in}=-Z_d-\left(\frac{j2Z_{eff}}{\pi}\right)\left(\frac{{C_1}^3+{C_2}^3+{C_3}^3-3C_1C_2C_3}{{C_1}^2-C_2C_3}\right) \quad \textbf{(2.48)}$$

In (2.48), the input impedance of the circulator is defined in terms of Z_d, Z_{eff} and C_1, C_2 and C_3. Although C_i values are infinite series expansions (2.42-2.44),using terms up to third order is claimed to be sufficient for accurate circulator designs [4].

Before going into details of the *one octave* circulator design, the operation region of the circulator should be determined. There are two operation region possibility for circulator designs, which are below resonance and above resonance the details of which is given in Part 2.1.3.2. In below resonance operation, the internal static magnetic field (H_i) equivalent frequency is below the microwave signal frequency ($f_o < f$). However, in the above resonance operation, static magnetic field equivalent frequency is larger than the microwave signal frequency ($f_o > f$). Thus, below resonance operation is clearly more suitable for our application, because it provides larger bandwidth and requires smaller magnets. In the below resonance operation, exciting the ferrite slightly above the saturation is sufficient. Due to the below resonance operation, permanent magnets with B_r values slightly larger than *saturation magnetization* of the ferrite materials are chosen [1,22].

For below resonance operation, a zero internal magnetic field approximation can be made because of very low static internal fields [22],

$$\overrightarrow{H_i} \approx 0 \tag{2.49}$$

$$\omega_o = 2\,\pi\,(f_o) = 2\pi\,(\overrightarrow{H_i}\,\gamma) \approx 0 \tag{2.50}$$

As $\omega_o \approx 0$ for below resonance operation, the elements of the Polder Tensor given in (2.4) and (2.5) are approximately equal to [22],

$$\mu = 1 \tag{2.51}$$

$$\kappa = -\frac{f_m}{f} \tag{2.52}$$

In order to get perfect circulation, the scattering element, β contributing to isolation should be zero. In other words, one of the ports must be completely isolated. For complete isolation, the denominator of (2.46) should be zero

$$C_2{}^2 = C_1 C_3 \tag{2.54}$$

As C_1 , C_2 and C_3 are complex number, (2.54) can be decomposed into 2 separate equations due to real and imaginary parts. (2.55) and (2.56) are also named as first and second perfect circulation conditions, respectively

$$\text{P}=\frac{M\,(M^2-3N^2)}{(M^2+N^2)} \tag{2.55}$$

$$\text{Q}=\frac{N\,(3M^2-N^2)}{(M^2+N^2)} \tag{2.56}$$

Where P,Q,M,N values are

$$\text{P=Re}\,(C_1)=\frac{\Psi B_o}{2A_o}+\sum_{n=1}^{\infty}\left(\frac{sin^2 n\Psi}{n^2\Psi}\right)\frac{A_n B_n}{A_n{}^2-\left(\frac{n\kappa}{\mu SR}\right)^2 B_n{}^2} \tag{2.57}$$

$$\text{Q=Im}\,(C_1)=\frac{\pi Z_d}{2Z_{eff}} \tag{2.58}$$

$$\text{M= Re}\,(C_2)=\frac{\Psi B_o}{2A_o}+\sum_{n=1}^{\infty}\left(\frac{sin^2 n\Psi}{n^2\Psi}\right)\frac{A_n B_n \cos\left(\frac{2n\pi}{3}\right)}{A_n{}^2-\left(\frac{n\kappa}{\mu SR}\right)^2 B_n{}^2} \tag{2.59}$$

$$\text{N= Im}\,(C_2)=\sum_{n=1}^{\infty}\left(\frac{sin^2 n\Psi}{n^2\Psi}\right)\frac{\left(\frac{n\kappa}{\mu SR}\right)B_n{}^2 \sin\left(\frac{2n\pi}{3}\right)}{A_n{}^2-\left(\frac{n\kappa}{\mu SR}\right)^2 B_n{}^2} \tag{2.60}$$

The P, Q, M, N values are infinite series, but higher terms than the 2nd term do not contribute to significant changes in the result. In *continuous tracking technique*, Wu and Rosenbaum state that it is enough to consider the series up to the 3rd order [5]. The equations in (2.55) and (2.56) contribute to 2 circulation conditions and the results are drawn in the 2 perfect circulation graphs given in Figure 2.8 and 2.9.

By using the 2 perfect circulation graphs, it is possible to design a circulator for specific frequencies, but designing wideband circulators with an octave band requires a more special approach . In Chapter 2, the operation region of the ferrite material is decided to be below resonance which simplifies the tensor elements to the values given in (2.51) and (2.52).

According to Bosma, Wu and Rosenbaum [3.4], circulation starts approximately from *saturation magnetization* frequency, f_m . Below f_m frequency, the low-field losses become dominant and the insertion loss values become too high due to these losses [7]. By assuming the below resonance operation, the impedance ratio is approximately given by

$$\frac{Z_{eff}}{Z_d} = \left(\frac{\varepsilon_d}{\varepsilon_f}\right) (1 - \left(\frac{\kappa}{\mu}\right)^2)^{1/2} \quad \textbf{(2.61)}$$

For below resonance operation, the gyromagnetic splitting value $|\kappa/\mu|$ is approximately equal to f_m/f by (2.51) and (2.52). Thus, it can be said that the x-axis of the first and second perfect circulation graphs does not span only the $|\kappa/\mu|$, but also the f_m/f value. As the f_m is frequency found by the *saturation magnetization* of the ferrite material, the x–axis of perfect circulation graph varies in terms of the inputted microwave signal frequency, f.

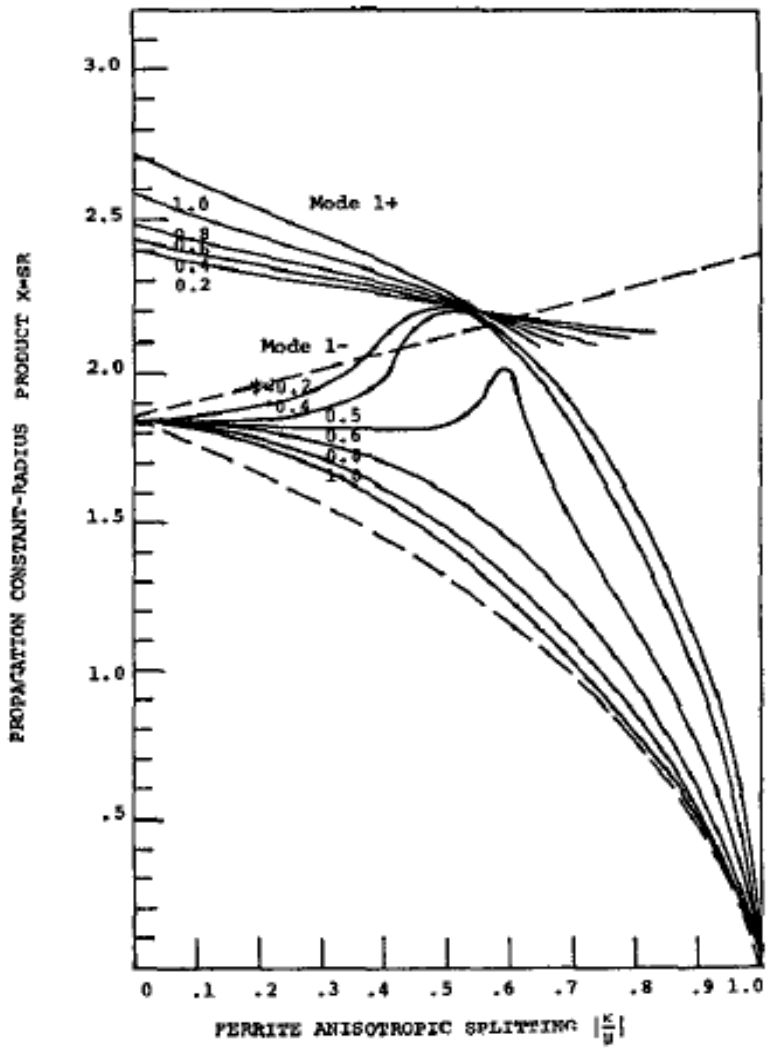

Figure 2.8 Perfect circulation roots for the first circulation condition (2.55) for various coupling angles [4]

In continuous tracking circulator approach, a method for *one octave* circulator design is provided. As we know the lower microwave frequency band limit is $f = f_m$, the upper microwave frequency band limit is $f = 2f_m$ due to *one octave* band. Finally, the band of continuous tracking circulator is determined by the f_m , which is the saturation magnetization frequency given in (2.6).

For lower frequency band limit, if $f = f_m$,

$$|\kappa/\mu| \approx 1 \tag{2.62}$$

For upper frequency band limit, if $f = 2f_m$,

$$|\kappa/\mu| \approx 0.5 \tag{2.63}$$

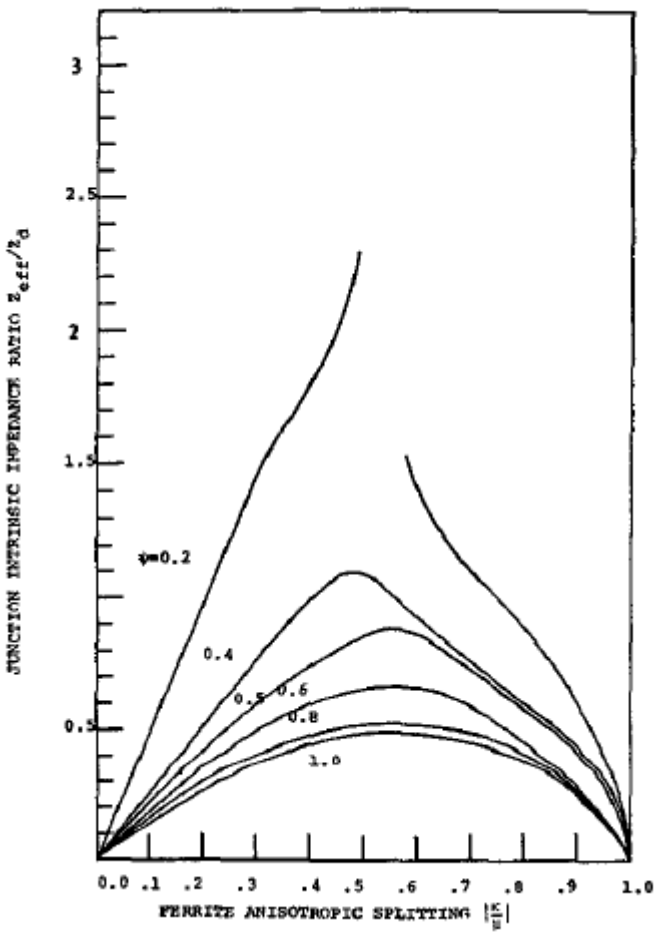

Figure 2.9 Normalized junction impedance ratio as a function of anisotropic splitting factor calculated from the second circulation condition (2.56) for various coupling angles[4]

In Figure 2.8 and 2.9, *one octave* band of the circulator lies between $|\kappa/\mu| \approx 0.5$ and $|\kappa/\mu| \approx 1$ by (2.62) and (2.63). For circulator operation to be realized between f_m and $2f_m$, the second perfect circulator graph should intersect with (2.61) between $|\kappa/\mu| \approx 0.5$ and $|\kappa/\mu| \approx 1$.In order to make one octave circulator design, a procedure like the following one can be followed. Firstly, proper dielectric and ferrite materials

should be chosen, and then the $\frac{Z_{eff}}{Z_d}$ value should be drawn as a function of |κ/ μ| value on second perfect circulation graph. Now, a proper coupling angle ψ for second circulation curve should be chosen to guarantee the intersection of the drawn $\frac{Z_{eff}}{Z_d}$ equation given in (2.61) and second circulation curve. If both curves intersect for small regions, it can be said that the circulator operation is limited to a very narrowband region, but if they intersects between |κ/ μ|≈0.5 and |κ/ μ|≈1, then a one octave circulation is from possible from f_m to 2 f_m. After deciding the coupling angle ψ value, the only parameter remaining to be determined is the radius of the ferrite disk (R) from the first perfect circulation graph.

As operation region is chosen as below resonance, $\frac{Z_{eff}}{Z_d}$ ratio can be found from (2.60). If the ferrite material and dielectric material have the same dielectric constant ($\frac{\varepsilon_d}{\varepsilon_f}$=1), then (2.61) becomes

$$\frac{Z_{eff}}{Z_d} = (1 - \left(\frac{\kappa}{\mu}\right)^2)^{1/2} \quad \textbf{(2.64)}$$

If this new $\frac{Z_{eff}}{Z_d}$ curve for equal dielectric constants of ferrite and dielectric is drawn on top of second perfect circulation graph, an optimized coupling angle (ψ) value can be found for wideband operation which assures intersection of two curves between |κ/ μ| =0.5 and |κ/ μ| = 1. In Figure 2.10, (2.64) is drawn on top of second perfect circulation roots for ψ=0.51 and it is observed that two curves intersect from |κ/ μ| =0.5 to |κ/ μ| = 1. Thus, if the coupling angle ψ is chosen as 0.51 and dielectric constant of ferrite and dielectric is chosen equal, a one octave circulation operation is possible between f = f_m to f= $2f_m$. For comparison, second perfect circulation graph of the ψ=0.2 is also drawn in Figure 2.10 which shows that it intersects with (2.64) only at one point around |κ/ μ| is 0.2 which shows that if the coupling angle is chosen as ψ=0.2, the circulation is restricted to a very narrow frequency band.

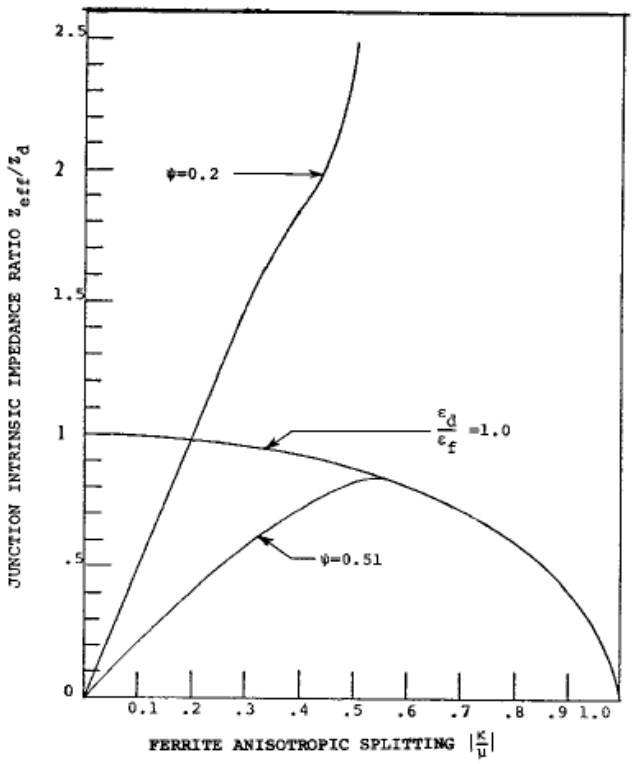

Figure 2.10 Equation 2.63 vs. second circulation graph for both ψ=0.2 and ψ=0.51[4]

Although Wu and Rosenbaum establishes the design process for equal dielectric constant ferrite and dielectric material choice, the approach can be modified for the designs in which ferrite and dielectric material have different dielectric constants. For this case, equation (2.61) is drawn for desired $\left(\frac{\varepsilon_d}{\varepsilon_f}\right)$ ratio and a coupling angle ψ value is found for the best intersection in second perfect circulation graph for the region between $|\kappa/\mu| = 0.5$ and $|\kappa/\mu| = 1$. Then, by using the first circulation condition, it is straightforward to find the radius of the ferrite disk.

Wu and Rosenbaum provide a straightforward method for the design of *one octave* frequency band circulators. In the following Chapter, a 9-18 GHz circulator design is made by using the approach explained here.

CHAPTER 3

THE DESIGN, SIMULATION, REALIZATION AND MEASUREMENT OF ONE OCTAVE FREQUENCY BAND STRIPLINE CIRCULATOR

In Chapter 2, the theoretical design approach for *one octave* circulator design has been provided. The main goal in this chapter is to realize a 9-18 GHz circulator. However, the design process of one octave circulator has many phases. Firstly, analytical approach given in Chapter 2 is used to achieve a starting point for the design parameters of the 9-18 GHz one octave frequency band circulator. Secondly, analytically found parameters are optimized by using a simulation tool, CST. Thirdly, optimized structures are realized and measured. Finally, the measurement results are compared with the simulation results which show whether the simulation tools are reliable in terms of ferrite device modeling. At the end of the chapter, the measurement results are shared and analyzed, which is also a good indicator whether the *continuous tracking technique* is reliable for one octave designs or not.

Another importance of the design of *one octave* frequency band circulator is that it is an intermediate step for the design of *more than one octave* circulator, which is our next target in this study. In the following chapter, the one octave circulators given in this chapter are modified to have wider frequency performances.

3.1 Analytical Design of One Octave Frequency Band Circulator

In this part, the main goal is to find a starting point for the *one octave* circulator design, analytically. This analytical approach possibly does not give the best circulator structure, because many approximations like uniform static field distribution and magnetic walls have been made during the theoretical approach in

Part 2.2.2.1 [3,4]. However, it is certain that the analytically found values provide a satisfying starting point for the optimization of the circulator structure. In the following parts, the *continuous tracking technique* is used to define the geometry and material requirements for a 9-18 GHz *one octave* circulator structure. Then, multi-section impedance transformers are designed to match the impedance of the circulator to 50 Ω for one octave frequency band. After the analytical results have been determined, the structure is simulated in 3D electromagnetic simulator, CST to observe the performance.

In continuous tracking technique, the two perfect circulation conditions in Figure 2.8 and Figure 2.9 have been presented [4]. In addition to this, it is stated that if a specific coupling angle (Ψ) and impedance ratio ($\frac{Z_{eff}}{Z_d}$) couple is chosen, it is possible to design wideband circulators up to 1 octave. Besides, a solution has been proposed for *one octave* circulation which requires the parameters $\frac{\varepsilon_d}{\varepsilon_f}$=1 and Ψ=0.51. In the following parts, the *continuous tracking technique* is followed to find the properties of the 9-18 GHz circulator, analytically.

3.1.1 Determination Of Ferrite Material

During the development of *continuous tracking technique*, it is shown that a circulator operation is possible between f_m and 2 f_m. As a 9-18 GHz circulator operation is desired,

$$f_m = 9\text{GHz} \quad \textbf{(3.1)}$$

If equation (2.6) is modified by considering the effect of Lande factor (g), it becomes

$$f_m = 4\pi M_s \Upsilon\ (g/2) \quad \textbf{(3.2)}$$

As gyromagnetic ratio Υ is a constant and equal to 2.8 MHz/Oe, then for $f_m = 9GHz$,

$$4\pi M_s = 3214\ (2/g) \tag{3.3}$$

In equation (3.2), a required *saturation magnetization* value in terms of Lande factor is derived by (3.1). Lande factor (g) is a ferrite material parameter, which generally has a value very close to 2 for ferrimagnetic materials. A ferrite material satisfying our requirements can be chosen from the datasheets of well-known ferrite manufacturers like TCI or TTECH. In Appendix A, a list of ferrites and dielectric materials provided by these manufacturers can be found. If nickel ferrite options of TTECH are examined, nickel ferrites like TT2-2750 and TT1-102 seem to be proper for our aim. In Table 3.1, some properties of proper ferrite materials mentioned above can be seen.

Table 3.1 Possible TTECH ferrites for 9-18 GHz circulator

	SAT.MAG.(4PIMs)	LANDE FAC.	RESONANCE LINEWIDTH(ΔH)	DIELECTRIC CONST. (ε)	fm (GHz)
TT2-2750	2750G ±10%	2,2	≤540 Oe	12.8 ±5%	8,47
TT2-101	2150G ±10%	2,19	≤315 Oe	13.0 ±5%	9,24

A ferrite material with an f_m value of 9 GHz is required for 9-18 GHz circulation. In Table 3.1, the related f_m are given for both TT2-2750 and TT2-101. Although both ferrites have very close f_m values, it is preferred to choose ferrites with slightly lower f_m values than the required one to minimize gyromagnetic losses.

In *continuous tracking technique*, it is shown that a one octave circulation is possible if $\left(\frac{\varepsilon_d}{\varepsilon_f}\right)$ =1 and Ψ =0.51 are satisfied. If the $\left(\frac{\varepsilon_d}{\varepsilon_f}\right)$ ratio is not chosen as unity, the $\frac{Z_{eff}}{Z_d}$ equation (2.61) should be drawn and the proper Ψ value should be gathered from the second perfect circulation graph. But, this way is not preferred, because there are plenty of dielectric materials which have the same dielectric constants with the chosen ferrite TT2-2750. As shown in Table 3.1 and Appendix A, the dielectric

constant of TT2-2750 is 12.8 which makes SMAT-13 very suitable for our design. The properties of SMAT-13 are given in the Table 3.2. Dielectric loss tangent, which is a measure of dielectric losses, is also critical for circulator performance. The loss tangent value of SMAT13 is given as lower than 0.00015 at 9.4 GHz which shows that SMAT13 is quite a low-loss material.

Table 3.2 Dielectric material chosen from TTECH catalog

	DIELECTRIC CONST. (ε)	DIELECTRIC LOSS. TAN. (ε)
SMAT-13	13.0 ±5%	≤0.00015

Finally, after summarizing the material choice procedure, it can be said that the frequency band determines the *saturation magnetization* of the ferrite material and the dielectric constant of the chosen ferrite material determines the dielectric constant of the dielectric material. SMAT-13 and TT2-2750 are chosen for the design of 9-18 GHz *one octave* circulator due to their proper properties in terms of the desired requirements.

3.1.2 Determination of Coupling Angle

For a circulator operating in below resonance region, the $\frac{Z_{eff}}{Z_d}$ is given by equation (2.64), $\left(\frac{\varepsilon_d}{\varepsilon_f}\right) \approx 1$.

Now as explained in part 2.2.2.2, should the second circulation condition intersect with (2.63) between |κ/ μ|=0.5 and |κ/ μ|=1. Circulation is possible for the band of f_m to 2 f_m. In Figure 3.1, it is shown that if the coupling angle (Ψ) is chosen as 0.51 and $\left(\frac{\varepsilon_d}{\varepsilon_f}\right)$ is chosen as unity, both curves intersect each other for the desired range.

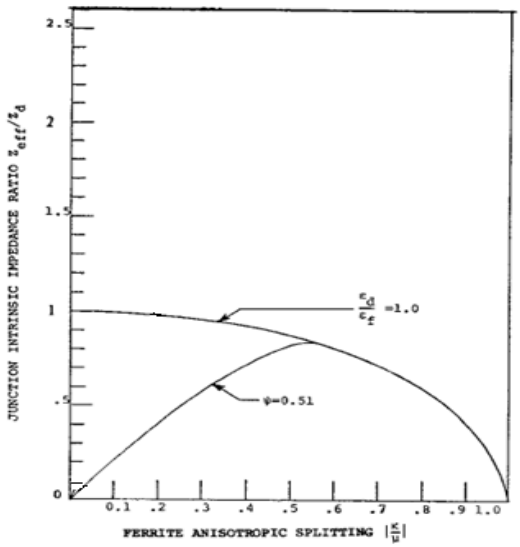

Figure 3.1 The second circulation condition for Ψ=0.51 and impedance ratio equation [4]

From Figure 2.6, it is clear that the coupling angle (Ψ) and the radius of the ferrite disk (R) cooperatively determine the width of the strip-transmission line (w_{int}). Thus, w_{int} is determined in the next part after finding the radius of the ferrite disks (R).

3.1.3 Determination of Radius and Thickness of Ferrite Disk

In Figure 3.2 , the first perfect circulation curve for a coupling angle of 0.51 radian is shown. As the operation region is below resonance, anisotropic splitting value |κ/ μ| directly equal to the ratio f_m/f [22]. In figure 3.2, each |κ/ μ| value contributes to a different SR value. In other words, for each frequency value in the band a different radius is required. As a wideband circulation is desired, an intermediate frequency f_o should be chosen to find an optimum radius value. Geometric mean of f_m and $2f_m$ is a good approximation for f_o.

$$f_o = \sqrt{f_m 2f_m} = f_m\sqrt{2}$$

$$f_o = \sqrt{9.18} = 12.72 \text{ GHz} \quad \textbf{(3.4)}$$

At f_o=12.72 GHz, by (2.51) and (2.52)

$$|\kappa/\mu| = f_m/f = 8.47/12.72 \approx 0.67 \quad \textbf{(3.5)}$$

By derived (3.4) and (3.5) the defined f_o results an anisotropic splitting value of $|\kappa/\mu|$=0.67 which corresponds to SR=1.58 for the first circulation condition to be satisfied. R is the radius of the ferrite disk and S is the propagation constant in the ferrite which are given in 2.38.

$$S = (\omega/c)\ (\mu_{eff}\varepsilon_f)^{1/2}$$

$$\mu_{eff} = (\mu^2 - \kappa^2)/\mu$$

For below resonance $\mu \approx 1$, $\kappa \approx f_m/f$ [22],

$$\mu_{eff} = (\mu^2 - \kappa^2)/\mu$$

$$\mu_{eff} = (1^2 - 0.67^2)/1$$

$$\mu_{eff} = 0.55 \quad \textbf{(3.6)}$$

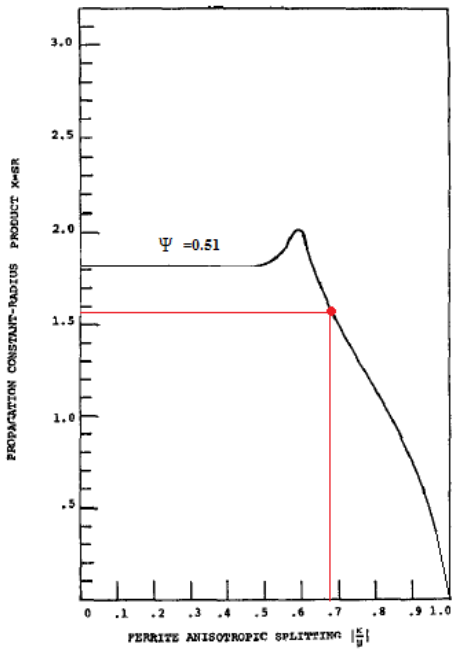

Figure 3.2 The first circulation condition for Ψ=0.51[4]

As $\mu_{eff}$is found in (3.6), propagation constant S is found for f_o=12.72 GHz as

$$S = (2\,\pi\,12.72\,10^9\,/3\,10^8)\,(0.55\,12.8)^{1/2}$$

$$S=706.85 \qquad \textbf{(3.7)}$$

As SR=1.58, by using (3.7)

$$R=2.23\text{mm}.$$

But Wu and Rosenbaum suggest using smaller radius for the ferrite disks especially improves the performance in the tightly coupled designs ($\Psi > 0.5$) [4]. Moreover, they state using a constant value SR≈1.2 is a good approximation for tightly coupled designs.

By using the SR≈1.2 approximation, the radius of the ferrite disk is found as

$$R=1.73mm \tag{3.8}$$

At the end of Part 3.1.2, it is stated that the width of the strip transmission lines (w_{int}) can be found if the coupling angle and radius of the ferrite disks are both determined. In Part 3.1.2, Ψ is found as 0.51 and R is found in (3.8), so by triangular properties considering Figure 2.6,

$$w_{int} = 1.7\ mm \tag{3.9}$$

The thickness of the ferrite disks is a design parameter which does not come out from first and second circulation curves. In Chapter 2, before explaining the theoretical basis of *one octave* circulator design, some approximations have been done. Firstly, the walls of the ferrite disks are assumed to be perfect magnetic conductor (PMC), which means tangential HF magnetic fields do not present on the walls. Secondly, the HF E and H fields do not vary through z direction. In other words, the thickness of the ferrite disks should be so small in terms of the wavelength to reduce field variations through z-direction. If the frequency band of the operation region is considered, 18 GHz signal has the smallest wavelength which contributes to the worst case limitation. Note that the permeability (μ) of a ferrite is unity through the direction of excitation (z), so the wavelength(λ) of the HF signal through z direction can be found as [19],

$$\lambda=c/ (f\sqrt{\varepsilon_f})$$

$$\lambda=3\ 10^8/ (18\ 10^9\ \sqrt{12.8})$$

$$\lambda=4.65\ mm \tag{3.10}$$

While the upper limitation for the thickness of the ferrite disk is set by the wavelength of the HF signal, the lower limitation is set by practical issues. Firstly, ferrite materials are very brittle which prevents the usage of thin ferrite parts in the structure. Secondly, as the dielectric material around the ferrite has the same thickness with ferrite disks, ferrite thickness also defines the dielectric thickness. Likewise, dielectric thickness defines the width of the conductor lines in the circulator structure. If the dielectric is chosen very thin, then the width of the conductor lines becomes very low, which makes them unrealizable.

By assuming λ/10 ferrite thickness is enough for homogeneous field distribution through z-direction, the ferrite thickness is chosen as 20 mil. (0.508mm) which is also a good choice for durability of ferrite substrate and realizable transmission line widths.

$$t=0.508\text{mm} \tag{3.11}$$

3.1.4 Analytical Design of Impedance Transformer

Up to this point, although many structural parameters of the one octave circulator have been determined, the matching sections are not taken into consideration. Generally, input impedance of a circulator is matched to the line impedance of the port, which is generally different than 50 Ohm. However, the circulator can be matched to 50 Ohm in the one octave band by using multi-section quarter wave transformers. Firstly, a proper number of sections should be determined. The most practical value seems to be three, because two-section transformers are not sufficient for *one octave* operation and four-section transformers increase the planar dimension of the circulator. As the width of the strip-transmission line (w_{int}) and the thickness of the ferrite (t) have already been determined, the port impedance can be found by using strip-line impedance calculation approximations [19,23] or some microwave simulations, like CST and AWR. (Figure 3.3)

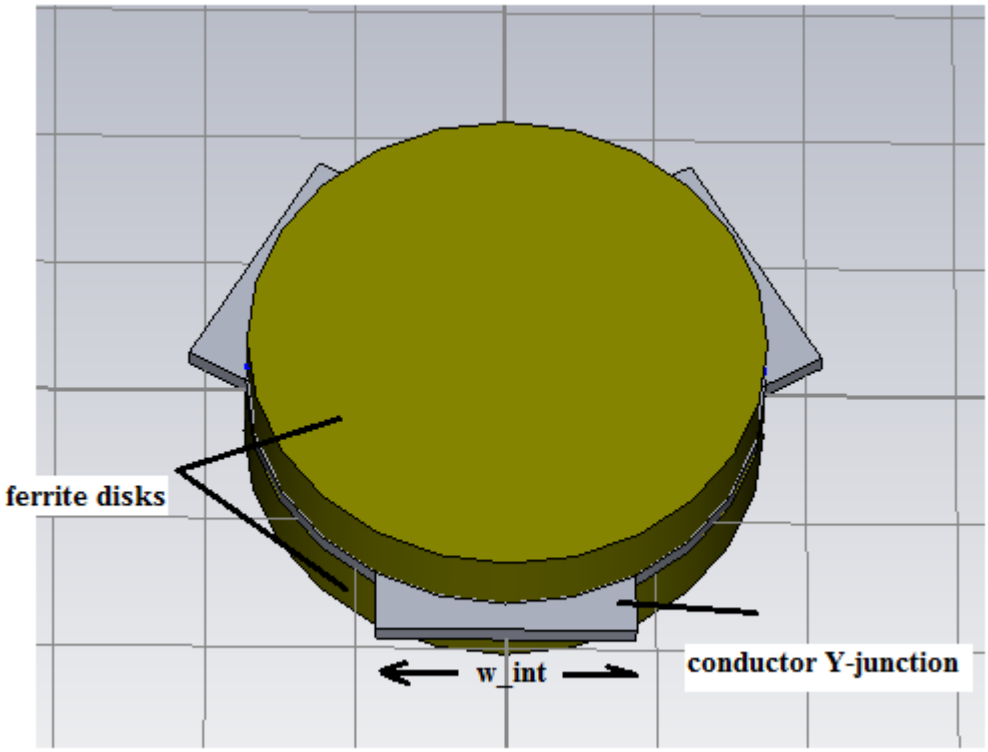

Figure 3.3 Circulator structure without impedance transformers

In Figure 3.4, the port impedance-frequency relation of the unmatched circulator can be observed. The frequency dependence is resulted by the frequency dependent dielectric losses of the dielectric and ferrite material. If we take 12 GHz as the reference frequency, from Figure 3.4.

$$Z_{circulator} = 11.67\ \text{Ohm}$$

As the Chebyshev transformers offer wider bandwidth than Butterworth or Binomial transformers, the characteristic impedances of quarter-wave sections is found with the help of Chebyshev transformer tables [19,23]. By using the impedance ratio table for reflection coefficient Γ=0.05, the characteristic of the sections are found approximately as

$$Z_{system} = 50\ \Omega$$

$$Z_1 = 37\ \Omega$$

$$Z_2 = 25\ \Omega$$

$$Z_3 = 15\ \Omega$$

$$Z_{circulator} = 11.67\ \Omega$$

The corresponding line widths for the found impedances are

$$w_1 = 0.2\ mm.$$

$$w_2 = 0.5\ mm. \qquad \textbf{(3.12)}$$

$$w_3 = 1.25\ mm.$$

The length of the quarter wave sections for 12 GHz reference frequency is

$$\lambda/4 = 3\ 10^8 / (12\ 10^9\ \sqrt{12.8}) \approx 1.75\text{mm}$$

The length of the subsections are 1.75 mm.

$$l_1 = 1.75\ mm.$$

$$l_2 = 1.75\ mm. \qquad \textbf{(3.13)}$$

$$l_3 = 1.75\ mm.$$

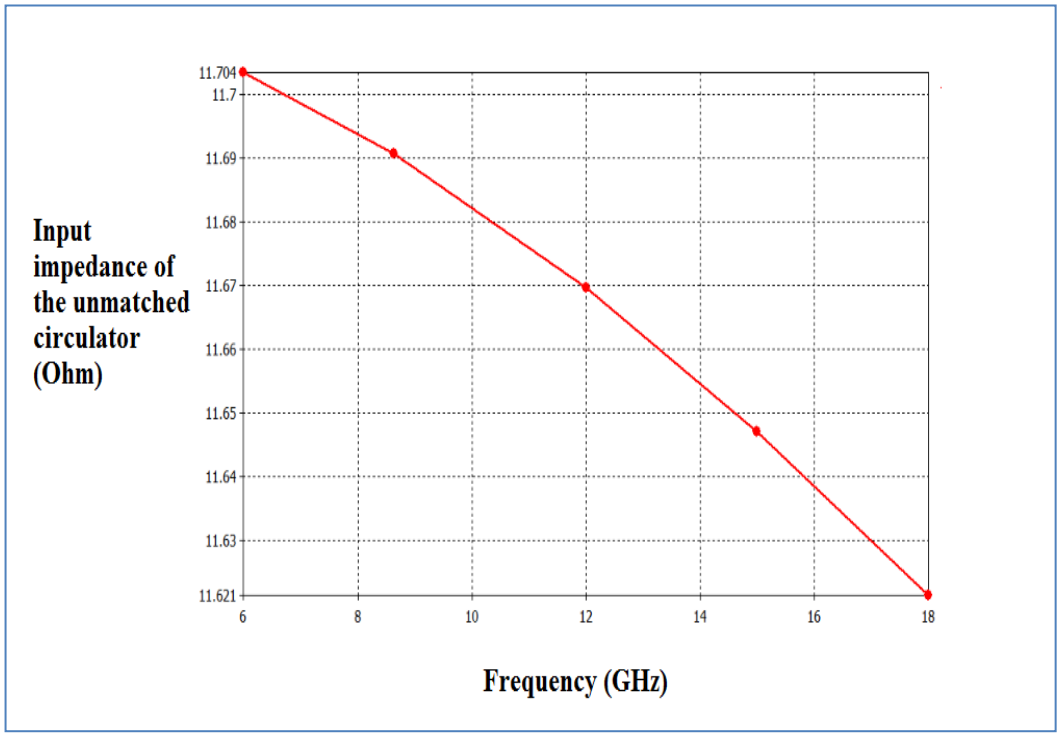

Figure 3.4 The port impedance vs frequency relation of the unmatched structure

In Figure 3.5, the y-junction conductor with impedance transformers is diplayed. This structure involves the impedance transformers connected to the central conductor disk the dimensions of which are determined in (3.8), (3.9), (3.12) and (3.13). The overall structure is matched to 50 Ω and can be directly connected to a 50 Ω microstrip line or a connector. In the measurement process, the ports of the strip-line circulator is connected to 50 Ω micro-strip lines in order to see the effect of the stripline to microstrip transition.

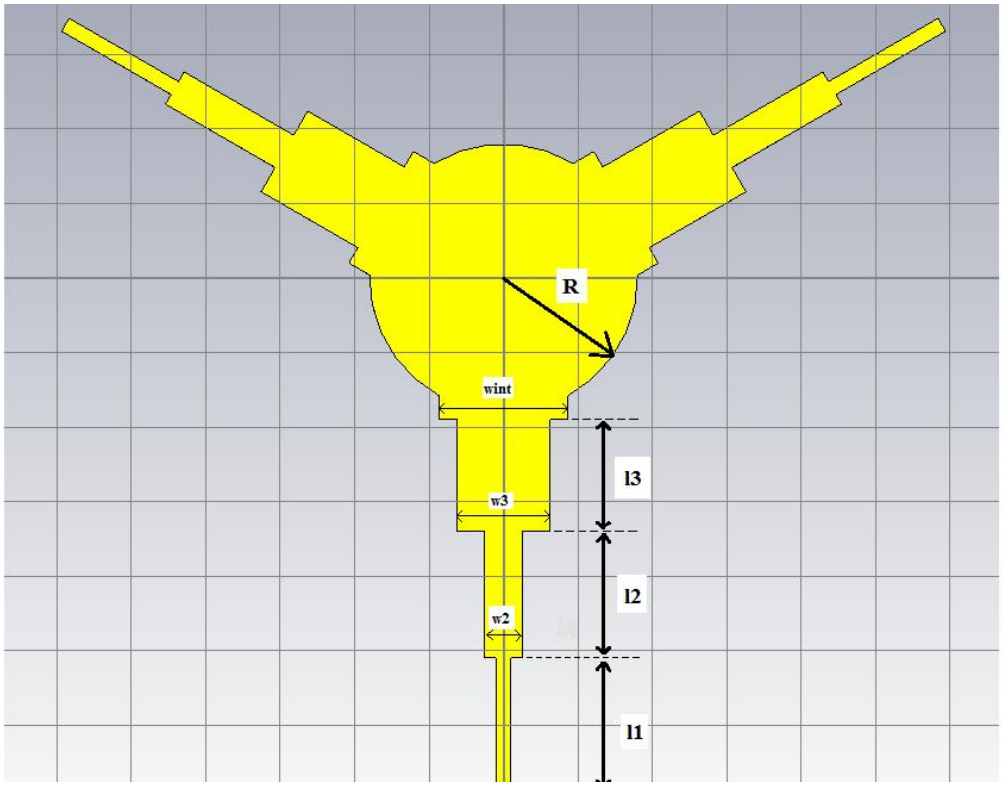

Figure 3.5 Conductor y-junction with three section Chebyshev impedance transformers

3.1.5 Determination of Static Field Excitation

In order to reveal the gyrotropic characteristics of the ferrite material, ferrite disks should be excited by a permanent magnet or an electromagnet [19]. These devices are static magnetic field sources, the strength of which determines the operation region. For wideband circulator operation, below-resonance region is more logical due to many advantages which is explained in Part 2.1.3.2. For below resonance operation, applying slightly a larger static magnetic field than $4\pi M_s$ value is sufficient which enables the designer to apply weaker magnets or small currents to electromagnets. In Part 3.1.1, TT2-2750 nickel ferrite has been determined to be proper for 9-18 GHz operation which means that a static magnetic field in the range of 3000-4000 G is sufficient for below resonance circulation.

3.2 Simulation of One Octave Frequency Band Circulator

Although analytical approaches like *continuous tracking technique* provide enough data to realize a circulator, it is very important to check their performance by using 3D simulation tools. Disk structures are non-ellipsoidal bodies which means that their internal static field distribution is non-uniform even if the external static field excitation is uniform. Some 3D magnetostatic solvers have the capability of solving the internal static field distribution of such kind of structures. CST EM STUDIO is one of them. However, it is not possible to take into account the demagnetization effect in analytical calculations. If demagnetization effect is desired to be taken into consideration, CST EM STUDIO and CST MICROWAVE STUDIO can be operated cooperatively to find the circulator performance. Firstly, CST EM STUDIO solves and finds the internal static magnetic field (H_i) distribution of the ferrite disks. Secondly, CST MICROWAVE STUDIO takes these data and solves the s-parameters of the circulator structure.

In the previous section, dimensions and material properties for a 9-18 GHz circulator have been determined. On top of this, appropriate ferrite and dielectric materials are chosen from the TTECH catalog [13], the details of ferrite and dielectric materials produced by TRANS-TECH and TCI can be found in Appendix A. With the defined values given in Table 3.3, the circulator is modeled in CST which can be observed in Figure 3.6. The simulated structure also contains the stripline to microstrip transitions. Although yoke and magnet structures are included in the simulation, they are not shown in Figure 3.6 to show the structure clearly.

Table 3.3 Analytically found design parameters

dielectric	ferrite	ferrite radius	ferrite thickness	coupling angle(Ψ)	magnet strength
SMAT-13	TT2-2750	1.73 mm.	0.508mm.	0.51rad	3800 G

In Figure 3.6, the exploded view of the simulated circulator can be observed. This structure contains ferrite disks (green), hexagonal dielectric (blue), conductor y-junction (yellow) and microstrip lines. The yoke and magnet disk are hidden in Figure 3.6.

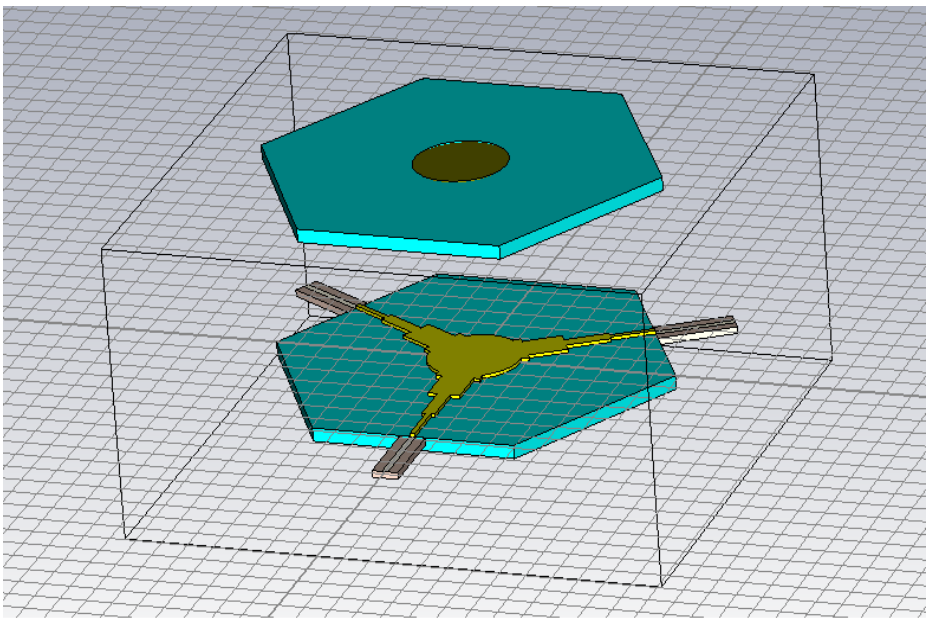

Figure 3.6 Exploded view of the 3D circulator structure

3.2.1 Definition of Field Excitation in CST

In CST, there are two ways of defining the excitation of ferrite materials. Firstly, a constant internal magnetic field (H_i) can be defined for the ferrite material which is not suited well to our situation because of the non-uniform demagnetization factors of disk structures. The other way is to define a static magnetic field source like a magnet for ferrite excitation which enables to determine the deteriorating effects of non-uniform field distribution. Thus, it is preferred to use the second way because it is certain that more realistic results can be found by considering the non-uniform field distribution. As a static magnetic field source, a magnet with residual flux (B_r) value of 3800 Gauss is determined in Part 3.1.5. However, an optimum thickness and radius for the magnet still needs to be found. In the following parts, simulation and theoretical sources are used cooperatively to find optimum dimensions of a

permanent magnet to create a uniform static magnetic field (H_{ext}) on the ferrite disks.

At the beginning of the circulator design, it is stated that the externally applied static field is assumed to be uniform above the ferrite disks [7]. If the thickness of the magnet is not chosen properly, the assumption of uniform external field fails. In other words, an optimized magnet thickness and radius should be found for the most uniform static field (H_{ext}) distribution on the ferrites. Magnet thicknesses like 1mm., 2.54 mm and 4 mm are available in market, so these values can be compared to find the most optimized thickness. In magneto-static solver CST EM Studio, two ferrite disks are placed face to face and the static H_z is found in the gap between them (Figure 3.7).

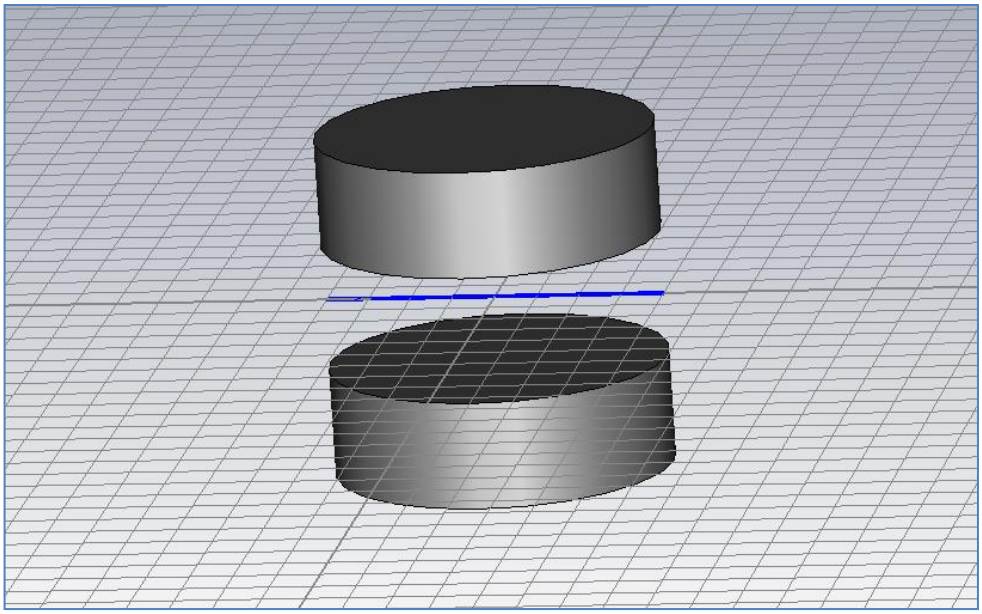

Figure 3.7 Two magnet disks and the curve on which the static field is calculated

The static H_z is found on the curve for different thickness of ferrite disks. In Figure 3.8 the field distribution (A/m) on the curve for the magnet thicknesses of 1mm., 2.54mm and 4 mm. can be observed. During the simulation, the gap thickness between two ferrite disks are fixed to a certain value which is equal to 2 ferrite thickness. Figure 3.8 shows that there is an optimum magnet thickness value at

which the field distribution is very close to uniform. For low thickness of the ferrite disk, the field distribution at the central parts is lower than the side field distribution, but as the thickness increases the field at the middle prevails against the field distribution at the side. By considering this fact, it can be said that there exist an intermediate value for thickness which makes the static field distribution as uniform as possible. A magnet thickness of 2.54 mm. clearly creates the most uniform static field among other thickness values.

An optimized thickness has been found with regard to the uniform field distribution requirement on the ferrite disk. Likewise, the optimum magnet radius can be found with the same approach. According to Helszajn [20], if the ratio of magnet radius to ferrite radius is 1.25, the most uniform field can be achieved which is shown in Figure 3.9. In the composite substrate case designed for *more than one octave* circulator, an outer ferrite radius of 3.4mm is determined which requires approximately a 4 mm magnet radius due to the ratio given. Finally, in the fabrication procedure, a magnet disk with a B_r 3800G, thickness 2.54mm. and radius 4mm. is used.

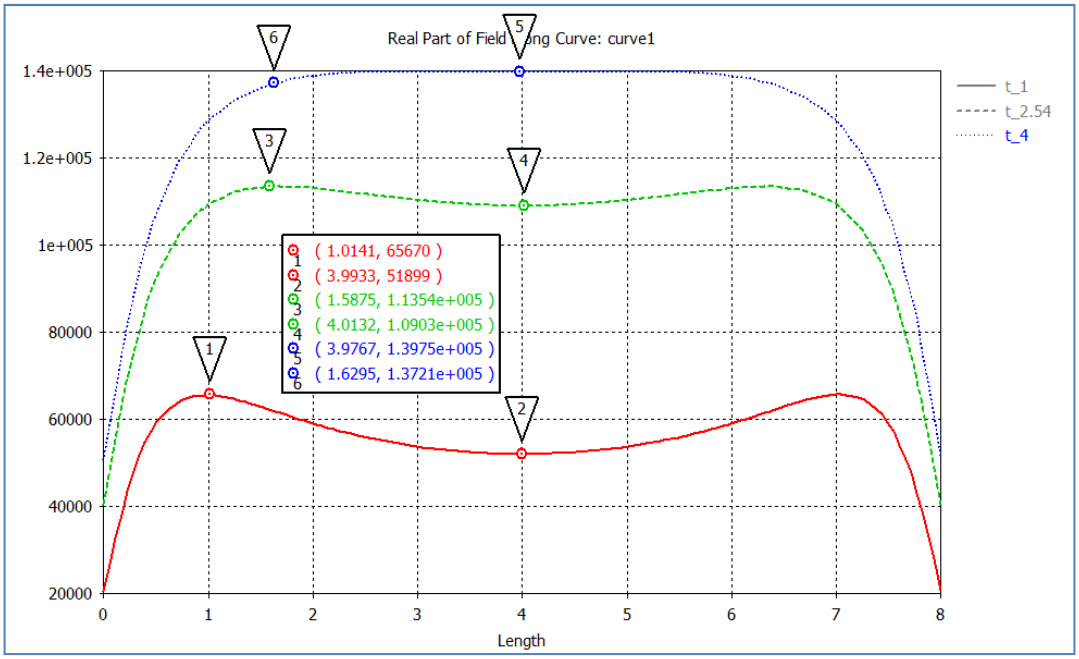

Figure 3.8 Static H_z distribution (A/m) versus position

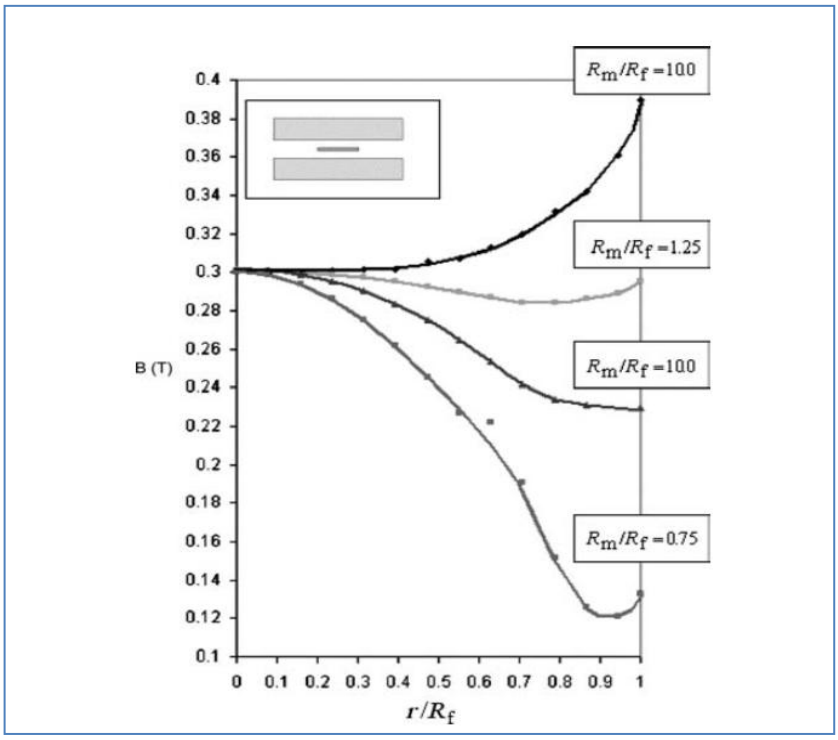

Figure 3.9 Field distribution for different R_m/R_f (R_m:magnet radius, R_f:ferrite radius)[20]

3.2.2 Definition of Yoke Structure in CST

To generate a closed loop path for static magnetic field, a yoke structure made of a magnetic material should be employed. Thus, the material can be chosen among one of magnetic materials like iron or steel. During the simulation process, the material of the yoke is defined as steel, because steel is more prone to fabrication process. In Figure 3.10, the overall simulated structure is displayed. However, the upper side of the yoke is not shown in order to display the interior parts of the structure clearly.

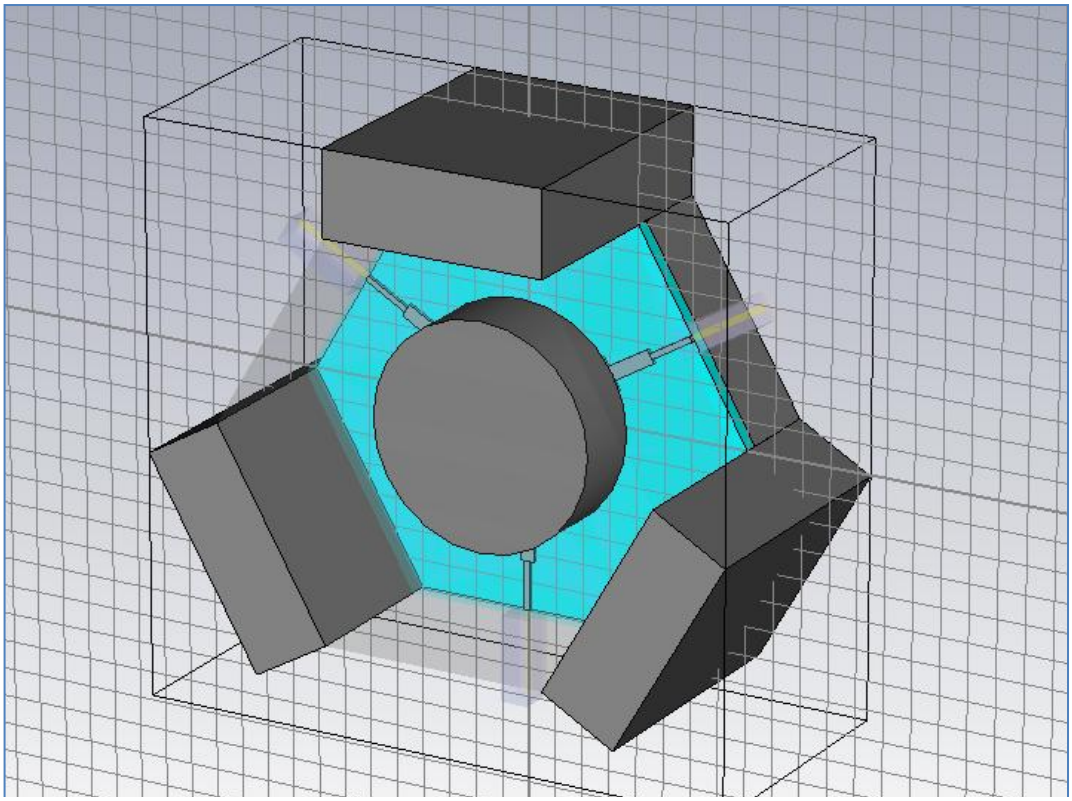

Figure 3.10 The overall circulator structure with the magnet and yoke

3.2.3 Simulation Results of Analytically Found One Octave Frequency Band Circulator

In the previous parts, analytical design procedure of a 9-18 GHz circulator is summarized. Adding to this, in Table 3.3 analytically found parameters are listed. In Figure 3.11, the simulation results of the analytically designed circulator are given. Between 9-18 GHz, isolation (S_{31}) curve is below the level of -14.5 dB which is a satisfying result. Likewise, return loss (S_{11}) values are below the level of -15 dB level for the most of the band. However, the insertion loss is worse than 2 dB at the edges of the frequency band which is not an acceptable performance. However, during this study, 1.4 dB is accepted as the maximum insertion loss value. The details of this choice are given at the beginning of Part 3.4.

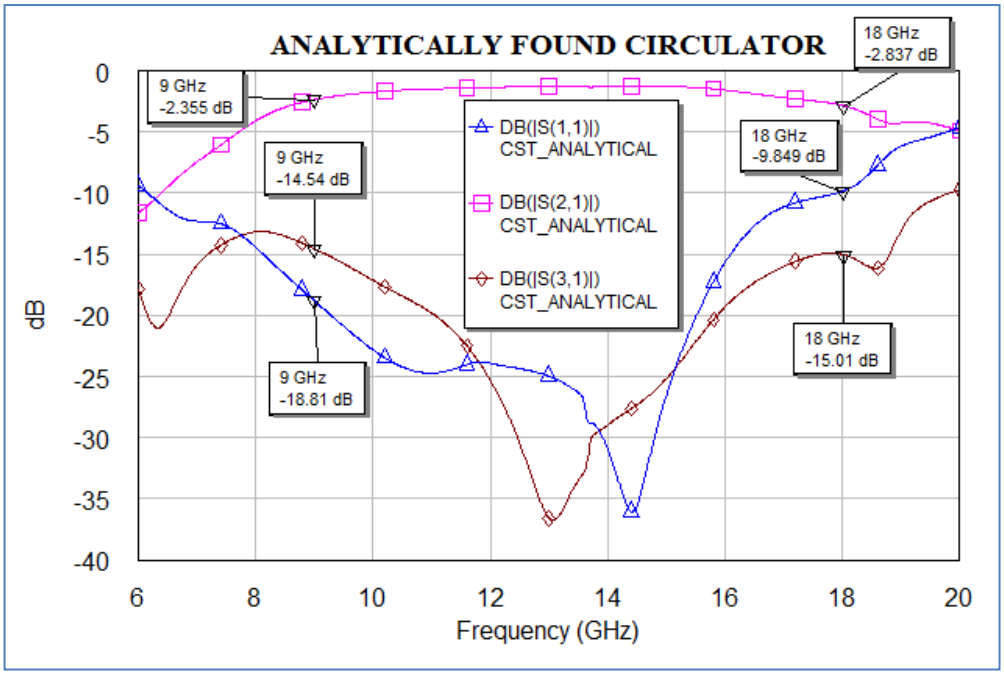

Figure 3.11 S-parameters of analytically found circulator

Simulation results show that the insertion loss of the analytically found circulator is relatively high , which can be resulted by dielectric, conductor and magnetic losses. In the simulation of the circulator, gold is assigned as the material of the conductor. Thus, conductor losses does not have a significant contribution to the insertion loss due to the high conductivity of gold. Likewise, dielectric losses can be said to have a very weak effect in the insertion loss, because ferrite materials and dielectric materials have very low dielectric loss tangent (tanδ) which can be observed in Appendix A or ferrite producer datasheets [13,24,25]. However, gyromagnetic losses, the principle of what has been explained in detail in Part 2.1.3.2, are the most dominant factors for the insertion loss of the circulator. Thus, *resonance linewidth* (**ΔH**), which defines the magnetic loss characteristic of the ferrite, is the parameter that should be assigned carefully to observe realistic simulation results.

At the beginning of the simulation process, we need to assign *resonance linewidth* (**ΔH)** of TT2-2750, which is the ferrite material chosen for the one-octave circulator design. (Part 3.1.1) However, the only data known about these materials were the ones given in product datasheets [13, 24, 25]. Thus, max **ΔH** value is assigned for the

simulated ferrite material. In Figure 3.11, it can be observed that the insertion loss (S_{21}) is between 1dB and 3 dB in the band. This insertion loss is the maximum loss that can be observed, because the maximum **ΔH** is assigned for the ferrite material.

When the desired materials are made produced, a Certificate of Analysis (CoA), which includes the exact measured properties of the ferrite and dielectric materials, has been supplied by TRANS-TECH. In Table 3.5, a comparison of measurement (by TRANS-TECH) and datasheet values of mentioned materials are given. Note that the produced material properties are much better than the worst case given in the datasheet in terms of dielectric losses and *resonance linewidth*s. For example, the *resonance linewidth* (**ΔH**) value for TT2-2750 in the datasheet was max 540 Oe; however, the measured **ΔH** given in CoA is 279 Oe, which is nearly half of the datasheet value. Because the *resonance linewidth* (**ΔH**) directly determines the magnetic losses, it is expected that relatively lower CoA values gives better insertion loss characteristics..

Table 3.4 Material properties in datasheet and CoA

	DIELECTRIC CONSTANT	DIELECTRIC LOSS TAN @9.4 GHz	SAT.MAG.(4PIMs)	RESONANCE LINE WIDTH @-3dB
TT2-2750(datasheet)	12,80	0.0025	2750 G	540 Oe
TT2-2750(Cert of Analysis)	12,69	0.0014	2758 G	279 Oe
SMAT-13(datasheet)	13	0.00015	N/A	N/A
SMAT-13(Cert of Analysis)	12,91	0.00007	N/A	N/A

In Figure 3.12, the insertion loss comparison of datasheet and measurement (CoA) values can be observed. Although the return loss and isolation of the two options do not differ much, it is possible to say that insertion loss highly depends on *resonance linewidth* (**ΔH**). Figure 3.12 displays that assigning CoA values for **ΔH** values improves the performance at least 0.5 dB throughout the frequency band. Adding to that, as CoA values are measured values, simulation results gained with CoA values are expected to be more realistic.

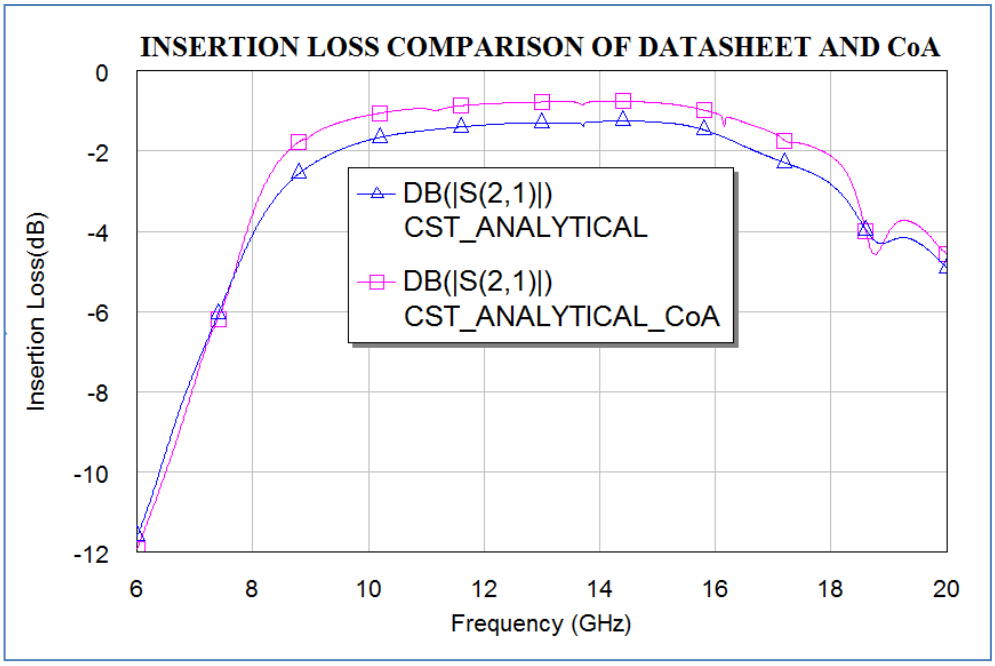

Figure 3.12 Insertion loss comparison of datasheet and CoA

3.2.4 Optimized Structures for 9-18 GHz Circulation

In the simulation process, it is observed that analytically found parameters give satisfying results. However, these parameters can be optimized to have better circulations. By using optimization process in CST, 3 different structures are optimized for the best performance. The fundamental difference between these structures is the radius of the ferrite disks. Thus, the goal here is to compensate the frequency band discrepancies between the measurement and simulation. In Table 3.5, the radius of the ferrite and the optimized dimensions of the impedance transformers are tabulated. Note that the same thickness and materials are used with the analytically found circulator given in Table 3.3

Table 3.5 3 optimized structures

	R(mm)	wint(mm)	w3(mm)	w2(mm)	w1(mm)	l3(mm)	l2(mm)	l1(mm)
STRUCTURE1	1,6	1,53	1,1	0,5	0,2	1,7	1,7	1,7
STRUCTURE2	1,8	1,73	1,25	0,5	0,2	1,5	1,7	1,7
STRUCTURE3	2	1,92	1,4	0,6	0,2	1,5	1,6	1,7

From *Structure 1* to *3*, the radius of the ferrite disk is varied. This parameter does not only change w_{int}, but also changes the width of the other impedance transformer sections (w_1, w_2, w_3). Moreover, appropriate length of matching sections are found with the help of CST optimization processes.

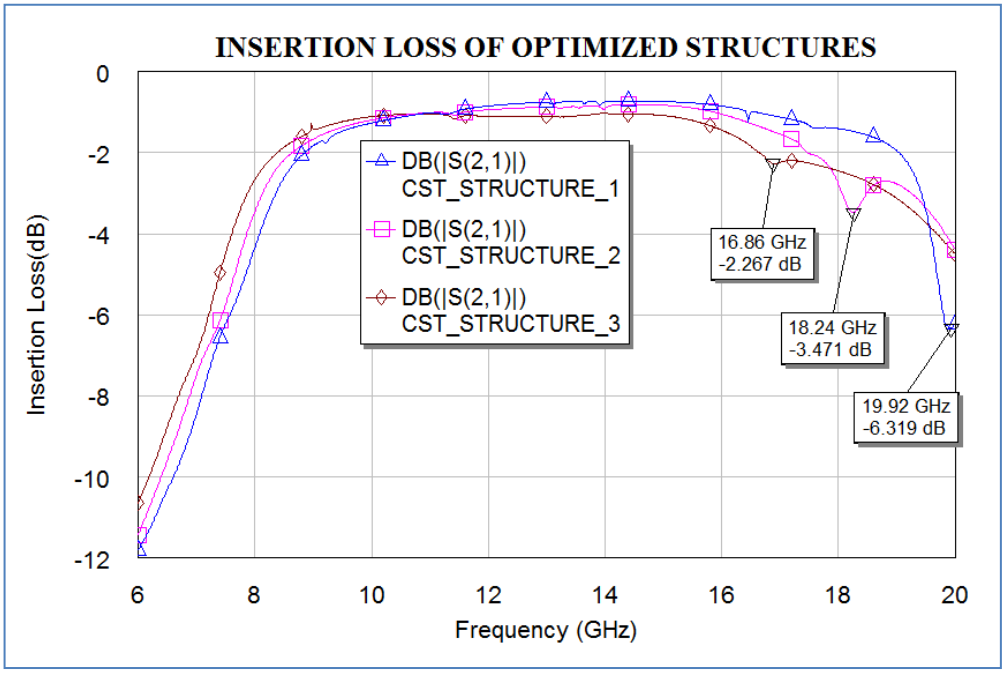

Figure 3.13 Insertion losses of the 3 optimized structures (CST)

Each of the three optimized structures have been simulated and their behavior is presented in the three figures given. If Figure 3.13 is analyzed, it is possible to say that the insertion loss performance in the low frequency band (8-10GHz) deteriorates as the radius of the ferrite decreases. Two reasons may be proposed for this phenomena. Firstly, as the ferrite disk radius increases, the internal static magnetic field density per area decreases which means an improvement in the performance especially in the low frequencies of the band, because a more ideal below-resonance operation is achieved. Secondly, as the ferrite radius decreases, the band of the frequency shifts to higher frequency values which is a very well-known resonance cavity property.

If the insertion loss of structures in the high frequency band (16-20GHz) is observed, it is clear that the notches, which are signed with markers have different locations. These notches are due to the second order modes excited in the ferrite resonators and their locations are determined by the bessel functions and radius of the ferrite disks. Figure 3.13 shows that all structures have 1-2 dB insertion loss throughout the band; however, *Structure 3* has 2.23 dB notch at 16.86 GHz, which can cause some trouble in "real life".

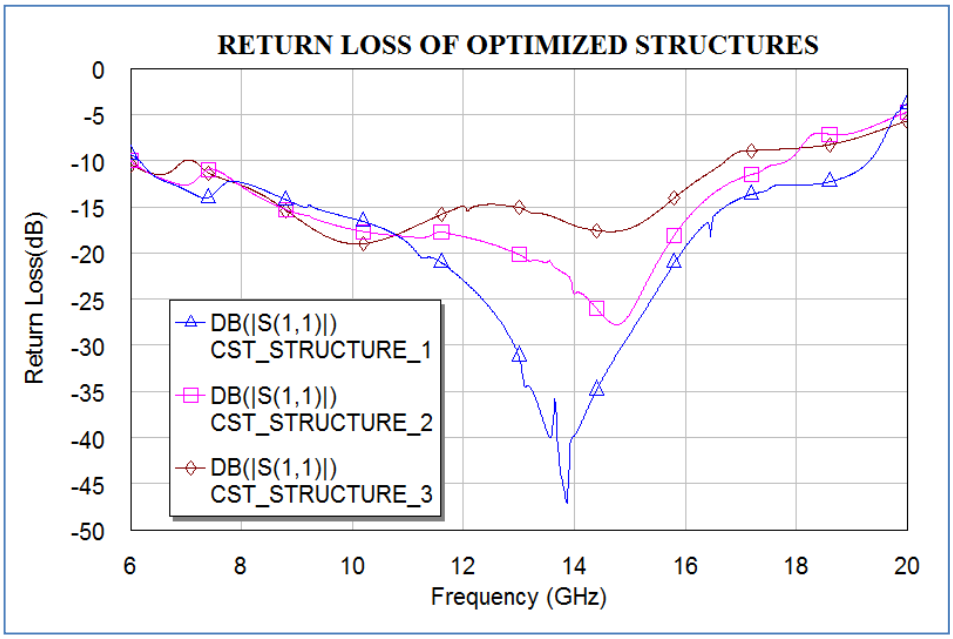

Figure 3.14 Return losses of the 3 optimized structures (CST)

Figure 3.14 displays the return loss performance of each optimized structure. Firstly, as a performance target, a return loss 10dB at the edges and 15dB at the middle of the frequency band is acceptable. Figure 3.14 shows that the best matching conditions are achieved in *Structure 1*. However, *Structure 2* and *Structure 3* have satisfying matching conditions.

Figure 3.15 shows the isolation performance of the optimized structures. The same performance target with the return loss is still applicable. It is clear that each of the structures satisfy the 10dB isolation values throughout the band. However, *Structure 1* and *Structure 2* have better isolation performance in the middle of the band than *Structure 3.*

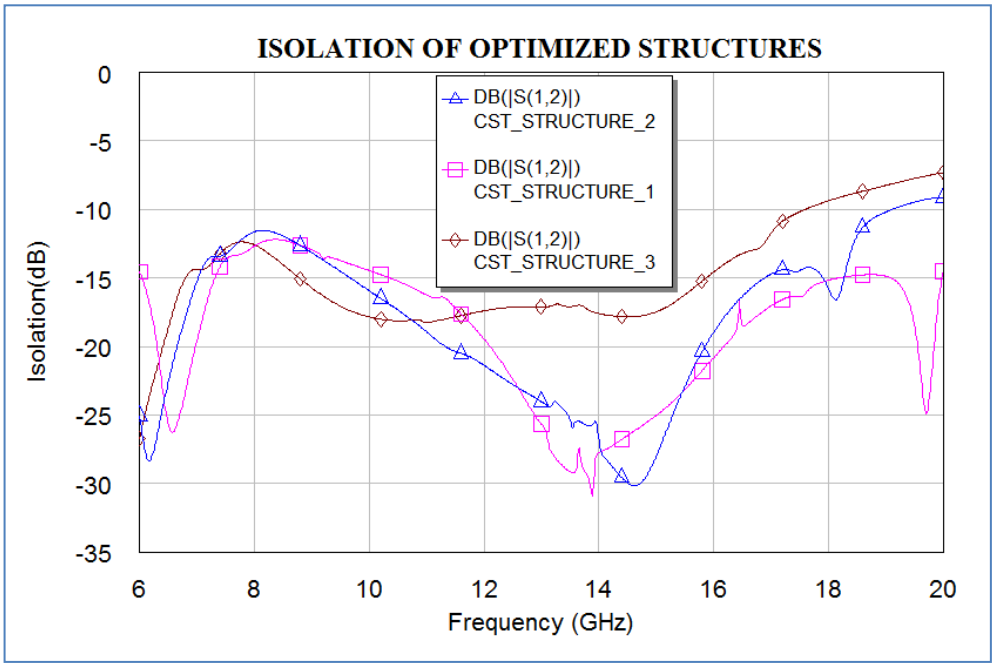

Figure 3.15 Isolation of the 3 optimized structures (CST)

In this part, simulation results of the three optimized structures have been provided. On top of this, it is observed that each optimized structure has satisfying performances. Now, these structures can be realized to observe their "real life" performances.

3.3 Realization of One Octave Circulator

In Part 3.2.4, three structures have been optimized by using CST. In this part, the aim is to summarize the fabrication process of these structures. Firstly, the ferrite substrates are explained in detail. Then, some properties of the conductor y-junction is given. Finally, the permanent magnet choice and mechanical structure design process are clarified.

3.3.1 Ferrite Substrates

In Part 3.1.1 , TT2-2750 and SMAT-13 have been chosen as the appropriate ferrite and dielectric materials for the 9-18 GHz *one octave* circulator. In addition to this, three different structures have already been determined for 9-18 GHz circulation the details of which are given in Table 3.5.

Before the ferrite substrate production, we had contacted with three 3 well-known ceramic manufacturers, AFT, TRANS-TECH and TCI. However, TRANS-TECH is preferred, because their materials are frequently mentioned in academic studies.

The shape of the substrate is another question mark. Although the shape of the ferrite substrate can be chosen as hexagonal or circular, hexagonal shape is preferred, because it makes the transition between stripline and microstrip line easier. In Figure 3.16, the ferrite substrate made produced to TRANS-TECH is displayed. One side of some hexagonal substrates are metalized to observe the effect of metallization. However, it is observed that using unmetalized substrates and using indium sheets instead offers much better circulation.

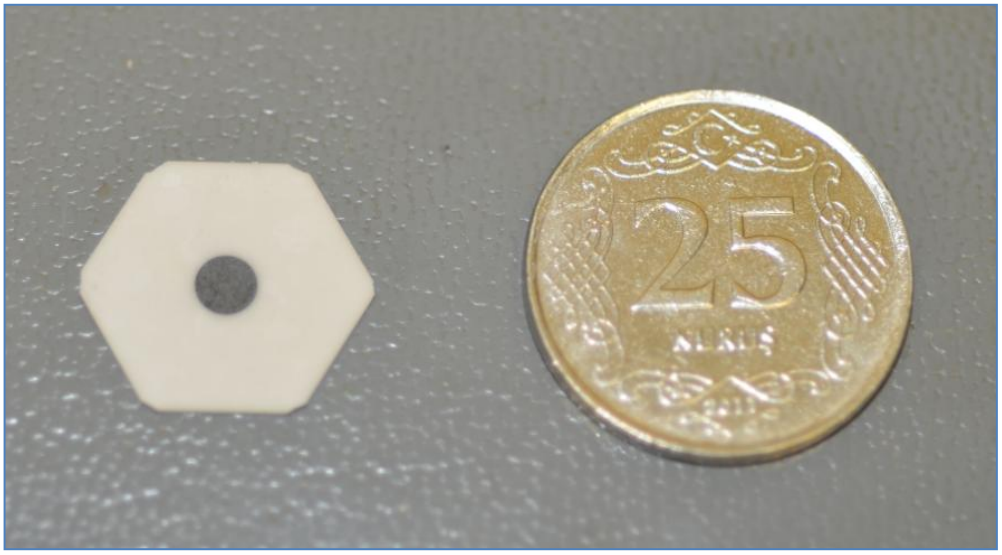

Figure 3.16 Photograph of single ferrite substrate

3.3.2 Conductor Y-junction

In Table 3.5, the overall dimensions of the optimized structures are provided. Figure 3.5 can be seen to understand what these dimensions contribute to. Although the dimensions are determined, the choice of conductor material is still important due to many considerations. Firstly, the conductor material should have a high conductivity to lower conductor losses. Secondly, conductor should be in the sheet form down to small thicknesses to lower the air gap thickness between the ferrite disks . Finally, it should have a mechanical strength to protect its shape. Thus, silver or gold plated conductors can be chosen to satisfy these requirements. However, they are expensive and available with thick sheet dimensions. After comparing many materials, we observed that CuBe2 (Copper Berilium) seems to be a good choice, because it has a good conductivity due to the copper element. In addition to that, berilium element in the compound increases the durability of the material. Moreover, low thicknesses around 0.13mm. are available for this material ,and it is prone to shaping by a laser cutter. Because of the explained advantages, BeCu2 is chosen as the material of the y-junction conductor. In Figure 3.17, a shaped y-junction can be observed.

Figure 3.17 Berilium Copper (CuBe2) Y-junction

3.3.3 Permanent Magnet

In Part 3.2.1, it is explained that a permanent magnet with a B_r value of 3000-4000 G is sufficient for below resonance operation. However, in circulator applications, different permanent magnet types can be required according to the operation region chosen. In Appendix B, different magnet grades with short explanations can be found. Generally speaking, magnets are classified as ceramic, alnico, rare-earth magnets. In Table 3.6, some important characteristics of different magnet grades are given [26].

Table 3.6 Some magnet types and their characteristics [26,38]

Material	Residual Flux Density Br(G)	Coercive Force Hc(Oe)	Max energy Product (MGOe)
Ceramic 1	2300	1860	1,05
Ceramic 5	3800	2400	3,4
Ceramic 8	3850	2950	3,5
Alnico 5	10900	620	3,9
Alnico 8	8200	1650	5,3
Samarium Cobalt 20	9000	8000	20
Samarium Cobalt 28	10500	9500	28
Neodymium N45	13500	10800	45
Neodymium 33UH	11500	10700	33

In Table 3.6, Ceramic1, Ceramic5 and Ceramic8 are hard ferrite magnets. They are made of composite of iron oxide and barium carbonate ($BaCO_3$) or strontium carbonate ($SrCO_3$). They are brittle and hard which makes their shaping very difficult. Thus, diamond wheels are required to grind and shape them. Ceramic 1 is an isotropic material unlike Ceramic 5 and Ceramic 8. The anisotropic magnet grades are achieved by applying magnetic field during the production process. While their advantages are low cost, high coercive force, resistance to corrosion, their disadvantage is low magnetic strength. For the applications where weak magnet strengths are desired, they are very advantageous in terms of their low cost [26].

After analyzing different magnet types, it can be said that ceramic magnets are appropriate for our operation. Firstly, their *residual flux density (B_r)* is in the desired range. Secondly, they are cheap and there are many C5 magnet disk dimensions

available in the market. Due to the stated facts, Ceramic 5 magnets seem to be the best option for using in the circulator.

Ceramic material has already been determined as proper in terms of residual flux density, but the thickness and the radius of the permanent magnet should also be optimized for uniform static field requirement. The thickness of the magnet is important in terms of the strength of the magnetic field. In order to tune the thickness of the magnet, the yoke structure is designed to be compatible with different thicknesses of permanent magnets. By using magneto-static solvers, it is possible to observe the effect of the thickness. As the thickness is increased, the permanent magnet strength increases, but at the same time the uniformity of the field distorts. In Part 3.2.1, it is concluded that a magnet disk with a radius of 4mm. and a thickness of 2.54 mm. offers the best performance in terms of uniform external static magnetic field distribution. In Figure 3.18, C5 disk magnets used in circulator structures can be observed.

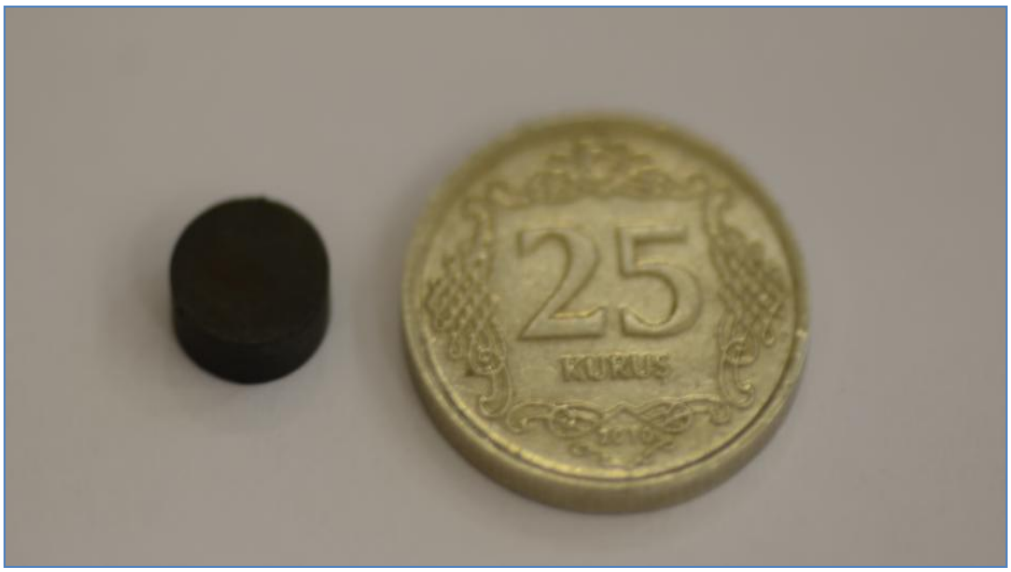

Figure 3.18 C5 disk magnets

3.3.4 Mechanical Structure

The design of mechanical structure is critical for circulator performance in terms of two main reasons. Firstly, the structure should create a closed loop path for static magnetic field generated by permanent magnet. Thus, the material of the yoke should have magnetic properties like iron or steel. As steel is more prone to production process, it is preferred as the material for the structure. Secondly, mechanical structure needs to hold substrates, y-junctions and permanent magnets together which is important especially for ground connection issues..

In microwave modules, microstrip connections are widely used because they are cheaper and an easier for assembly issues. However, our design is a stripline circulator. Thus, we need to observe and compensate the distorting effects of the microstrip to stripline transitions. In order to do that, microstrip lines are added to the mechanical structure, can be observed in Figure 3.19 .

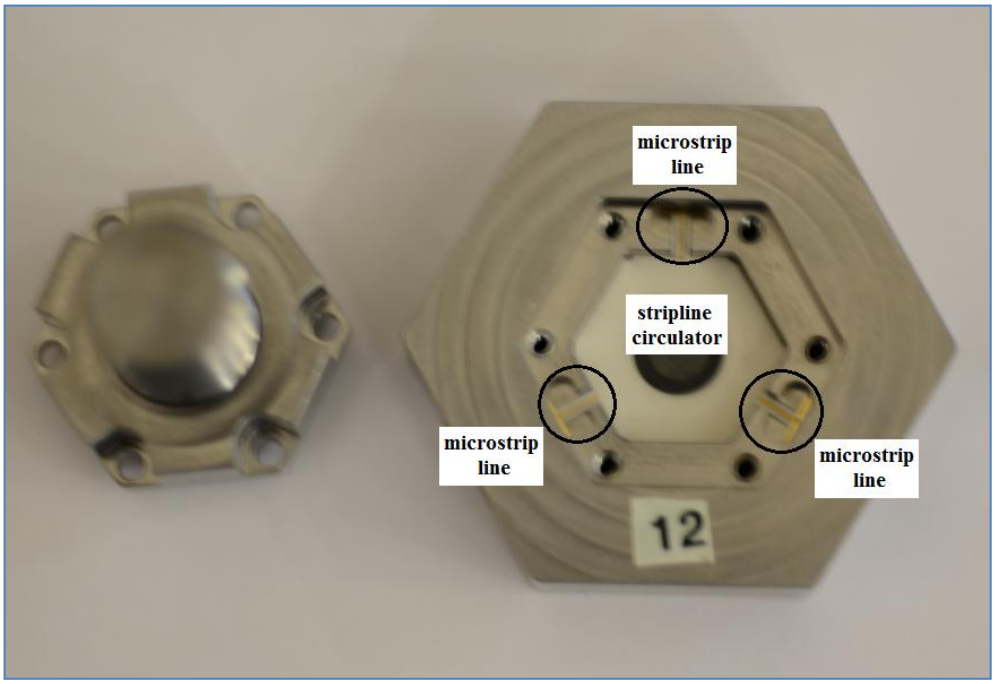

Figure 3.19 An open view of the circulator

In Figure 3.20, the overall circulator structure ready to measurement can be observed. As can be seen, SMA connectors are mechanically appended to the structure.

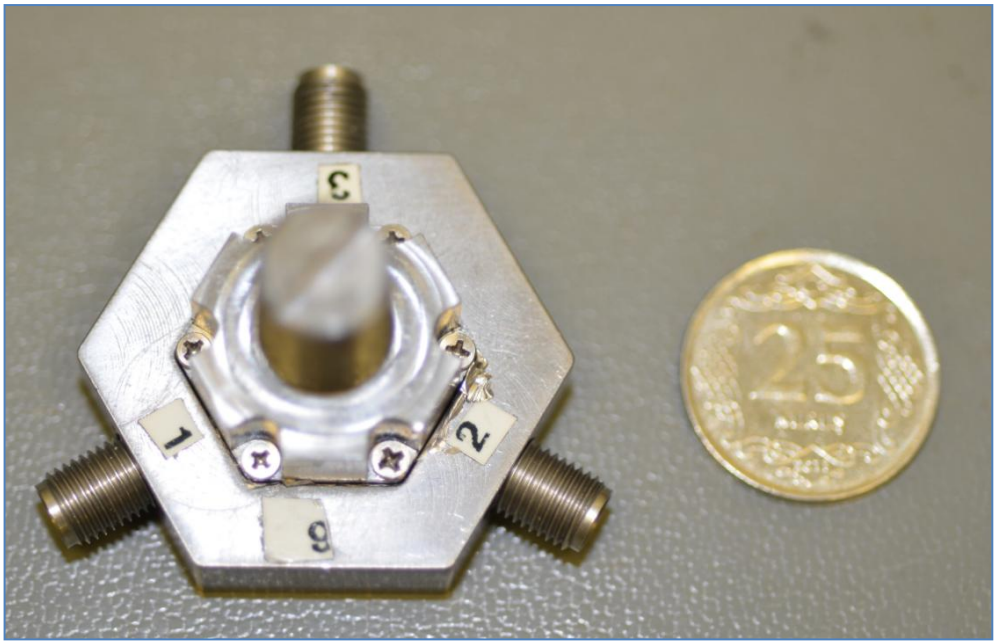

Figure 3.20 Photograph of the measured circulator structure

3.4 Measurement Results of One Octave Frequency Band Circulators

In this part, the measurement results of the three optimized structures are given. The properties of these structures can be found in Table 3.5. Another aim of this study is to determine whether the simulation tools are reliable in ferrite material modeling. So, the measurement results are given together with the corresponding simulation results.

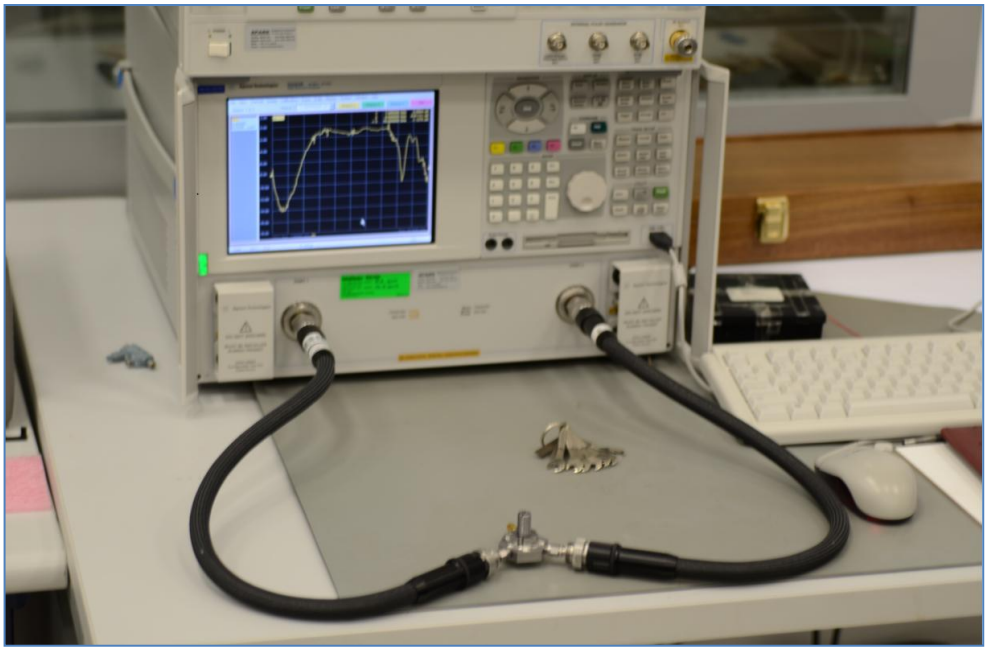

Figure 3.21 Agilent E8364B network analyzer is used for measurement

In the measurement results given in the following parts, the results gained directly from connectors of circulator are provided. This means that measurements display the harming effects of microstrip to stripline transitions. In Figure 3.19, it is shown that microstrip lines are included to the structure to see the effect of microstrip to stripline transitions. However, this microstrip lines and transitions result additive losses for the structure. Thus, in order to understand the performance of pure stripline circulator, the distorting effect of the transmission lines and connectors should be removed from the measurement results. For this aim, two connectors and a microstrip transmission line with the same dimensions used in circulator are prepared on a carrier which is shown in Figure 3.22. When the structure is measured, it is observed that the insertion loss of the structure is around 0.3-0.4 dB through 6-11GHz band. For frequency values larger than 12 GHz, insertion loss of the lines and connectors starts to deteriorate. This measurement shows that additive microstrip lines result at least an additive 0.3-0.4 dB insertion loss to the performance of the circulator. So, 1.4dB insertion level can be said to be acceptable in the circulation band.

Figure 3.22 Photograph of measured transmission lines and connectors

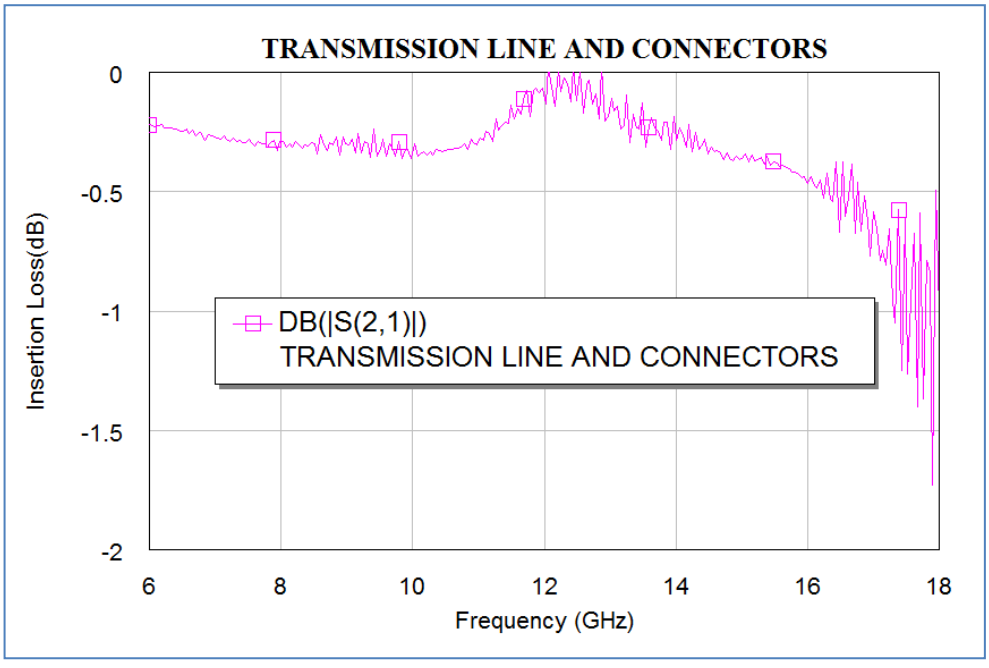

Figure 3.23 Measured insertion loss of microstrip lines and connectors

3.4.1 Measurement Results of *Structure* 1

In the following 3 figures, comparison of the measurement and simulation results of *Structure 1*are given. In Table 3.5, the parameters of S*tructure 1* can be found.

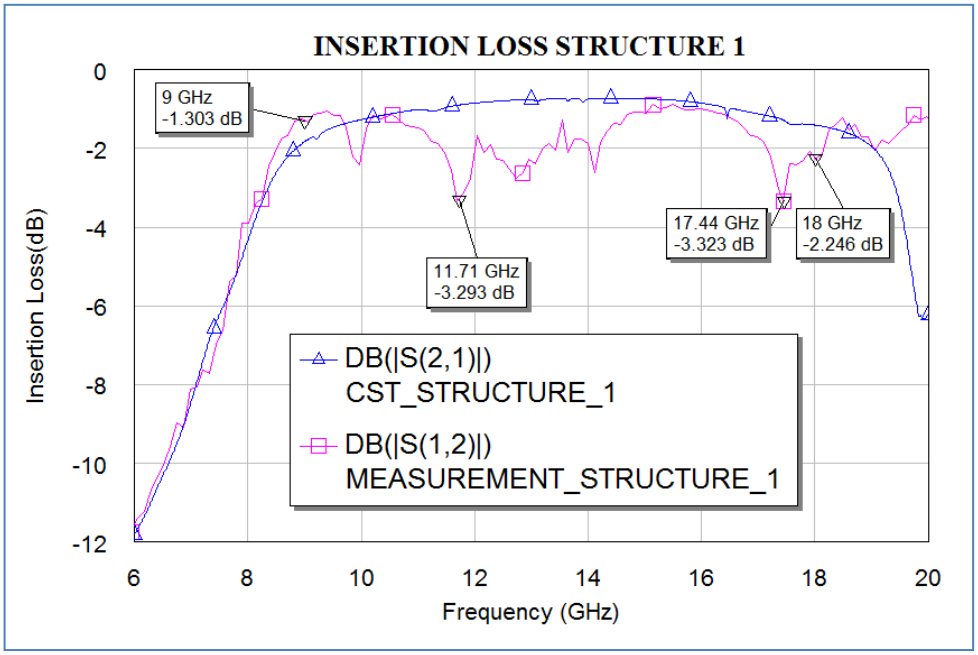

Figure 3.24 Insertion loss of *Structure* 1

In Figure 3.24, measurement and simulation results of insertion loss are shown. General characteristics of the measurement and simulation are similar. However, some notches do exist at 11.71GHz and 17.44 GHz in the measurement. We observed that the places of notches changed with changing position of upper yoke structure. At the same time, it is well-known that the performance of circulator structures highly depends on the upper and lower ground connections. In stripline circulator case, the lower ground connection is made through the lower yoke structure connected the ground of the SMA connectors. However, upper yoke ground connection is made through a longer way which can result a distortion in upper ground connection. The ground connection problem can be solved by using indium layers both between mechanical structures and the ferrite substrates, another way to solve this problem can be to design a different mechanic to avoid screw usage as much as possible. So in the next iteration, a new mechanic without screws is planned

to make produced. The results of *Structure 1* are included in the thesis to show how ground connection is crucial for the circulator operation.

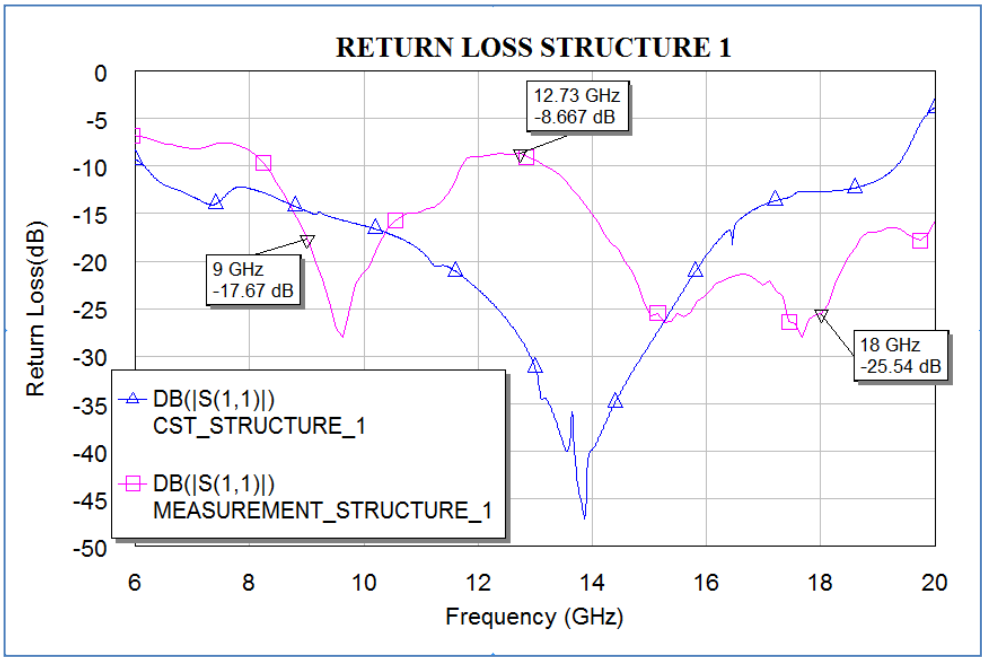

Figure 3.25 Return loss of *Structure* 1

In Figure 3.25, the return loss of the measured structure is worse than 10dB level which is not acceptable for circulator operation. However, these matching conditions can be improved if the ground connection problems are solved.

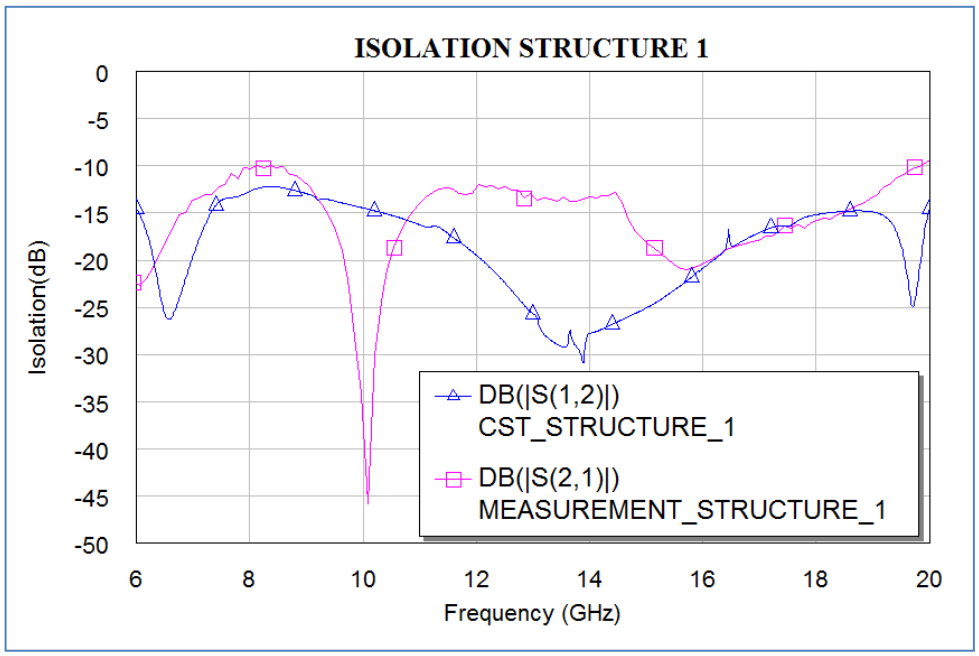

Figure 3.26 Isolation of *Structure* 1

In Figure 3.26, isolation characteristics of *Structure 1* can be observed. If the measurement is analyzed, it can be said isolation is better than 10dB in the desired frequency band .However, the discrepancies between measurement and simulation is resulted by the problematic ground connection of the upper side.

3.4.2 Measurement Results of *Structure 2*

In Figure 3.27, the insertion loss characteristic of *Structure 2* is shown. The notches up to -3dB values are not observed as they are in *Structure 1* which shows that ground connection problem is partly solved in *Structure 2*. If the insertion loss of the measurement and simulation results are compared, it can be said that simulation gives relatively close results to the real performance of the circulator; however, still some discrepancies exist. Firstly, low frequency (6-10 GHz) characteristics of the simulation and measurement are very similar, but the simulation anticipates a 1 GHz shifted-to-the-right insertion loss characteristics. This discrepancy is thought to be resulted by the higher static magnetic field distribution in simulation. If the static magnetic field value increases in the ferrite, the low frequency performance of the structure distorts which is due to the below resonance operation. The details about below resonance operation can be found in Part 2.1.3.2 .

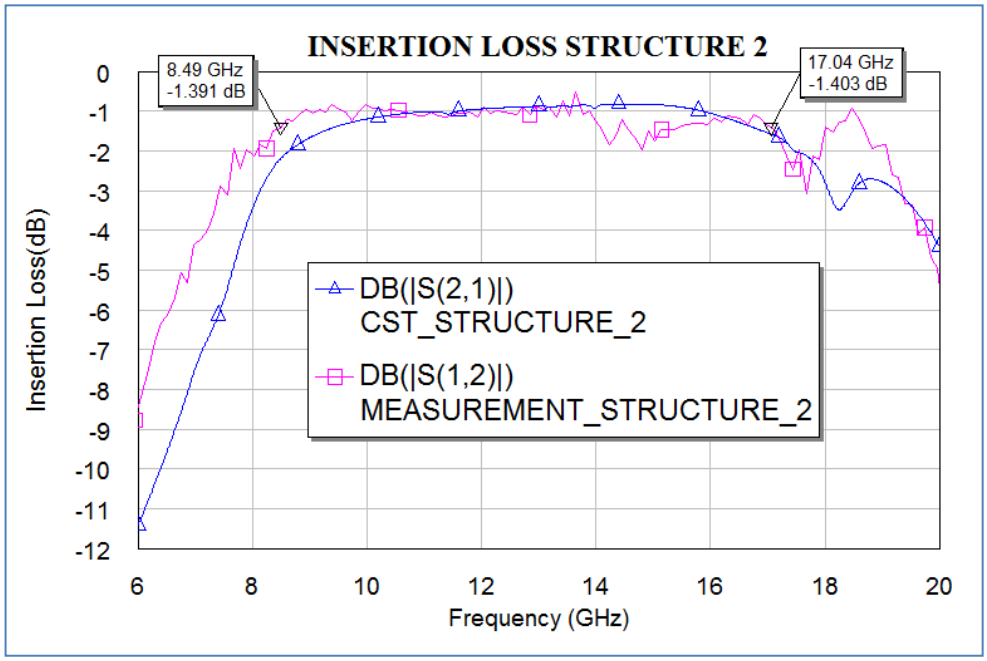

Figure 3.27 Insertion loss of *Structure* 2

In the previous paragraph, it is clarified that shifted-to-the-right insertion loss characteristics is resulted by the relatively higher internal static field (H_i) assumption in simulation than reality. During the simulation, a permanent magnet with 3800 G Br value is assigned and a closed magnetic field path is structured with the help of mechanical structure; however, in real life although there is a closed loop path for static magnetic field, there are indium layers and air gaps which distorts the closed-loop static magnetic field path. For example, the air gaps between upper and lower parts of the mechanical structure and the indium layers result distortions for the closed magnetic field path. These distortions result lower static magnetic field distribution in the ferrite material which results a better operation in lower frequencies in real life. Ironically, the distortions in the magnetic field path result a better performance for lower frequencies which is resulted by the nature of below resonance operation.

If the larger frequency values are examined in the insertion loss, it can be said that insertion loss is around 1.2 dB in the band of 9-18 GHz, this value seems to be relatively high for a circulator operation, but it should be considered that the measurement results also include the transition between microstrip and stripline transmission lines, which are explained at the beginning of Part 3.4. If the effect of the connectors and transmission lines are considered, it can be said that 1 dB insertion loss requirement is satisfied through 8.5-17 GHz band which is one octave but a little bit shifted-to-the-left in terms of 9-18 GHz desired circulator. But that is not a problem, because the optimized structures are designed with different radius values to eliminate this kind of "band shift" problems.

If the return loss and isolation characteristics of *Structure 2* are observed in Figure 3.28 and 3.29 respectively, it is clear that both values are better than 10 dB which is an acceptable level. As the ground connection is improved in *Structure 2*, return loss and isolation do not lower below 10dB level as they do in *Structure 1*.

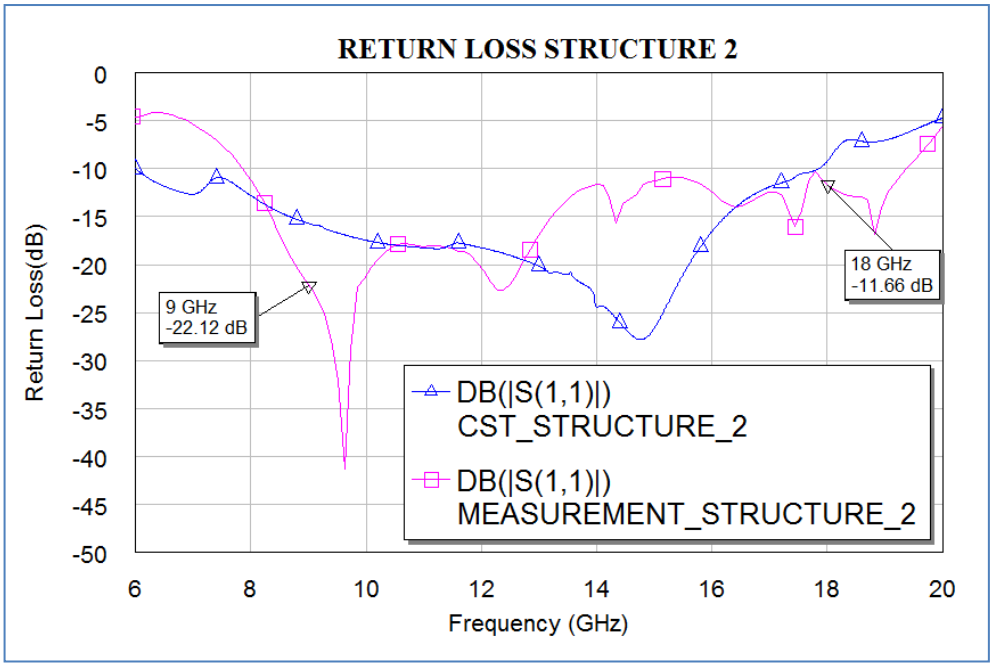

Figure 3.28 Return loss of *Structure* 2

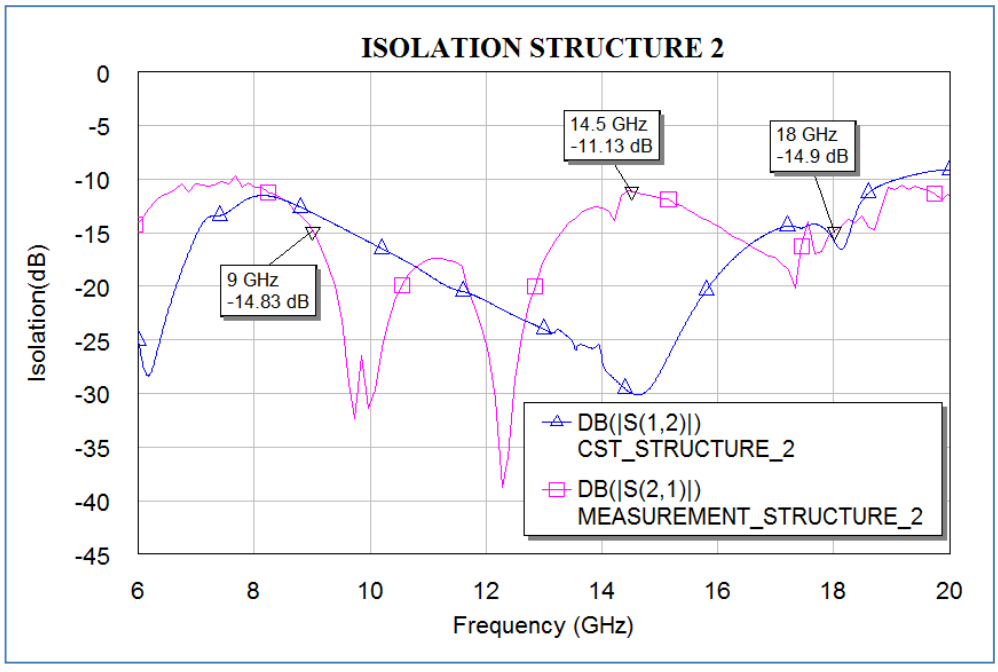

Figure 3.29 Isolation of *Structure* 2

3.4.3 Measurement Results of *Structure 3*

If the insertion loss characteristic of *Structure 3* is observed in Figure 3.30, it is clear that the results are better in terms of many considerations than *Structure 1* and *Structure 2*. Firstly, notches observed in *Structure 1* and *Structure 2* are not observed in Structure 3 which means that ground connections are established successfully. Secondly, the insertion loss characteristic is very similar to the simulation results. However, still the simulation gives nearly 1 GHz shifted-to-the- right due to the reasons explained in part 3.4.2. Thirdly, a *one octave* band circulator operation is achieved between 8.74GHz and 18.25GHz which shows that our design requirement of 9-18 GHz *one octave* circulator operation is achieved.

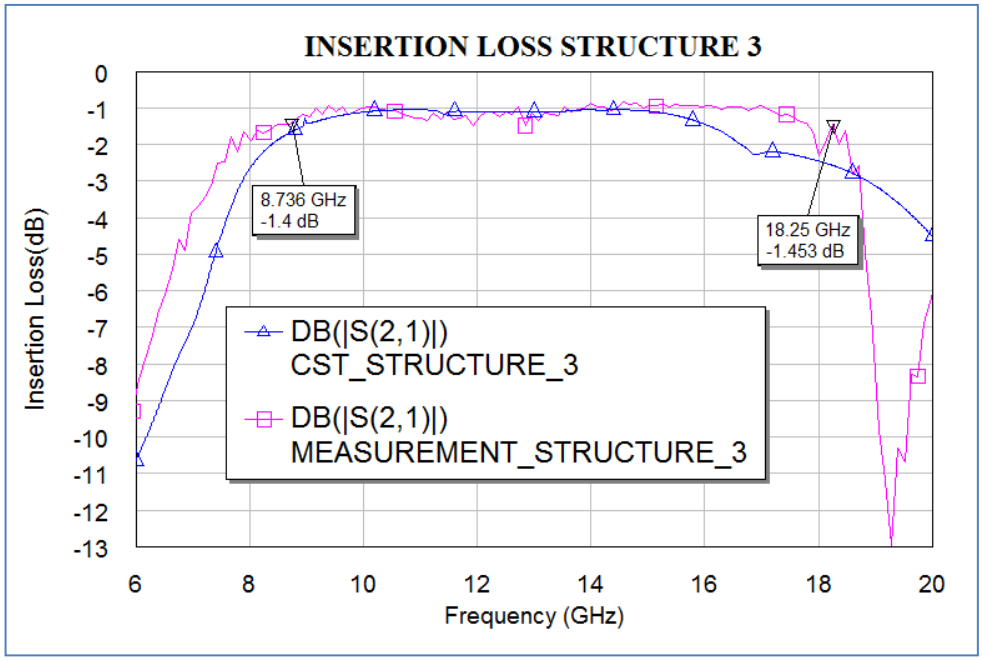

Figure 3.30 Insertion loss of *Structure 3*

In Figure 3.31, the measurement of return loss shows that for the frequency band of 9-14 GHz, return loss is in the band of 13-15 dB, between 14-18GHz return loss values improves and exceeds the 15 dB level. Adding to that, the similarity between measurement and simulation shows that simulation tools provide reliable data in the design of wideband circulators.

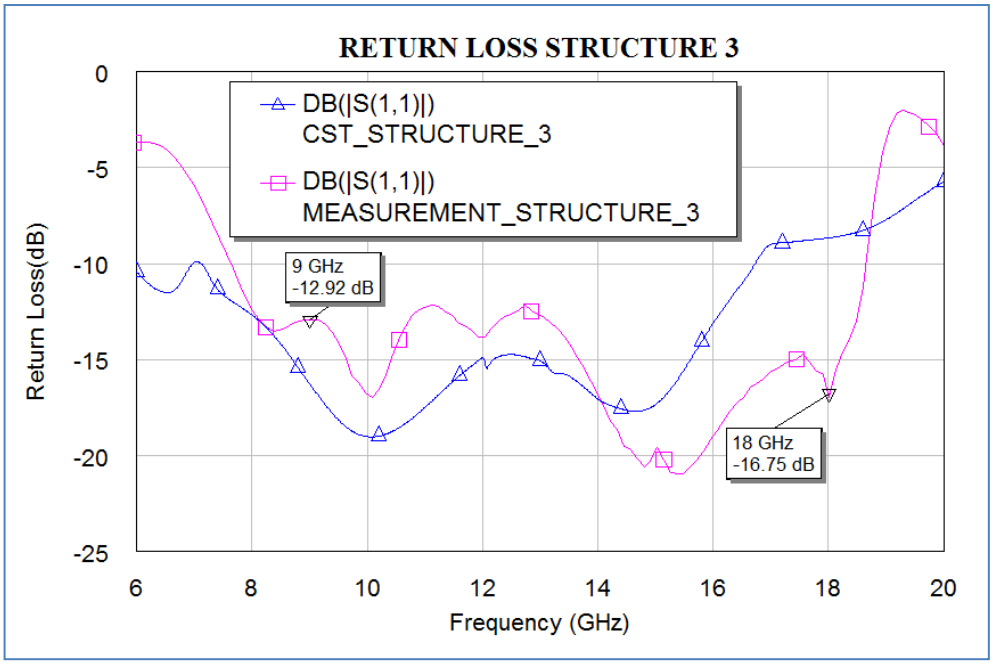

Figure 3.31 Return loss of *Structure 3*

In Figure 3.32, the isolation characteristics of *Structure 3* is observed. In the 9-12GHz frequency band, isolation is around 13-15 dB band. However, between 14-18GHz isolation improves and goes below -20dB level.

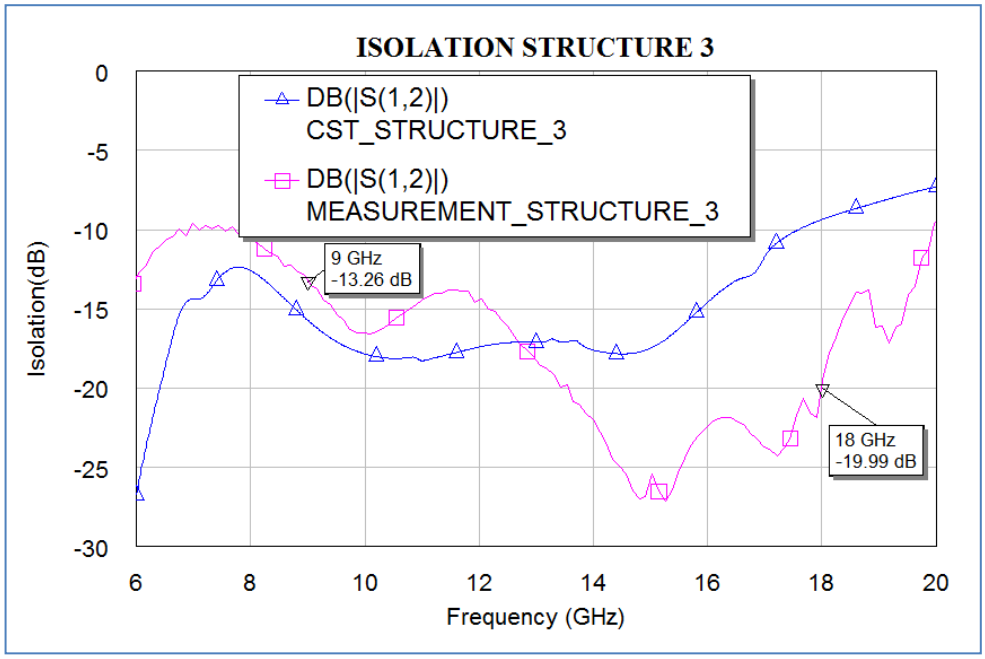

Figure 3.32 Isolation of *Structure 3*

3.4.4 General Review of Measurement Results

In part 3.4, the measurement results of three optimized structures have been given and a comparison of measurement and simulation results has been provided. If the overall results are analyzed, it can be said that *Structure 1* has a weak insertion loss performance due to ground connection problems. The results of the *Structure 1* is given in the thesis on purpose so as to show how ground connections are important for the performance of the circulation. In Figure 3.24,3.25 and 3.26, it is clear that ground connection problems do not only distort the insertion loss, but also result a decrease in the isolation and return loss performances.

In Figure 3.27, 3.28 and 3.29, the measurement results and their comparison with simulation results of *Structure 2* have been provided. As generally the ground connection problems are partly solved in this structure which results an improvement with regard to *Structure 1*. However, insertion loss performance deteriorates between 14-16 GHz, which is a negative behavior for 9-18 GHz circulator operation.

Figure 3.30, 3.31 and 3.32 show that the overall performance of *Structure 3* is very satisfying for the 9-18 GHz circulator operation. Firstly, the insertion loss value is better than nominally 1dB, which is well enough, because this value also includes the deteriorating effects of microstrip to stripline transitions. Secondly, return loss is better than -12.92dB for the overall band. Finally, isolation is below -13.26dB for the low frequency values and it improves and goes below -20dB level for the higher frequencies in the band. These results show that one octave circulation is achieved through the band of 8.75 GHz and 18.25 GHz.

If the three optimized structures are compared, *Structure 3* is superior in terms of insertion loss, return loss and isolation performances for 9-18 GHz circulator operation. This structure also proves that *continuous tracking technique* proposed by Wu and Rosenbaum is a reliable method to design *one octave* circulators [4]. Adding to that the measurement results show that the simulation tools provide a trustworthy and precise predictions for the circulator performance.

CHAPTER 4

THE DESIGN, SIMULATION, REALIZATION AND MEASUREMENT OF MORE THAN ONE OCTAVE FREQUENCY BAND STRIPLINE CIRCULATOR

In Chapter 3, the design, simulation, realization and measurement of a 9-18 GHz *one octave* circulator have been explained in detail. In this chapter, the main target is to widen the frequency band of *one octave* circulator to a larger value. In fact, the design of the *one octave* circulator is an intermediate step for the design of the *more than one octave* frequency band circulators [7,8,14]. In this chapter, the design and realization of *more than one octave* circulators do not need to be explained in detail, because these processes are very similar to the ones of *one octave* circulator design. However, in Chapter 4, the main focus is on widening the frequency band. Thus, firstly, the phenomena called *demagnetization affect* that limits the frequency band of the circulator is discussed. Then, some methods to widen the frequency band are proposed, one of which is used to realize the *more than one octave* circulator. Finally, the produced more than one octave circulator is measured and measurement results are provided to decide whether the method is efficient and simulation results are reliable.

4.1 Theoretical Basis of More Than One Octave Frequency Band Stripline Circulator

In the Chapter 2, during the explanation of *continuous tracking technique*, it is claimed that a maximum one octave circulation is possible for stripline circulators[3,4]. However, according to Schloemann and Blight, the previous theoretical work is misleading, because it totally rejects the possibility of using the frequency values below f_m or $\mu_{eff}<0$ [7]. But, it is possible to operate circulators

for frequency values lower than f_m, if some precautions are taken for the non-uniform field distribution in the ferrites.

According to (2.38), effective permeability (μ_{eff}) is related to permeability tensor elements μ and κ .

$$\mu_{eff} = (\mu^2 - \kappa^2)/\mu$$

If $f < f_m$, then

$$\mu_{eff} < 0$$

The former researchers, Bosma, Wu and Rosenbaum assume that frequency values resulting negative μ_{eff} values are very lossy due to the low field losses. Schloemann and Blight state that it is possible to operate circulators below f_m or for negative μ_{eff} values, if and only if the low field losses are avoided [7]. Schloemann and Blight claim that low field losses are resulted by the non-uniform static magnetic field distribution in the ferrite disks. Although the ferrite disks are placed in a magnet structure that creates uniform static field distribution (H_{ext}), the static field inside the ferrite disks (H_i) is not uniform which is due to the non-uniform demagnetizing factors of the ferrite disks. Generally speaking, the demagnetizing fields are due to the magnetic poles at the ferrite disk surfaces and their direction is opposite to the applied static fields.

4.1.1 Demagnetization Effect

The internal (H_i) and external (H_{ext}) static magnetic field distribution of ferrimagnetic materials are related to each other with a well-known phenomena called *demagnetization effect (*Figure 4.1) [32,33,34]. If a ferrimagnetic material is

placed in a z-directed uniform static magnetic field (H_{ext}), the internal static magnetic field distribution (H_i) is determined by demagnetization factor N_z and *saturation magnetization* of the ferrite material ($4\,\pi\,M_s$) with a well-known equation given in (4.1). During the development of equation, H_{ext} is assumed to be z-directed which enables to use only z directed demagnetization factors, N_z. However, same approach can be applied by defining N_x and N_y for uniform x and y directed external fields, respectively. The relation for z-directed H_{ext} and z directed H_i is given in (4.1).

$$H_i = H_{ext} - N_z\,(x,y)\,4\,\pi\,M_s \qquad \textbf{(4.1)}$$

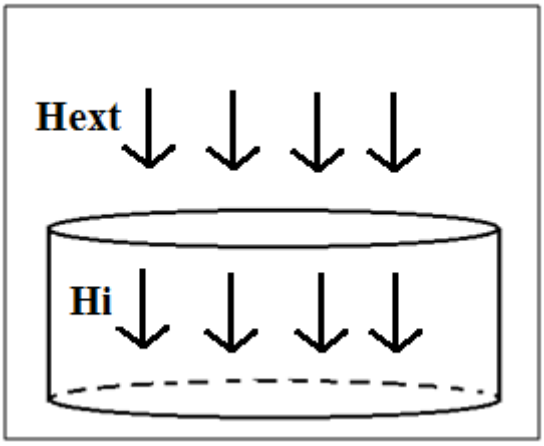

Figure 4.1 The internal and external static field distribution

In (4.1), it is assumed that H_{ext} is applied through z-direction which results a z-directed internal static magnetic field, H_i. Although *demagnetization factor* (N_z (x,y)) is given as a position dependent variable. For some specific material shapes, it is a constant that does not depend on position. For example, ellipsoidal bodies have constant *demagnetization factors* $N_{x,y,z}$ which results uniform H_i distribution throughout the body. In Figure 4.2, some shapes that have uniform demagnetization factors can be observed [19].

Shape	N_x	N_y	N_z
Thin disk or plate 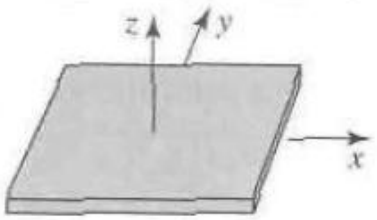	0	0	1
Thin rod 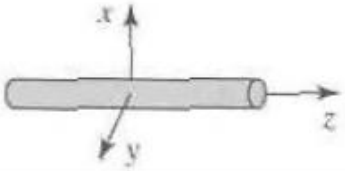	$\frac{1}{2}$	$\frac{1}{2}$	0
Sphere 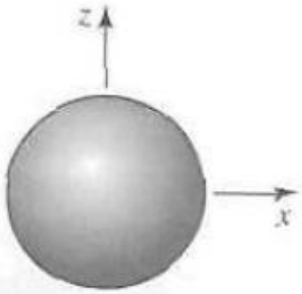	$\frac{1}{3}$	$\frac{1}{3}$	$\frac{1}{3}$

Figure 4.2 Some simple shapes that have constant demagnetization factor [19]

However, for non-ellipsoidal bodies like disks, cylinders or cubes, the demagnetization factor N_z(x,y) becomes dependent to the position which results non-uniform internal field distribution (H_i) throughout the structure [31,35].

In stripline circulator structures, ferrite disks are employed, so demagnetization factors of the ferrite disks N_z (x,y) are position dependent, which contributes to non-uniform H_i distribution. However, their values are also determined by another term called aspect ratio, which is the height-to-diameter ratio of the ferrite disk. It is possible to determine the demagnetization factor of a ferrite disk with a known aspect ratio by looking at the tables given in the literature[27,29,35]. For example, for a ferrite disk with a height-to-diameter ratio of 1:10, N_z (x,y) value is 0.9 close to disk center and 0.5 close to disk perimeter [7]. Thus, by using equation (4.1) with the given N_z (x,y) values, the internal field distribution of a TT2-2750 disk with an

aspect ratio of 1:10 can be determined. In the following derivations, an $H_{ext}\ of\ 3000\ G$ is assumed.

At the disk center

$$H_{i\_cen}=3000-0.9\ 2750$$

$$H_{i\_cen}=525G$$

At the perimeter

$$H_{i\_per}=3000-0.4\ 2750$$

$$H_{i\_per}=1900G$$

The example above shows that the internal static magnetic field of a ferrite disk increases from center to the perimeter. The demagnetization phenomena can also be demonstrated in magnetostatic solvers like CST EM STUDIO the details of which will be given in the following parts.

In order to saturate a ferrite material, a certain threshold, $N_z 4\pi M_s$, of external static field should be applied to the ferrite material. Thus, saturating the central region of the ferrite disk requires much larger static field excitation than the one required for saturating the regions around periphery, because demagnetization factor N_z(x,y) decreases while going to the perimeter. If a uniform H_{ext} is applied just enough to saturate the ferrite at the central region, the internal field at the perimeter becomes is relatively large which results the operation to go away from the below-resonance operation. Thus, the performance in the low frequency values of the band worsens due to the high fields at the periphery. According to Schloemann and Blight, high static magnetic fields around periphery should be lowered to widen the frequency

band [7]. In the following parts, two different methods are discussed to eliminate the static magnetic field non-uniformity in the ferrite disks.

4.1.2 Methods To Widen The Frequency Band

In Part 3.1, it is analytically demonstrated that a *one octave* circulation is possible in the frequency band between $f_m \; and \; 2f_m$. Thus, in order to widen the frequency band, circulator performance needs to be improved around frequencies f_m or $2f_m$. Achieving this seems impossible for $2f_m$, because second modes do not allow. However, the performance at f_m can be improved, if the gyromagnetic losses are eliminated.

In order to comprehend the loss mechanism due to internal fields, a local resonant frequency f_{res} is defined. f_{res} depends f_m and f_o with the relation given in (4.2). f_{res} puts a lower limit below which the low-field losses become so dominant and the performance deteriorates [7].

$$f_{res}=\sqrt{f_o\,(f_o+f_m)} \qquad \textbf{(4.2)}$$

By using (4.2), f_{res} values can be found for different regions of an arbitrary ferrite structure. The required values are the internal static field at the desired region and saturation magnetization of the ferrite to determine f_o and f_m, respectively [7]. In this part our aim is to understand which regions of the ferrite disk limit the frequency band of circulation. In order to do this, f_{res} values for different regions of a TT2-2750 disk with a height-to-diameter ratio of 1:10, the demagnetization factors which are provided in the previous part, are calculated.. Firstly, the internal static magnetic field distribution of ferrite disk is analytically found at the center (H_{i_cen}) and at the perimeter (H_{i_per}). Then, by using the calculated values, f_{res} values are determined for the the center and perimeter of the ferrite disk. In order to simplify equations, it is assumed that H_{ext} is adjusted just to saturate the central region of the ferrite disk which means a zero internal static field at the center is employed.

If H_{i_cen}≈0, H_{ext} is found by (4.1) as,

$$H_{ext}=N_{z\_cen}\ 4\ \pi\ M_s \tag{4.3}$$

$$H_{ext}=0.9\ 2750$$

For central region, H_{i_cen}≈0 so by (2.6)

$$\mathrm{f}_{res\_center}\approx 0 \tag{4.4}$$

For the perimeter of the given ferrite disk, by (4.1)

$$H_{i\_per}=H_{ext}-N_{z\_per}4\ \pi\ M_s$$

$$H_{i\_per}=N_{z\_cen}4\ \pi\ M_s-N_{z\_per}4\ \pi\ M_s$$

As N_{z_cen} and $N_{z_per}$are 0.9 and 0.4 for a disk with an aspect ratio 1:10,

$$H_{i\_per}=0.5\ \ 4\ \pi\ M_s$$

By (4.1), f_{res_per} is found as

$$\mathrm{f}_{res\_per}\approx\sqrt{0.5\ \mathrm{f}_m\ (0.5\ \mathrm{f}_m+\mathrm{f}_m)}=\sqrt{\frac{3}{4}}f_m=0.87f_m \tag{4.5}$$

(4.4) shows that circulation operation down to 0 GHz is theoretically possible for the regions at the center of the ferrite disk. However, (4.5) indicates that at the perimeter, high gyromagnetic losses occur for the frequencies below $0.87f_m$. Thus, it is clear that the lower limit of the band is determined by the high static magnetic fields at the perimeter. In conclusion, if the high static magnetic fields at the perimeter is lowered, the circulator operation at lower frequencies is possible.

In the previous derivation, it is concluded that lower frequency limitation of the circulation operation is resulted by the high static magnetic fields at the perimeter. Thus, the frequency band of circulation can be widened by lowering the H_{i_per} values. A method to achieve this is to lower the H_{ext} by using weaker magnets; however, the magnets should not be lower than a threshold value which is required to saturate the central parts of the ferrite disk that is given in (4.3). So, the magnet strength should be chosen according to two different considerations. Firstly, it should be larger than a threshold value to guarantee the saturation at the central regions of the ferrite disk [30]. Secondly, H_{ext} should be as low as possible not to result high internal static magnetic fields around the perimeter. In conclusion ,by (4.4) and (4.5), it is clear that the high static magnetic field around the periphery of the ferrite disk limits the low frequency boundary of the circulator operation, so if H_{i_per} is lowered, it is possible to operate the circulator below f_m. In the following two parts, two different approaches are proposed to widen the frequency band by lowering H_{i_per} values.

4.1.2.1 Dome Method

In Part 4.1.1, it is stated that ellipsoidal structures have constant demagnetization factors that do not depend on position. On top of this, in the previous part, it is determined that the frequency band of the circulator operation is limited by the non-uniform demagnetization factors of the ferrite disks. By considering these two facts, if there is a method that replaces non-ellipsoidal ferrite disks with ellipsoidal ferrite spheres , the non-uniform demagnetizations factor would not be a problem any more. Schloemann and Blight propose to use ferrite domes on top of the ferrite disks to gain a uniform field distribution inside the ferrite disks which is shown in Figure 4.4

[7]. However, some precautions should be taken to apply this method to structure. Firstly, ferrite materials used for the domes and the ferrite disks should have the same *saturation magnetization*. Secondly, ground sheets should be placed between ferrite disks and ferrite domes. Finally, the ferrite domes should be made of pure single crystal ferrites that require a special form of ferrite production.

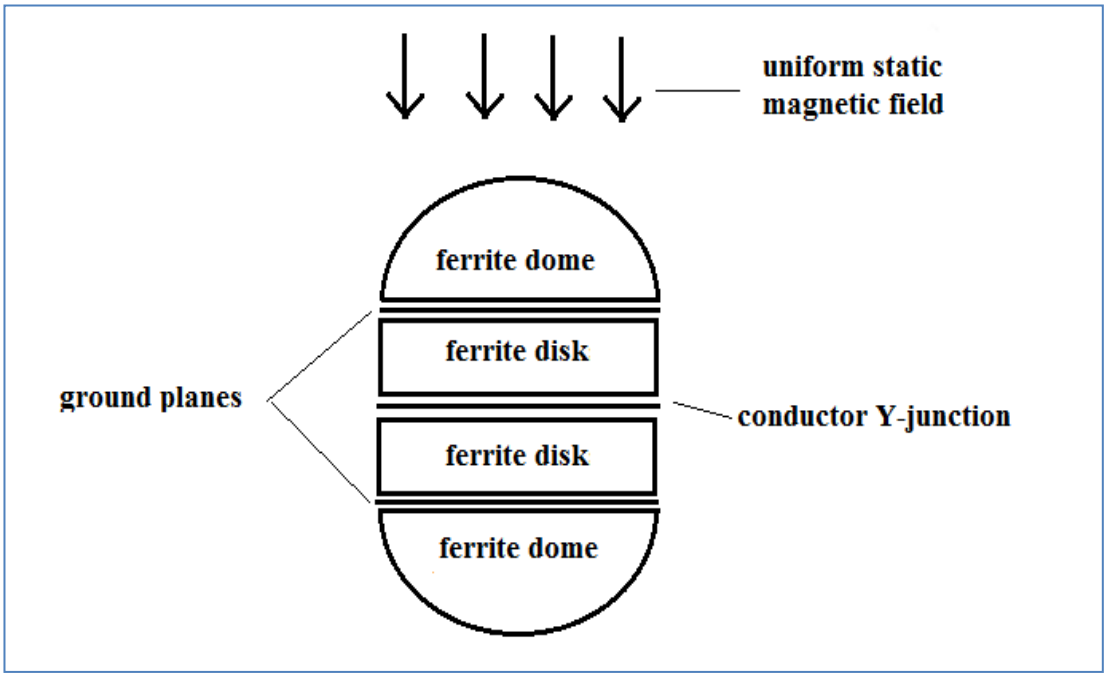

Figure 4.3 Ferrite dome embedded in conventional circulator

In Figure 4.4, a circulator structure designed with dome method can be observed. If the ferrite domes and ferrite disks are considered together, the overall structure has a shape of a slightly elongated sphere. As this shape is ellipsoidal, the demagnetization factor is constant and equal to a value around 1/3 which is the demagnetization factor of sphere given in Figure 4.2. According to the results given in Schloemann and Blight's article [7], this method is efficient in widening the frequency band of circulator operation. However, this method has many disadvantages, too. Firstly, ferrite domes increase the thickness of the overall circulator structure. Especially in RADAR applications, the thickness of the circulator is very important, because so many transceiver modules are tried to be stacked in very small volumes. Secondly, the necessity to use single crystal ferrite for the ferrite domes increases the cost

extremely, because single crystal ferrites have a special production process which contributes high costs. To sum up, because of the mentioned reasons, this method seems unpractical to realize [7].

4.1.2.2 Composite Substrate Method

Another method to eliminate low-field losses is to use composite substrates. Up to this point, it is observed that the high internal fields are constrained to the periphery of the ferrite disk. So, a ferrite ring can be located radially outside of the central ferrite disk to get rid of the high fields at the center. As the high static magnetic fields (H_{i_per}) around the periphery are constrained to the ferrite ring at which the circulation does not occur, the onset frequency of the band is naturally lowered. However, for doing this a ferrite material with a lower *saturation magnetization* should be used for the ferrite ring [8].

In order to observe the effect of composite substrate approach, two different structures are simulated in CST EM STUDIO to observe the internal static field distribution of ferrite disks. The first structure is a single ferrite disk given in Figure 4.4, and the second one is a composite substrate which includes a ferrite disk and a ferrite ring given in Figure 4.5..

In Figure 4.4, internal static magnetic field (H_i) of a 3.6 mm. diameter TT2-2750 ferrite disk can be observed. In this structure, an additional ferrite ring is not used and the ferrite disk is radially covered by a TRANS-TECH dielectric material, SMAT13. The details of the ferrite and dielectric materials can be found in Appendix A. If the internal static magnetic field H_i is observed, it is clear that H_i value goes up to 105kA/m at the periphery, and it is around 73 kA/m around the center. This field distribution is certainly because of the non-uniform demagnetization affect depending on position in non-ellipsoidal bodies like disks. In the regions out of the ferrite disk, very high H_i values up to 150kA/m is observed, this is because of the non-magnetic characteristics of SMAT13 in this region. As this material has a

permeability (μ) value of unity, the B_i results relatively much higher H_i than magnetic materials.

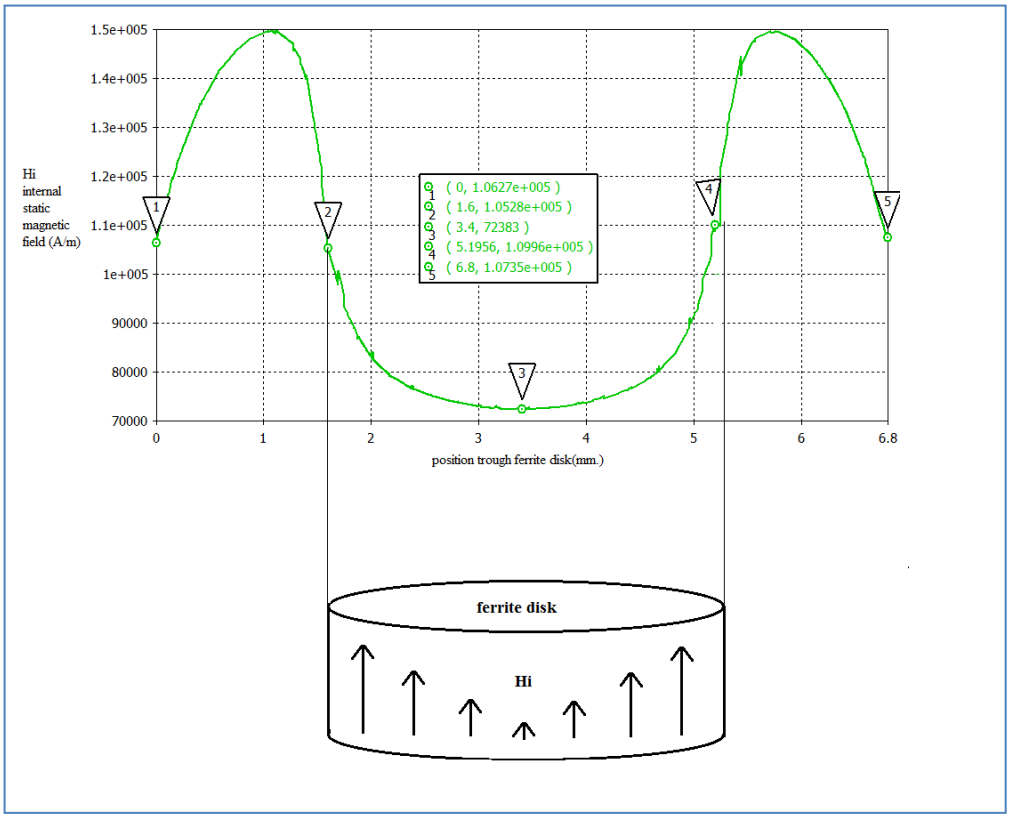

Figure 4.4 Internal static magnetic field distribution of a single ferrite substrate

In Figure 4.5, $\boldsymbol{H_i}$ distribution of a composite substrate can be observed. The composite structure enables the $\boldsymbol{H_i}$ value to become lower and more homogeneous in the ferrite disk, where the circulation takes place. Firstly, the ferrite ring around the ferrite disk provides a larger cross-section for the static magnetic field than the single ferrite substrate; and this results lower static magnetic field density per area ($\boldsymbol{B_i}$) which results lower $\boldsymbol{H_i}$. Secondly, even if still high $\boldsymbol{H_i}$ fields do exist, these fields are confined to the ferrite ring in which circulation does not occur. In Figure 4.5, $\boldsymbol{H_i}$ internal static field distribution of the ferrite disk ($\boldsymbol{H_i}$) can be observed by the help of *marker 1*, *marker 2* and *marker 3*. *Marker 1* and *marker 3* are located at the periphery of the ferrite disk; and *marker 2* is placed just at the center of the ferrite disk. At the periphery of the ferrite disk in composite structure, $\boldsymbol{H_i}$ value is 57kA/m and at the center, it is 50kA/m

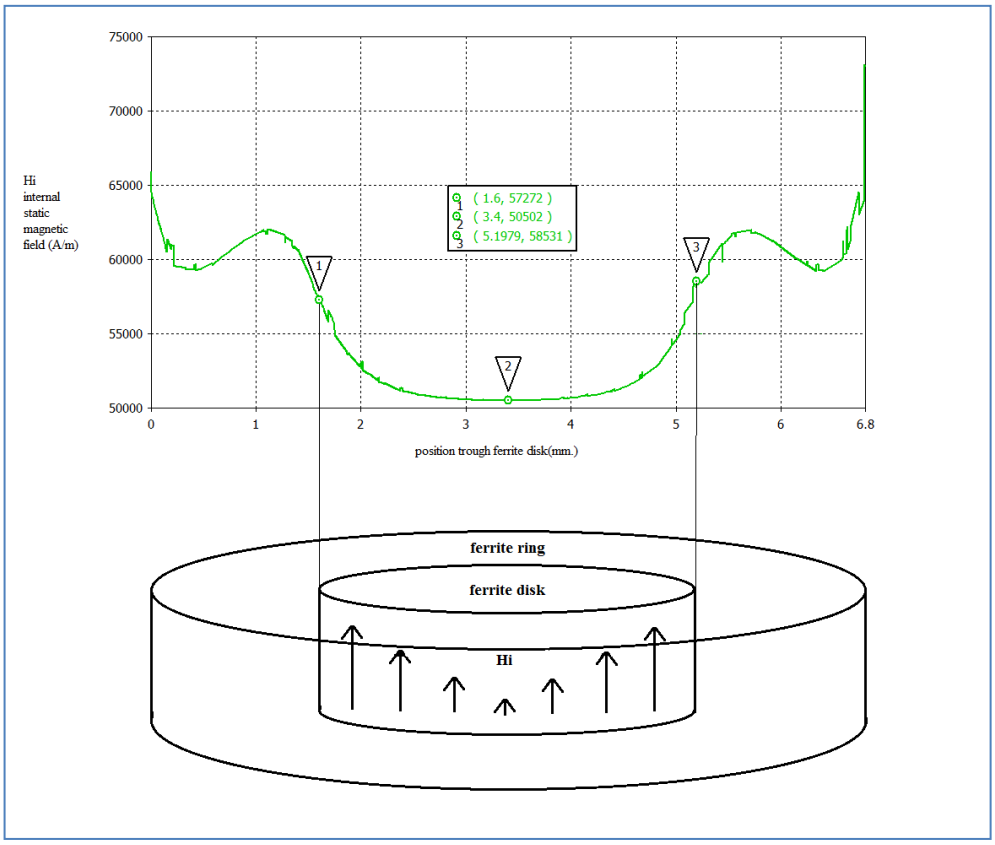

Figure 4.5 Internal static magnetic field distribution of composite substrate

To compare the homogeneity of the field distribution in first and second structure, a homogeneity ratio can be defined as

$$\boldsymbol{Homogeneity\ ratio} = \frac{\boldsymbol{H_{i\_periphery}}}{\boldsymbol{H_{i\_center}}}$$

Homogeneity ratio of the single ferrite structure,

$$\boldsymbol{Homogeneity\ ratio} = \frac{\boldsymbol{H_{i\_periphery}}}{\boldsymbol{H_{i\_center}}} = \frac{\mathbf{105kA/m}}{\mathbf{73kA/m}} = \mathbf{1.43}$$

Homogeneity ratio of the composite structure,

$$\boldsymbol{Homogeneity\ ratio} = \frac{\boldsymbol{H_{iperiphery}}}{\boldsymbol{H_{icenter}}} = \frac{\mathbf{57kA/m}}{\mathbf{50kA/m}} = \mathbf{1.14}$$

By the homogeneity ratios, it is clear that the composite substrate provides a much more homogeneous static field distribution in the ferrite disk. At the same time, lower static magnetic fields can be created in the ferrite disk with the help of the ferrite ring. To sum up, if the results of homogeneity equations are considered, it is certain that using a composite substrate with two different ferrites is an effective way of stabilizing internal static magnetic field distribution of the ferrite disk.

For circulators with a band *more than one octave*, it is known that composite substrates are effectively used. If composite substrate approach is compared with the dome approach, it is superior in terms of many considerations. Firstly, composite substrate does not have a contribution to the thickness of the overall structure unlike the dome structure. Secondly, it is not necessary to use single crystal ferrites in the composite substrate method. Moreover, it is certain that single-crystal dome structures increase the cost much dramatically than composite substrates. However, the cost of a composites substrate can be slightly larger than normal substrates. Because of the terms explained, it is concluded that using the composite substrate method to design *more than one octave* circulators is the most logical way to follow.

4.2 Design of More Than One Octave Frequency Band Stripline Circulator

In the previous parts of this chapter, 2 different methods have been explained to widen the frequency band by modifying *one octave* circulators. At the end of the discussion, composite substrate method has been concluded to be superior to widen the frequency band. In order to implement the explained band widening methods, a 9-18 GHz *one octave* design can be used as an intermediate step. In part 3.2.4, 3 different structures have been optimized for 9-18 GHz circulator operation. Thus, it

is logical to use the most proper structure among them as an intermediate step for the wider bandwidth design.

The insertion loss characteristics of the three optimized structures have been given in Part 3.2.6 separately. However, in Figure 4.7 these characteristics are displayed together to determine which structure should be used as an intermediate step for the *more than one octave* circulator design. The desired property for the intermediate *one octave* structure is the width of the frequency band. It is observed that *Structure 2* and *Structure 3* have very similar insertion loss characteristic; however, *Structure 1* has a relatively weak insertion loss performance for low frequencies. But, if the second mode placement is considered, *Structure 2* has a second mode notch at 20.32 GHz, while *Structure 3* has the same kind notch at 19.23. Thus, in terms of the insertion loss performance at the beginning of the band and second mode frequencies, *Structure 2* is the best optimized structure for the design of *more than one octave* circulator design.

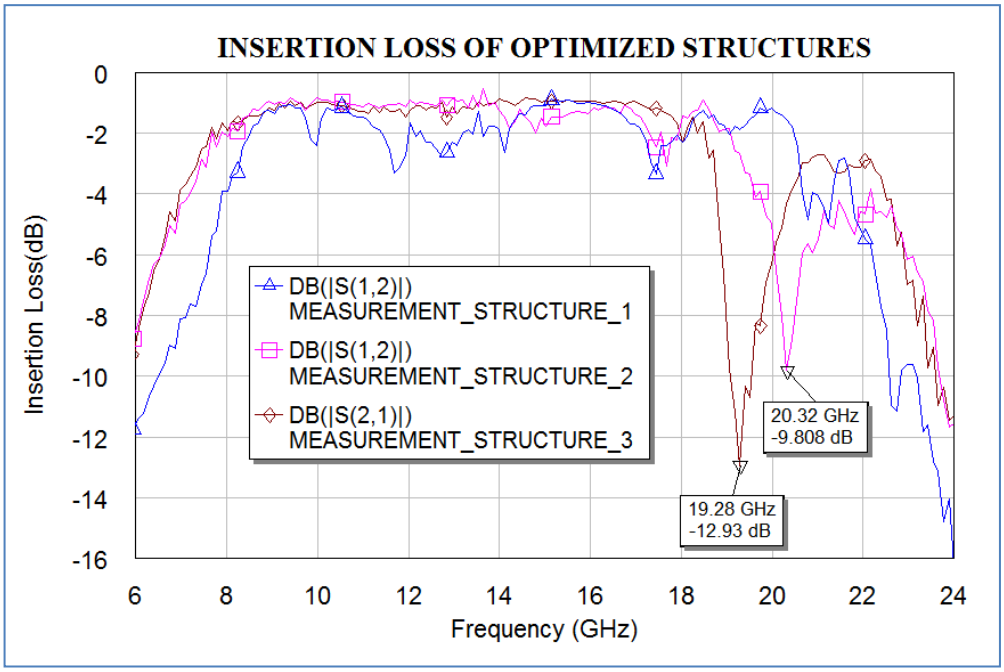

Figure 4.6 Insertion loss comparison of the optimized structures determined in Chapter 3

In Table 3.5, the geometrical parameters of 3 optimized structures are shown. As *Structure 2* has been determined as the intermediate step for further design steps, the geometrical parameters of *Structure 2* are used for the design of *more than one*

octave circulator design. The additional parameters need to be determined are the outer radius (R_{outer}) and material of the ferrite ring.

Table 4.1 Geometrical parameters of the *Composite Structure*

	R(mm)	R_outer(mm)	wint(mm)	w3(mm)	w2(mm)	w1(mm)	l3(mm)	l2(mm)	l1(mm)
COMPOSITE	1,8	3,4	1,73	1,25	0,5	0,2	1,5	1,7	1,7

In Table 4.1, the geometrical parameters for the *more than one octave* circulator are given. In this table, w_{int}, w_1, w_2 and $w_3$values are the width of the impedance transformer sections; l_1, l_2 and l_3 are the lengths of the impedance transformer sections; R is the radius of the ferrite disk; and R_{outer} is the outer radius of the ferrite ring. It is clear that all the geometrical dimensions are the same with the *Structure 2* given in table 3.5. The only difference is the newly defined parameter R_{outer}, the outer radius of the ferrite ring. This parameter is simply found by using l_3, the idea here is the third section of the impedance transformer lays just below the ferrite ring.

Another design consideration for composite substrate is the material of the ferrite ring. In Part 4.1.2.2, it is stated that *saturation magnetization* of the ferrite ring should be lower than the *saturation magnetization* of the ferrite disk [8]. Although why this kind of a choice should be made is not explained in the literature, it can be said that the main reason is to constrain the magnet strength to the ferrite disk more than the ferrite ring. In fact, *saturation magnetization* is a measure of the non-linear permeability characteristics of the materials. Thus, if the *saturation magnetization* of the material is higher, static magnetic field prefer to go through this material. In this case, by choosing the ferrite ring material with a lower *saturation magnetization*, it is possible to apply much static field to the ferrite disk which enables the designer to focus the field on the ferrite disk, where the operation takes place. From the catalog of TRANS-TECH, a magnesium ferrite TT1-390 is chosen as the material of the ferrite ring. The details of the material can be found in Appendix A.

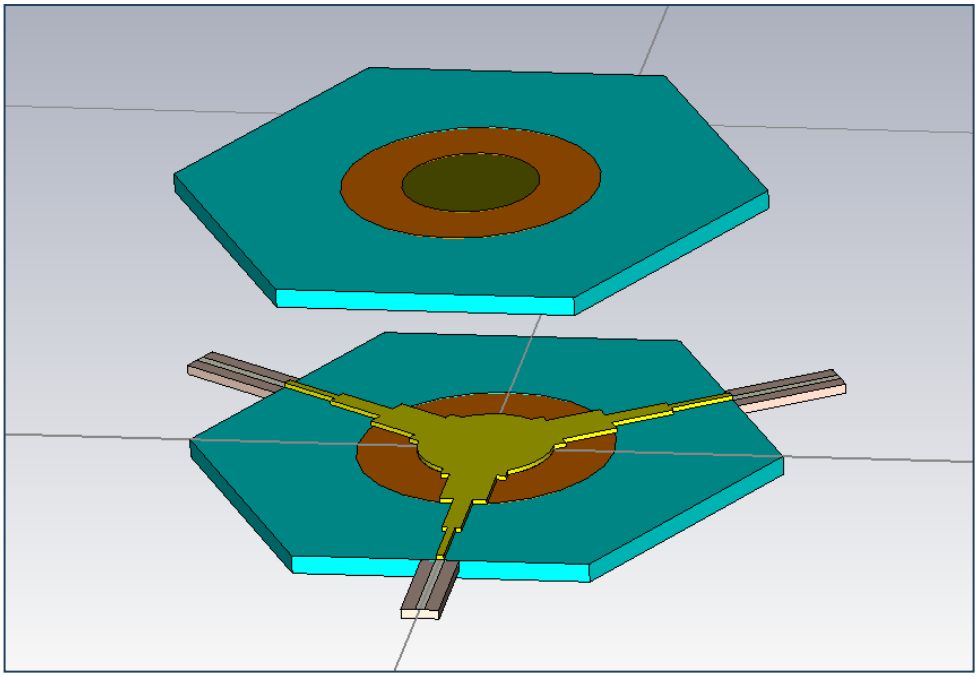

Figure 4.7 Exploded view of the *Composite Structure* (magnet and yoke are hidden)

In Figure 4.7, exploded view of the designed composite circulator is shown. Unlike the 9-18 GHz circulator shown in Figure 3.6, a ferrite ring (orange) is radially covers the ferrite disk. The outer radius of the ferrite ring is adjusted in terms of the length of the third section of the impedance transformers. The transitions between second and third section of the transformer and dielectric to ferrite ring are desired to occur at the same point to suppress the losses.

4.3 Measurement Results of More Than One Octave Frequency Band Circulator

In Figure 4.8, insertion loss characteristic of the designed *more than one octave* circulator is displayed. The insertion loss is satisfactory between 7.69 GHz and 18.66 GHz which shows that a wider frequency band is achieved with the composite substrate than the single ferrite *Structure 2*. If the simulation and measurement results are compared, it is clear that both results are very similar to each other. On top of this, a very stable 1 dB insertion loss is achieved throughout the mentioned band which means ground connection problems do not occur.

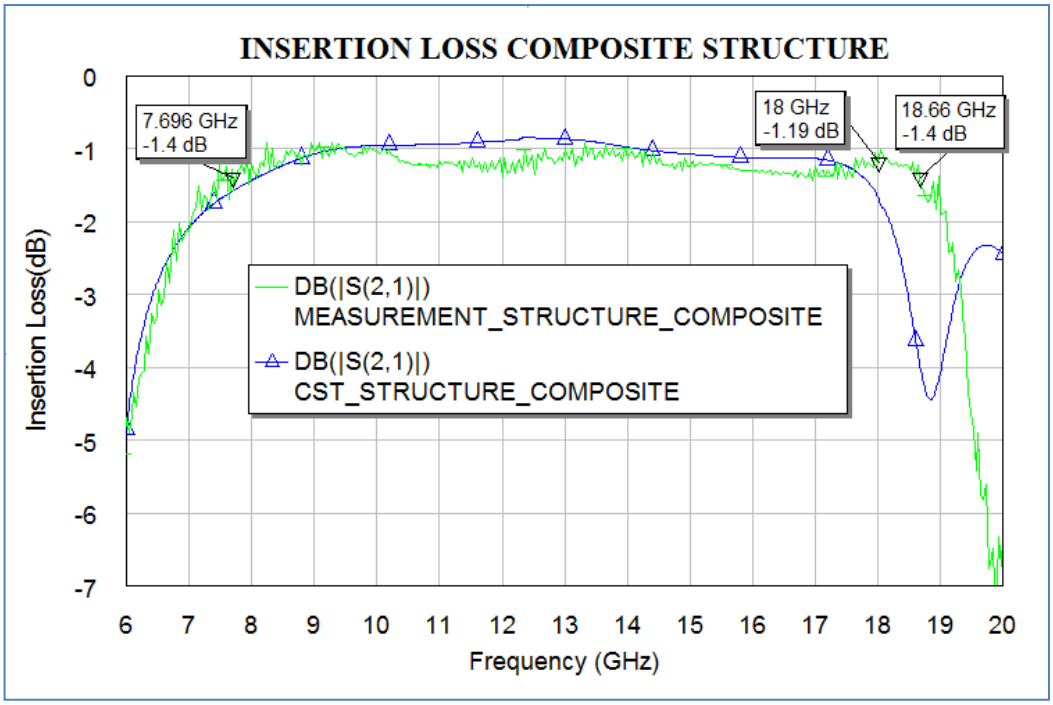

Figure 4.8 Insertion loss of the *Composite Structure*

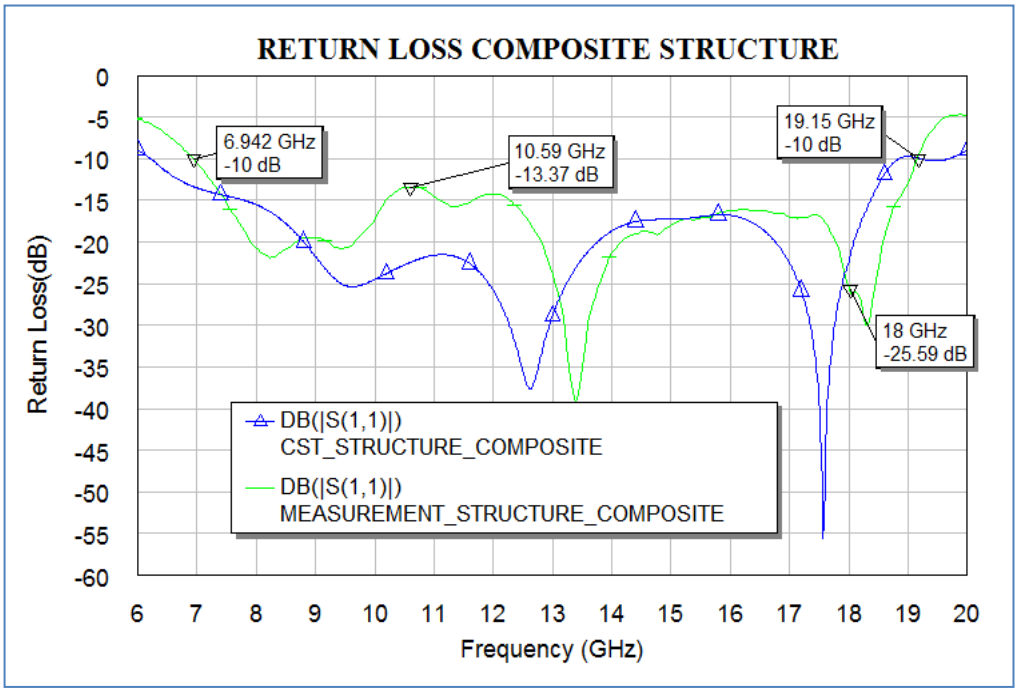

Figure 4.9 Return loss of the *Composite Structure*

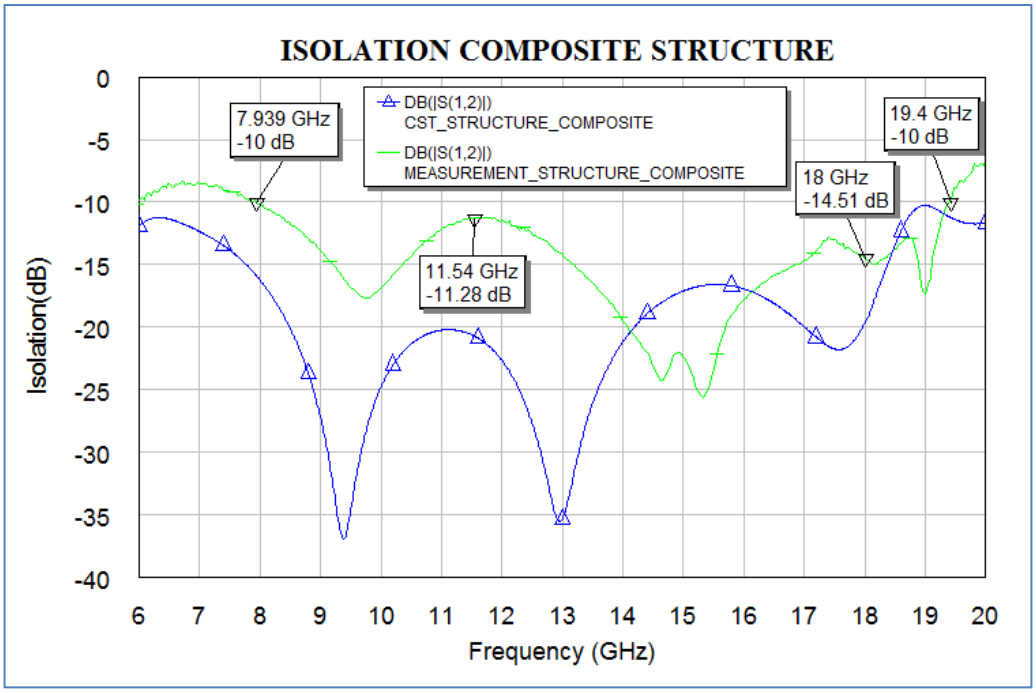

Figure 4.10 Isolation of the *Composite Structure*

In Figure 4.9, the return loss characteristics of the *more than one octave* circulator design can be observed. Firstly, 10 dB return loss requirement is satisfied between 7 and 19 GHz. On top of this, general characteristics of the measurement and simulation are similar. Note that for the high frequencies in the band (13.5-18 GHz), return loss is better than 15 dB.

In Figure 4.10, the isolation performance of the *Composite Structure* is displayed. For low frequencies around 10 dB isolation is achieved. However, with the increasing frequency, isolation performance improves and goes to values around 15 dB.

In conclusion, it is clear that a satisfying circulator operation has been achieved in the band of 7.7 and 18.66 GHz, which is a more than one octave frequency band. The measurement results also show that composite substrate method is a good way to design *more than one octave* circulators. Adding to that, a certain similarity is

observed between simulation and measurement results which prove that the simulation tools are reliable in predicting the circulator performance.

4.4 Comparison Of *Composite Structure* and *Structure 2*

In Chapter 3 and 4 , a one octave circulator and a more than one octave circulator are realized and measured. Now, as all the measurements have been made, the composite substrate method can be analyzed whether it is useful in widening the frequency band of circulators. Thus, In the following 3 figures, the measurement results of *Structure 2* and *Composite Structure* are displayed together.

Figure 4.11 displays the comparison of insertion loss of *Structure 2* and *Composite Structure*. It is clear that the low frequency performance of *Structure 2* is improved by applying composite substrate method. In *Composite Structure*, low frequency operation starts from 7.75GHz, while it starts from 8.49 GHz in *Structure 2*. The composite substrate method results a 0.7 GHz band improvement which shows that this method is useful for widening the frequency band of the circulator.

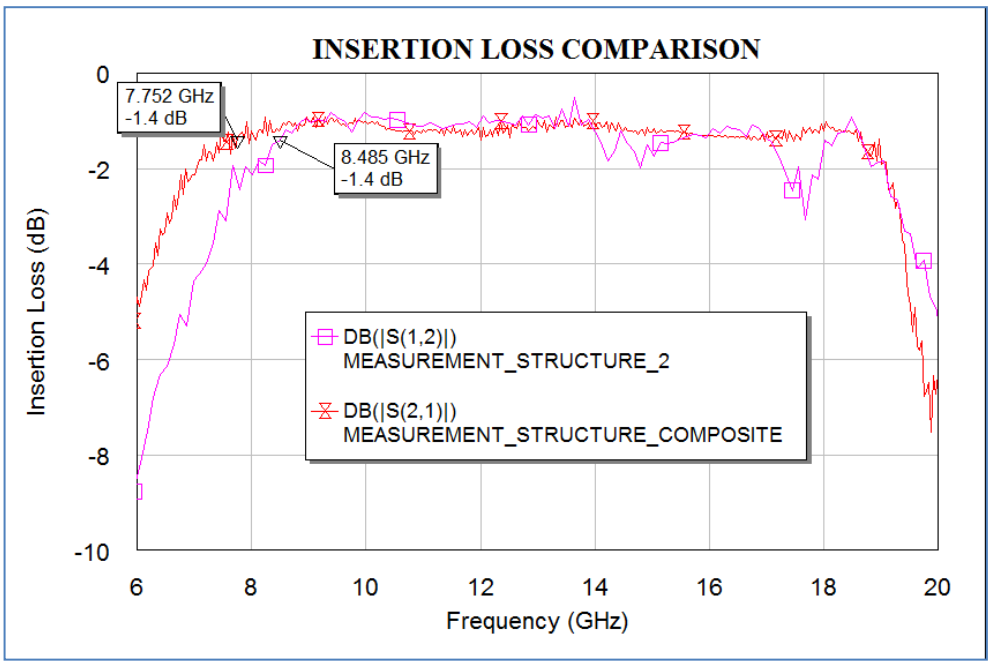

Figure 4.11 Insertion loss comparison of *Structure 2* and *Composite Structure*

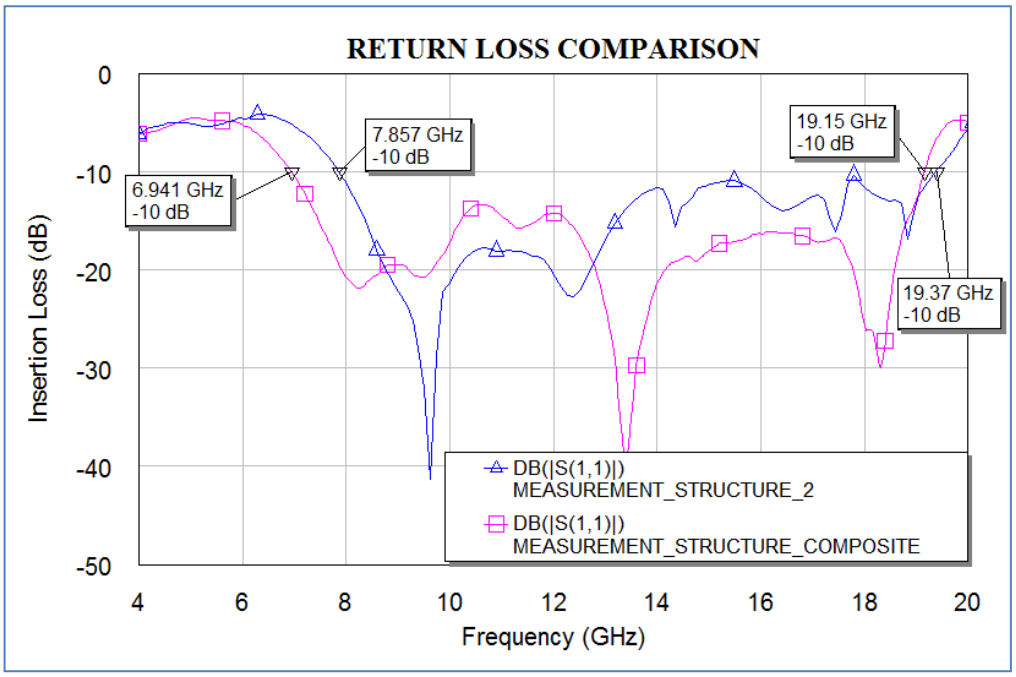

Figure 4.12 Return loss comparison of *Structure 2* and *Composite Structure*

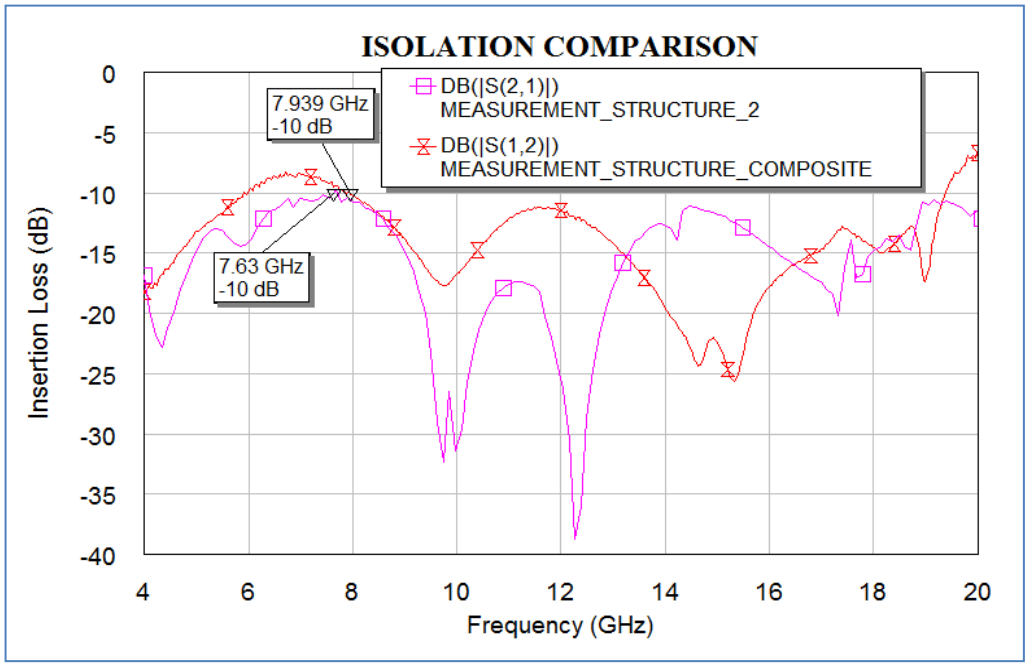

Figure 4.13 Isolation comparison of *Structure 2* and *Composite Structure*

Figure 4.12 shows that return loss of both structures are similar. However, a slight improvement can be observed for the *Composite Structure* especially for the low frequencies of the band. 10 dB return loss starts at 6.94 GHz and 7.86 GHz for *Structure 2* and *Composite Structure*, respectively. It is clear that composite substrate approach improves the frequency band of the return loss of the structure by 0.92 GHz.

Figure 4.13 displays that the isolation of the *Composite Structure* is slightly better than *Structure 2* in terms of the performance at the beginning of the band. In *Composite Structure,* 10 dB isolation starts at 7.63 GHz, while it starts at 7.93 GHz in *Structure 2* .

From Figure 4.4 and Figure 4.5, it is concluded that a composite substrate offers a more uniform static internal field distribution than a single ferrite substrate. After the overall measurements, it is observed that this uniformity in field distribution results an improvement of nearly 1 GHz in the frequency band of the circulation. To sum up, at the end of this chapter, two conclusions can be made. Firstly, a circulator operating between 7.69 and 18.66 GHz is realized which indicates that composite substrate method is a trustworthy way of designing more than one octave circulators. Secondly, a good correlation is achieved between the simulation and measurement results which shows that simulation tools can be used in the optimization process of circulator structures.

CHAPTER 5

CONCLUSION AND FUTURE WORK

Circulators are crucial components for T/R modules of RADAR systems. Thus, designing a wideband circulator is a significant issue in terms of designing wideband RADAR systems. In this thesis, it is aimed to give the details of the design, simulation, realization and measurement of the wideband stripline circulators. During the realization of each wideband stripline circulator, a general procedure is followed. Firstly, theoretical basis of wideband stripline circulator design is established. Secondly, circulator structures are modeled and optimized by using CST MW STUDIO and EM STUDIO. Then, the optimized structures are realized and measured. Finally, the measurement results and simulation results are compared whether the design method or simulation is reliable.

In Chapter 3, the main goal is to realize a *one octave* frequency band circulator between 9 and 18 GHz. By using *continuous tracking method*, design parameters of a one octave circulator have been analytically determined. Then, by using analytically found parameters as a starting point, three different structures have been optimized with the help of CST. These three structures are realized and measured, and it is observed that the overall performance of *Structure 1* is not satisfying because of the ground connection problems. In fact, the results of *Structure 1* are given on purpose to show how the ground connection problems deteriorate the performance. When the results of *Structure 2* are analyzed, it is clear that the ground connection problems are mostly solved, and a satisfying circulation is achieved in the band of 8.5 and 17 GHz. However, when *Structure 3* is analyzed, it is observed that all the ground connection problems have been solved throughout the frequency band between 8.7 and 18.3 GHz. In other words, *Structure 3* is observed to perform a 1dB insertion loss and 13 dB isolation and return loss, which satisfies the performance requirements in the frequency band of 8.7-18.3 GHz. On top of this, the measurement results indicate

two facts. Firstly, *continuous tracking method* is an efficient way of designing *one octave* circulators. Secondly, CST provides realistic results which shows that it can be used confidently during the design procedure.

In Chapter 4, it is aimed to design a *more than one octave* frequency band stripline circulator. At the beginning of the chapter, the demagnetization effect, which is the main limiting factor for the frequency performance of circulators, has been explained in detail. Two methods have been proposed for dealing with the demagnetization effect and widening the frequency band of the circulator. Among them, composite substrate method has been chosen due to some practical reasons. After the measurement procedure, it is observed that composite substrate method provides an additional band of 1 GHz than single ferrite structure does in Chapter 3. Moreover, it can be stated that a satisfying more than one octave circulation has been achieved for the frequency band of 7.7-18.7 GHz. In the mentioned frequency band, a 1dB insertion loss performance and a better than 13 dB isolation and return loss performances are achieved. The increased frequency band indicates that making the internal static magnetic field distribution of ferrite disks as uniform as possible improves the frequency band performance. In this study, the improvement has been achieved by using a composite substrate; however, another method called dome approach can be used for the same consideration.

At the beginning of this study, we were not sure about the ferrite modeling performance of CST. However, after measurement process, it is observed that it provides realistic results. But, still some discrepancies may occur between the measurement and simulation results due to many reasons. Firstly, the internal static field distribution may not be predicted very well, due to unexpected distortions in reality. Secondly, due to unpredictable behavior of partly-saturated ferrites, CST assumes that all the ferrites are saturated in the structure and this may cause some discrepancies between measurement and simulations. But, generally speaking, very realistic results are predicted by CST which shows that it can be used through the design process.

During this study, very satisfying wideband circulator operations have been achieved for desired frequency band; however, still some modifications can be done to improve the performance. During the measurement process, it is observed that the ground connections of the ferrite substrates are crucial especially for a successful circulator performance. The mentioned problem can be solved by designing a different mechanical structure at which ground connection made through a more reliable way. As a future work, it is planned to design new mechanical structures to eliminate ground connection problems.

In this study, main consideration is to design stripline circulators. However, the design and realization procedures are very similar for microstrip circulators. Thus, the design and realization of wideband microstrip circulators may be a future work with the help of experience gained in this study.

In conclusion, the main focus of this study is the design and fabrication of *a one octave* and *a more than one octave* circulator by using different design approaches. During this process, the reliability of different design methods and simulation tools are observed. Adding to that, this study can be a useful starting point for the newly – starting circulator designers and help them in the design, simulation and realization procedures of the wideband stripline circulators.

REFERENCES

[1]D.K. Linkhart, “Microwave Circulator Design,” Norwood, MA: Artech House, 1989.

[2] D.Polder, “On the Theory of Ferromagnetic Resonance,” Phil.Mag.,Vol.40, pp. 99-115, 1949.

[3] H. Bosma, ”On stripline Y-circulation at UHF,” IEEE Trans. Microwave Theory Tech., vol. MTT-12, pp. 61-72, January 1962.

[4] Y.S. Wu and F.J. Rosenbaum, “Wideband operation of microstrip circulators,” IEEE Trans. Microwave Theory Tech., vol. MTT-22, pp.849-856, October 1974.

[5] B.A. Auld, ”The synthesis of symmetrical waveguide circulators,” IRE Trans. On Microwave Theory and Techniques, vol. MTT-7, pp 238-246, April 1959.

[6] C.E. Fay and R.L. Comstock, “Operation of the ferrite junction circulator,” IEEE Trans. Microwave Theory Tech.,, vol. MTT-13, pp.15-27, January 1965.

[7] E. Schloemann and R.E. Blight, “Broad-band stripline circulators based on YIG and Li-Ferrit single crystals,” IEEE Trans. Microwave Theory Tech., vol. MTT-34, no.12, December 1986.

[8] E. Schloemann and R.E. Blight, “A compact broadband microstrip circulator for phased array antenna,” IEEE MTT-S Digest, pp. 1389-1392, 1992.

[9] A.M. Borjak and L.E. Davis, ”More compact ferrite circulator junctions with predicted performance,” IEEE Trans. Microwave Theory Tech., vol. MTT-40, no.12, pp.2352-2358, December 1992.

[10] Y.Konishi, ”Lumped element Y Circulator,” IEEE Trans. Microwave Theory Tech., vol. MTT-13, pp.852-864, November 1965.

[11]E.C. Snelling, ”Soft ferrites,” Second Edition, Boston:Butterworths, 1988.

[12] K. Chang, “Encyclopedia of RF and Microwave Engineering,” New York: John Wiley & Sons, 2005.

[13] Trans-Tech RF/Microwave Products Catalog, Revised: 2005.

[14] E. Schloemann and R.E. Blight, “Low-field loss in ferrites-relevance to broadband circulator design,” IEEE Trans. Magn., vol.28, no.5, pp.3291-3293, September 1992.

[15] IEC, “ International Standard for Gyromagnetic materials intended for application at microwave frequencies-Measuring properties for standards,” Second Edition, Geneva, 2006-04.

[16] R.A. Waldron, “Ferrites:An Introduction for Microwave Engineers,” D.Van Nostrand Co., 1961.

[17] B. Lax K.J. Button, “Microwave Ferrites and Ferrimagnetics,” McGraw-Hill, 1962.

[18] H. Bosma, “On the principle of stripline circulation,” Proc .IEE, vol.109, part B, suppl.21, pp. 137-146, 1962.

[19] D. M. Pozar, “Microwave Engineering,” Second Edition, John Wiley & Sons, NY., 1998.

[20] J. Helszajn, “The Stripline Circulator,” New York: John Wiley & Sons, 2008.

[21] D.B. Cruickshank, “Microwave materials for wireless applications,” Norwood MA: Artech House, 2011.

[22] S.Ayter and Y. Ayasli, “The frequency behaviour of stripline circulator junctions,” IEEE Trans. Microwave Theory Tech., vol. MTT-26, no. 3, March 1978.

[23] G.L. Matthaei, L.Young, and E.M.T. Jones, “Microwave Filters, Impedance Matching Networks, and Coupling Structures,” Artech House Books, Dedham, Mass, 1980.

[24] TCI Ferrite Material Catalog, Revised: 2007

[25] AFT Ferrite Material Catalog, Revised: 2006

[26] MAGCRAFT Permanent Magnet Design and Selection Handbook, Revised: 2007.

[27]J.A.Osborn, ”Demagnetizing factor for a general ellipsoid,” Phys.Rev., vol.67, pp.351-357, June 1945.

[28] J.Helszajn, “ Ferrite Phase Shifters and Control Devices,” London: McGraw Hill, 1989.

[29] R.I.Joseph and E. Schloemann, “Demagnetization field in non-ellipsoidal bodies,” J. Appl. Phys., vol.36, pp.1579-1593, May 1965.

[30] E.Scloemann, “Microwave behavior of partially magnetized ferrrites,”J. Appl. Phys.,vol.41, pp.204-214, January 1970.

[31] E.Scloemann, “Behavior of ferrites in the microwave frequency range,” Journal de Physique, vol.32, pp.C1-443-C1-451,Feb./Mar.1971.

[32] M. Pardavi-Horvath, “Non-uniform Internal Field In Planar Ferrite Elements,” IEEE Trans. Magnetics., vol.37, pp.3881-3884, Nov. 2001.

[33] X. Huang and M. Pardavi-Horvath , “Local Demagnetizing tensor calculation for rectangular and cylindrical shapes,” IEEE Trans. Magn., vol.32, pp.4180-4182, 1996.

[34] B. Lax and K.J. Button, “Microwave Ferrites and Ferrimagnetics,” New York: McGraw-Hill, 1962.

[35] Chen, D., Brug,J.A., Goldfarb,R.B., “Demagnetizing factors for cylinders,” IEEE Trans. Magn., vol.27, pp.3601-3619, 3619.

[36] C.M. Krowne and R.E. Neidert, “Theory and Numerical Calculations for Radially Inhomogeneous Circular Ferrite Circulators,” IEEE Trans. Microwave Theory Tech., vol.44, no.3, pp.419-431, March 1996.

[37] R.E. Neidert and P.M. Phllips, “Losses in Y-Junction Stripline and Microstrip Ferrite Circulators,” IEEE Trans. Microwave Theory Tech., vol.41, no.6/7, pp.1081-1086, June/July 1996.

[38] E-magnets UK Ltd. Grades of Ferrite. Retrieved from http://www.ferrite-info.com/ferrite_grades.aspx

[39] Magnetic Materials Producers Association, “Standard Specifications for Permanent Magnet Materials,” Chicago, 1964.

[40] Zhabao Magnet.Samarium Cobalt Magnet Grades. Retrieved from http://www.zhaobao-magnet.com/products_list/&pmcId=b58e780b-f65c-41f0-85a1-9973d99ad877&comp_stats=comp-FrontProductsCategory_show01-1315451312528.html

[41] Zhabao Magnet. Neodymium Iron Boron Magnet Grades. Retrieved from http://www.zhaobao-magnet.com/products_list/&pmcId=48842e9b-9acd-4b00-b91d-0d7b5aec9ec4&comp_stats=comp-FrontProductsCategory_show01-1315451312528.html

[42] Trans-Tech. (2007). No.661:Test for Complex Dielectric Constant. Retrieved from http://www.trans-techinc.com/documents/No661.pdf

[43] Trans-Tech. (2007). No.662: Test for Linewidth and Gyromegnetic Ratio. Retrieved from http://www.trans-techinc.com/documents/No662.pdf

[44] Trans-Tech. (2007). No.663: Test for Saturation Magnetization. Retrieved from http://www.trans-techinc.com/documents/No663.pdf

APPENDIX A

FERRITE AND DIELECTRIC MATERIALS AVAILABLE IN THE MARKET

In this part, it is aimed to provide a catalog that includes the variety of ferrite materials available in the market. The materials of the two well-known ferrite manufacturers, TRANS-TECH and TCI, are given, because materials of these manufacturers are produced for many years and the properties of them are clearly established. On top of this, these manufacturers have a great capability of producing different kind of shapes like hexagons and disks. In the following parts, garnets, nickel spinels, magnesium spinels and dielectrics provided by these two firms are provided with their properties.

A.1 Garnets

Garnets are efficiently used in microwave applications due to their low *resonance linewidth* values. However, the maximum *saturation magnetization* value for garnets is around 1780 G which limits the frequency of *one octave* circulator operation up to max 5-10 GHz. Thus, for higher f_m requirements, spinel ferrites can be preferred. Despite their limited saturation magnetization, it is very easy to optimize garnets for low line widths, square hysteresis loops and good power handling performance by applying rare earths like gadolinium or aluminum. In the tables below, garnets provided by TRANS-TECH and TCI are listed. Abbreviations for different family types are given at the beginning of the thesis.

Table A.1 Garnets provided by TCI [24]

Material code	Family	Saturation Magnetization (G)	ΔH (Oe)	ε	Tanδx (10)^4	Tn (C^o)
YG – 1780 – 45	YIG	1780	45	15,1	<2	280
YG – 1780 – 30	YIG	1780	30	15,1	<2	280
AL – 1510 – 45	AL	1510	45	14,9	<2	255
AL – 1510 – 35	AL	1510	35	14,9	<2	255
AL – 1400 – 45	AL	1400	45	14,8	<2	245
AL – 1380 – 45	AL	1380	45	14,9	<2	240
AL – 1210 – 45	AL	1210	45	14,8	<2	230
AL – 1200 – 45	AL	1200	45	14,8	<2	230
AL – 1200 – 35	AL	1200	35	14,8	<2	230
AL – 1030 – 45	AL	1030	45	14,5	<2	215
AL – 1000 – 45	AL	1000	45	14,5	<2	210
AL – 1000 – 35	AL	1000	35	14,5	<2	210
AL – 800 – 40	AL	800	40	14,4	<2	200
AL – 650 – 40	AL	650	40	14,4	<2	175
AL – 650 – 60	AL	650	60	14,3	<2	175
AL – 400 – 30	AL	400	30	13,9	<2	130
AL – 210 – 25	AL	210	25	13,7	<2	100
GD – 1600 – 45	GD	1600	45	15,1	<2	280
GD – 1600 – 35	GD	1600	35	15,9	<2	280
GD – 1300 – 75	GD	1300	75	14,9	<2	280
GD – 1200 – 75	GD	1200	75	15,2	<2	280
GD – 1200 – 60	GD	1200	60	15,2	<2	280
GD – 1200 – 120	GD	1200	120	15,0	<2	280
GD – 1000 – 100	GD	1000	100	15,3	<2	280
GD – 900 – 140	GD	900	140	15,4	<2	280
GD – 725 – 200	GD	725	200	15,4	<2	280
GA – 1400 – 50	GA	1400	50	15,1	<2	265
GA – 1300 – 30	GA	1300	30	15,1	<2	225
GA – 1300 – 60	GA	1300	60	15,1	<2	225
GA – 1200 – 50	GA	1200	50	15,1	<2	250
GA – 1200 – 30	GA	1200	30	15,0	<2	220
GA – 1150 – 30	GA	1150	30	15,1	<2	230
GA – 1000 – 55	GA	1000	55	14,7	<2	250
GA – 940 – 80	GA	940	80	15,1	<2	255
GA – 850 – 45	GA	850	45	15,0	<2	210
GA – 800 – 70	GA	800	70	14,7	<2	240
GA – 650 – 45	GA	650	45	14,8	<2	180
GA – 600 – 60	GA	600	60	14,5	<2	200
GA – 550 – 55	GA	550	55	14,5	<2	175
GA – 490 – 165	GA	490	165	14,5	<2	205

Table A.1 (cont'd)

Material code	Family	Saturation Magnetization (G)	ΔH (Oe)	ε	tanδx (10)^4	Tn (C^o)
GA – 450 – 40	GA	450	40	14,5	<2	140
GA – 400 – 90	GA	400	90	14,5	<2	160
NG – 1950 – 20	NG	1950	20	15,2	<2	205
NG – 1950 – 12	NG	1950	12	15,2	<2	205
NG – 1900 – 15	NG	1900	15	15,1	<2	220
NG – 1900 – 10	NG	1900	10	15,1	<2	220
NG – 1850 – 12	NG	1850	12	15,0	<2	225
NG – 1600 – 12	NG	1600	12	14,7	<2	225
NG – 1400 – 10	NG	1400	10	14,7	<2	215
NG – 1200 – 10	NG	1200	10	14,2	<2	180
NG – 1100 – 10	NG	1100	10	14,5	<2	205
NG – 1000 – 10	NG	1000	10	14,5	<2	190
NG – 900 – 10	NG	900	10	14,2	<2	180
NG – 800 – 10	NG	800	10	14,2	<2	170
NG – 520 – 10	NG	520	10	13,3	<2	120
HG – 1600 – 90	HG	1600	90	15,2	<2	280
HG – 1200 – 120	HG	1200	120	15,1	<2	265
HG – 475 – 130	HG	475	130	14,5	<2	225

Table A.2 Garnets provided by TRANS-TECH [13]

Material code	Family	Saturation Magnetization (G)	ΔH (Oe)	ε	tanδx (10)^4	Tn (C^o)
TTVG-800	NG	800	<=15	13,9	<2	192
TTVG-930	NG	930	<=10	14,0	<2	188
TTVG-1000	NG	1000	<=10	14,0	<2	199
TTVG-1100	NG	1100	<=10	14,1	<2	205
TTVG-1200	NG	1200	<=10	14,4	<2	208
TTVG-1400	NG	1400	<=10	14,5	<2	215
TTVG-1600	NG	1600	<=10	14,6	<2	220
TTVG-1850	NG	1850	<=10	14,8	<2	200
TTVG-1950	NG	1950	<=15	15,0	<2	235
G-610	NG	680	<=25	14,5	<2	185
G-810	NG	800	<=25	14,6	<2	200
G-1010	NG	1000	<=25	14,7	<2	210
G-1210	NG	1200	<=25	14,8	<2	220
G-113	NG	1780	<=25	15,0	<2	280

Table A.2 (cont'd)

Material code	Family	Saturation Magnetization (G)	ΔH (Oe)	ε	tanδx (10)^4	Tn (C^o)
G-1009	AL or GA	175	<=50	13,8	<2	85
G-250	AL or GA	250	<=45	13,8	<2	105
G-300	AL or GA	300	<=45	14,0	<2	120
G-350	AL or GA	350	<=45	14,0	<2	130
G-400	AL or GA	400	<=45	14,1	<2	135
G-475	AL or GA	475	<=45	14,1	<2	140
G-510	AL or GA	550	<=48	14,3	<2	155
G-610	AL or GA	680	<=48	14,5	<2	185
G-1006	AL or GA	400	<=78	14,2	<2	150
G-500	AL or GA	550	<=78	14,4	<2	180
G-600	AL or GA	680	<=72	14,6	<2	200
G-1004	AL or GA	800	<=90	14,8	<2	240
G-800	AL or GA	800	<=66	14,7	<2	230
G-1000	AL or GA	1000	<=66	14,7	<2	250
G-1021	AL or GA	1100	<=108	15,2	<2	280
G-1005	GD	725	<=300	15,4	<2	280
G-1003	GD	870	<=186	15,4	<2	280
G-1002	GD	1000	<=132	15,4	<2	280
G-1001	GD	1200	<=96	15,2	<2	280
G-1600	GD	1600	<=66	15,1	<2	280
G-113+Ho or Co	CHG	1780	depend doping	15,0	<2	280
G-4260	CHG	550	<=120	14,4	<2	180
G-4259	CHG	800	<=132	14,8	<2	240
G-4258	CHG	1000	<=156	15,4	<2	280
G-4257	CHG	1200	<=120	15,2	<2	280
G-4256	CHG	1600	<=84	15,1	<2	280

A.2 Spinels

The spinel family offers high *saturation magnetization* values up to 5000 G which is much larger than the values offered by the garnet family. Thus, it is possible to reach higher frequency circulator operations. Adding to that, the spinel family contains a broad range of intrinsic properties, which are square hysteresis loops, temperature stability and high power handling capacity. These properties are very important in

terms of millimeter wave applications. Spinel family has 2 main subdivisions, which are magnesium ferrites and nickel ferrites. In our wideband circulator designs, nickel and magnesium ferrites of TRANS-TECH are preferred for disk and ring structures, respectively.

A.2.1 Magnesium Ferrites

Table A.3 Magnesium ferrites provided by TCI [24]

Material code	Family	Saturation Magnetization (G)	ΔH (Oe)	ε	Tanδx 10^4	Tn (C^o)
MF – 3000 – 200	MF	3000	<=200	12,9	<30	240
MF – 2650 – 180	MF	2650	<=180	13,0	<28	250
MF – 2200 – 350	MF	2200	<=360	13,0	<20	360
MF – 1450 – 130	MF	1450	<=140	12,0	<20	140
MF – 1000 – 120	MF	1000	<=100	11,0	<45	100

Table A.4 Magnesium ferrites provided by TRANS-TECH [13]

Material code	Family	Saturation Magnetization (G)	ΔH (Oe)	ε	Tanδx 10^4	Tn (C^o)
TT1-414	MF	750	<=144	11,3	<2,5	90
TT1-105	MF	1750	<=270	12,2	<2,5	225
TT1-390	MF	2150	<=648	12,7	<2,5	320
TT1-2500	MF	2500	<=624	12,9	<5	275
TT1-3000	MF	3000	<=224	12,9	<5	240

A.2.2 Nickel Ferrites

Table A.5 Nickel ferrites provided by TCI[24]

Material code	Family	Saturation Magnetization (G)	ΔH (Oe)	ε	Tanδx 10^4	Tn (C^o))
NF – 5000 – 165	NF	5000	<=165	13	15	350
NF – 4000 – 350	NF	4000	<=350	13	15	480
NF – 3000 – 300	NF	3000	<=300	13	15	560
NF – 2500 – 500	NF	2500	<=500	13	15	530
NF – 2100 – 480	NF	2100	<=480	13	10	500

Table A.6 Nickel ferrites provided by TRANS-TECH [13]

Material code	Family	Saturation Magnetization (G)	ΔH (Oe)	ε	Tanδx 10^4	Tn (C^o)
TT2-125	NF	2100	<=575	12,6	10	560
TT2-102	NF	2500	<=610	12,7	20	570
TT2-2750	NF	2750	<=540	12,8	25	580
TT2-101	NF	2000	<=375	13	25	585
TT2-3500	NF	3500	<=500	12,8	25	540
TT2-4000	NF	4000	<=425	12,3	25	470
TT2-111	NF	5000	<=200	12,5	10	375
TT86-6000	NF	5000	<=200	12,5	2	363

A.3 Dielectric Materials

Table A.7 Dielectric materials provided by TCI [24]

Material	Dielectric Constant (ε') @ 9.4GHz	Dielectric Loss Tangent (ε'/ε'')	Temperature Coefficient Dielectric Constant x10^{-4}	Temperature Coefficient of Thermal Expansion x10^{-6}	Thermal Conductivity
K-4	4.3 ± 5%	<.0002	55	2.4	0.007
K-6	6.3 ± 5%	<.0002	107	10	0.009
K-9	9.0 ± 5%	<.0002	115	6	0.045
K-9,5	9.5 ± 5%	<.0015	100	7.5	0.025
K-12	12.0 ± 5%	<.0002	100	7.5	0.025
K-15	15.0 ± 5%	<.0002	100	7.5	0.025
K-16	16.0 ± 5%	<.0002	120	7.5	0.010
K-18	18.0 ± 5%	<.001	80 x	8	0.010
K-20	20.0 ± 5%	<.001	(-) 125	8.5	0.010
K-25	25.0 ± 5%	<.001	(-) 370	9	0.010

Table A.8 Dielectric materials provided by Trans-Tech [13]

Material	Dielectric Constant (ε') @ 9.4GHz	Dielectric Loss Tangent (ε'/ε'')	Temperature Coefficient Dielectric Constant $x10^{-4}$	Temperature Coefficient of Thermal Expansion $x10^{-6}$	Thermal Conductivity
SMAT-10	**10.0 ± 0.5**	**<.00015**	**100**	**7.5**	**0.025**
SMAT-11	**11.0 ± 0.5**	**<.00015**	**100**	**7.5**	**0.025**
SMAT-12	**12.0 ± 0.5**	**<.00015**	**100**	**7.5**	**0.025**
SMAT-13	**13.0 ± 0.5**	**<.00015**	**100**	**7.5**	**0.025**
SMAT-14	**14.0 ± 0.5**	**<.00015**	**100**	**7.5**	**0.025**
SMAT-9	**9.0 ± 0.3**	**<.00015**	**100**	**7.5**	**0.025**
SMAT-9.5	**9.5 ± 0.3**	**<.00015**	**100**	**7.5**	**0.025**

APPENDIX B

MAGNET SELECTION GUIDE

In this part, it is aimed to provide a permanent magnet selection guide for different circulator applications. An overview of different magnet types and properties of their grades are given in the following parts. The main classes of modern magnetic materials are ceramics, alnicos and rare earth magnets. Rare earth magnets can be divided into two subdivisions, which are Samarium cobalt type and Neodymium Iron Boron type.

B.1 Ceramic Magnets

Ceramic magnets, which are also known as hard ferrites, are made of a composite of iron oxide and barium carbonate ($BaCO_3$) or strontium carbonate ($SrCO_3$). Their low cost makes them useful for many areas since 1950s. Their production process has two main processes, which are pressing and sintering. Sintered magnet is simply the compressed powder of the alloy materials.

They are brittle and hard which makes diamond wheels to grind and shape compulsory. Their brittle structure is to be considered during the design of the mechanic in the circulator structure. They have many different grades but well-known grades are Ceramic 1, Ceramic 5 and Ceramic 8. Ceramic 1 is isotropic, unlike Ceramic 5 and 8, which means Ceramic 5 and 8 have static magnetic field through a defined direction.

As wideband circulators are below-resonance devices, just saturating the ferrite is enough for application which means that a 3000-4000 G permanent magnets are suitable for high frequency circulations. So, ceramic magnets are very suitable in

terms of their magnet strength. On top of this, their cost is very low, which makes them the best choice for below resonance circulator applications.

Table B.1 Ceramic magnet grades [38]

Grade	Br (kGs)	Hc (kOes)	(BH)max (MGOe)	Tmax (C^o)
Ceramic 1	**2,2**	**1,86**	**1,05**	**450,0**
Ceramic 5	**3,8**	**2,40**	**3,40**	**450,0**
Ceramic 7	**3,4**	**3,23**	**2,75**	**450,0**
Ceramic 8	**3,85**	**2,95**	**3,5**	**450,0**
Ceramic 10	**4,0**	**3,52**	**3,82**	**450,0**

B.2 Alnico Magnets

Alnico alloys consist of aluminum, nickel, cobalt, copper, iron and titanium. They have relatively larger residual flux density (Br) value than ceramic magnets. For instance Alnico 8 has a residual flux density of 8200 G which makes this material impossible to use in our application. However, they have a very good temperature stability and resistance to corrosion. Beside their good properties, they are prone to demagnetization due to shock. During production process, two different methods may be preferred. One of the production methods is sintering, which offers superior mechanical characteristics. The other method is casting, which delivers very high energy products (max. 5.5 MGOe). Alnico 5 and 8 are anisotropic grades and they offer a determined magnetic field direction as it happens in Ceramic 5 and 8. Despite their good properties like corrosion resistance and temperature stability, they are replaced by rare earth magnets and ceramic magnets due to their high costs. In below resonance circulator operation, their high magnet strengths make using them illogical.

Table B.2 Alnico grades [39]

Grade	Br (kGs)	Hc (kOes)	(BH)max (MGOe)	Tmax (C^o)
Alnico 1	**7,2**	**0,47**	**1,4**	**450**
Alnico 2	**7,5**	**0,56**	**1,49**	**450**
Alnico 3	**7,0**	**0,48**	**1,49**	**450**
Alnico 5	**12,8**	**0,64**	**5,5**	**450**
Alnico 6	**10,5**	**0,78**	**3,9**	**450**
Alnico 8	**8,2**	**1,65**	**5,3**	**450**
Alnico 9	**10,6**	**1,50**	**9,0**	**450**

B.3 Rare Earth Magnets

Rare earth magnets contain elements like Samarium (Sm) Neodymium (Nd), which are rare earth materials. Although there are a vast of alloy formulations, the most widespread formulations are Samarium Cobalt ($SmCo_5$, Sm_2Co_{17}) and Neodymium-Iron-Boron ($Nd_2Fe_{14}B$).

B.3.1 Samarium Cobalt Magnets

The most important property of samarium cobalt is its high resistance to oxidation. On top of this, their magnet strength is larger than ceramic magnets and alnico magnets. However, they are brittle and prone to cracking and their cost is very high.

Table B.3 Samarium Cobalt ($SmCo_5$) grades [40]

Grade	Br (kGs)	Hc (kOes)	(BH)max (MGOe)	Tmax (C^o)
1	8,3	7,8-8,3	14-16	250
2	8,5	8,3-8,8	16-18	250
3	9,2	8,5-9,1	19-21	250
4	9,4	8,9-9,4	20-22	250
5	9,8	9,2-9,7	22-24	250
6	8,7	8,3-8,8	17-19	250
7	9,2	8,5-9,1	18-20	250
8	9,4	8,9-9,4	20-22	250
9	6,1	5,8-6,2	8,5-10	250
10	7,2	4,5-4,9	10,0-13,0	200

Table B.4 Samarium Cobalt (Sm_2Co_{17}) grades [40]

Grade	Br (kGs)	Hc (kOes)	(BH)max (MGOe)	Tmax (C^o)
11	9,7	9	22-24	200
12	10,4	9,6	24-26	350
13	10,5	9,7	26-28	350
14	10,9	10,2	28-30	350
15	9,5	8,9	20-23	350
16	9,8	9,1	22-24	300
17	10,4	9,6	24-26	300
18	10,5	9,7	26-28	300
19	10,9	10,2	28-30	300
20	11,2	10,4	29-32	300
21	10,4	9,4	24-26	300
22	10,5	9,5	26-28	300
23	10,9	9,7	28-30	300
24	11,2	9,8	29-32	300
25	9,8	8	22-24	300
26	10,4	8,2	24-26	250
27	10,5	8,3	26-28	250
28	11,2	8,5	28-30	250
29	11,3	8,6	29-32	250
30	9,6	8,7	21-23	250

B.3.2 Neodymium Magnets

NdFeB is the most advanced commercial magnet material available in terms of high energy products and mechanical strength. However, they are more prone to oxidation and more unstable in terms of temperature than SmCO. They are more costly in terms of weight, but if the flux density per mass is considered, it can be said that their cost is lower than ceramic and alnico. Thus, they are very useful in complicated applications where high magnetic strengths are required. If they are used unprotected, they are very prone to corrosion. But this problem can be handled with the help of surface treatment, which include copper, silver, gold, nickel zinc, tin plating and epoxy resin coating. Finally, it can be said that beneficial properties of NdFeB are high energy product, high coercive force and moderate temperature stability. In addition to that, their corrosion inclination can be handled by applying surface treatment. Thus, nodymimum magnets are advantageous for high magnetic field requiring applications.

Table B.5 Neodymium-Iron-Boron ($Nd_2Fe_{14}B$) grades [41]

Grade	Br (kGs)	Hc (kOes)	(BH)max (MGOe)	Tmax (C^o)
N35	12,1	11,5	35	≤80
N38	12,6	11,5	38	≤80
N40	12,9	11,0	40	≤80
N42	13,2	11,0	42	≤80
N45	13,7	11,0	45	≤80
N48	14,1	10,8	48	≤80
N50	14,5	10,8	50	≤80
N35M	12,1	11,6	35	≤100
N38M	12,6	11,8	38	≤100
N40M	12,9	12,2	40	≤100
N42M	13,2	12,6	42	≤100
N45M	13,7	12,8	45	≤100

Table B.5 (cont'd)

Grade	Br (kGs)	Hc (kOes)	(BH)max (MGOe)	Tmax (C^o)
N48M	**14,1**	**12,8**	**48**	**≤100**
N33H	**11,7**	**11,0**	**33**	**≤120**
N35H	**12,1**	**11,5**	**35**	**≤120**
N38H	**12,6**	**12,0**	**38**	**≤120**
N40H	**12,9**	**12,0**	**40**	**≤120**
N42H	**13,2**	**12,6**	**42**	**≤120**
N45H	**13,6**	**12,8**	**45**	**≤120**
N48H	**13,8**	**12,8**	**47**	**≤120**
N30SH	**11,2**	**10,5**	**30**	**≤150**
N33SH	**11,7**	**11,0**	**33**	**≤150**
N35SH	**12,1**	**11,5**	**35**	**≤150**
N38SH	**12,6**	**12,3**	**38**	**≤150**
N40SH	**12,9**	**12,6**	**40**	**≤150**
N42SH	**13,2**	**12,6**	**42**	**≤150**
N45SH	**13,5**	**12,8**	**45**	**≤150**
N28UH	**10,8**	**10,2**	**28**	**≤180**
N30UH	**11,2**	**10,6**	**30**	**≤180**
N33UH	**11,7**	**11,0**	**33**	**≤180**
N35UH	**12,1**	**11,5**	**35**	**≤180**
N38UH	**12,4**	**12,0**	**38**	**≤180**
N40UH	**12,7**	**12,2**	**40**	**≤180**
N42UH	**13**	**12,4**	**42**	**≤180**
N28EH	**10,8**	**10,4**	**28**	**≤200**
N30EH	**11,2**	**10,6**	**30**	**≤200**
N33EH	**11,7**	**11,0**	**33**	**≤200**
N35EH	**12,1**	**11,5**	**36**	**≤200**
N38EH	**12,4**	**12,0**	**38**	**≤200**
N28AH	**10,8**	**10,4**	**28**	**≤240**
N30AH	**11,2**	**10,6**	**30**	**≤240**
N33AH	**11,7**	**11,0**	**33**	**≤240**
N35AH	**12,1**	**11,5**	**35**	**≤240**

APPENDIX C

FERRITE MATERIAL CHARACTERIZATION

In this appendix, it is aimed to explain the test procedures to find ferrite material parameters like complex dielectric constants, *resonance linewidth* and *saturation magnetization*. The given information is obtained from the application notes of Trans-Tech [42, 43, 44] and "international standard for gyromagnetic materials" [15].

C.1 Test For Complex Dielectric Constants

Determination of the complex permittivity (ε) is very important in terms of characteristic impedance and dielectric losses of the ferrimagnetic material. Permittivity (ε) is a complex number with the imaginary part ε'' and real part ε' [42].

$$\varepsilon = \varepsilon' - j\varepsilon''$$

In order to define energy dissipation, a well-known ratio called dielectric loss tangent (tanδ) is defined.

$$\tan\delta = \varepsilon''/\varepsilon'$$

Although a variety of methods have been proposed in literature to measure complex dielectric constant of ferrimagnetic materials, the cavity perturbation method has been widely accepted for microwave ferrimagnetic materials. This method simply compares resonant frequency (f) and quality factor (Q) of a cavity with and without a ferrimagnetic rod samples to measure ε' and ε''.

In Figure C.1, a TE_{103} cavity with an empty resonance frequency of 9.3 Ghz has been shown. For accurate results, the loaded Q of the empty resonator should be larger than 2000. The ferrite rod should have a diameter of 0.042 inch and it should be placed parallel to the microwave electric field in a region of substantially uniform microwave electric field and zero microwave magnetic field.

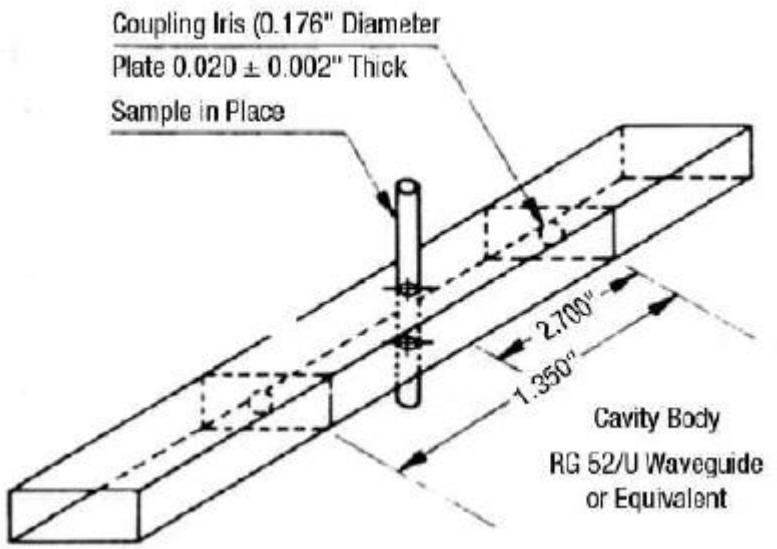

Figure C.1 TE_{103} cavity resonant at 9.4 GHz [42]

Applying the ferrite rod to the empty resonantor results a negative shift in the resonant frequency (f) and quality factor (Q) of the cavity. The governing equations to find ε' and ε'' are as below. The first equation gives the real part of the complex permittivity (ε'), Δf is the shift in the resonance frequency, V_s is the volume of the ferrite sample and V_c is the volume of the cavity.

$$\frac{\Delta f}{f} = 2\,(1-\varepsilon')\frac{V_s}{V_c}$$

In the second equation, the imaginary part of the complex permittivity (ε'') can be found in terms of the change in the quality factor (ΔQ).

$$\Delta\left(\frac{1}{Q}\right) = 4\varepsilon'' \frac{V_s}{V_c}$$

The measurement of the resonant frequency is straightforward. It can be made by applying different frequencies to the cavity and measuring the coupled output power. The frequency contributing the least output power is the resonant frequency. The measurement of Q is a little bit different. Between the input power and resonator an attenuator adjusted to 3 dB is placed and different frequencies are applied to find the central frequency (f). Then, attenuator is adjusted to 0 dB and the same output power with 3dB attenuator case is searched to find 2 half power frequencies. The difference between these frequencies give the $\Delta f_{1/2}$ and Q can be found as

$$Q = \frac{f}{\Delta f_{1/2}}$$

The procedure to find Q should be applied for both empty and ferrite sample located resonators to find ΔQ, then finding ε'' is a straightforward process from second equation.

C.2 Test For Resonance Linewidth (ΔH)

The ferrimagnetic *resonance linewidth* is defined as the separation of the two internal static magnetic field value at which the power is absorbed by the ferrimagnet is equal to half of the maximum absorption. As the measured sample is a sphere, the external field difference is the same with the internal field difference due to the uniform demagnetization factor [43]. Thus, analyzing the external static magnetic field does not contribute to different results.

For measuring the *resonance linewidth*, a perturbation method, which is similar to the one used for measuring complex dielectric constant, is used. But in this procedure, a TE_{106} cavity is employed. The details of a TE_{106} cavity for 9.3 GHz can be observed in Figure C.2 .

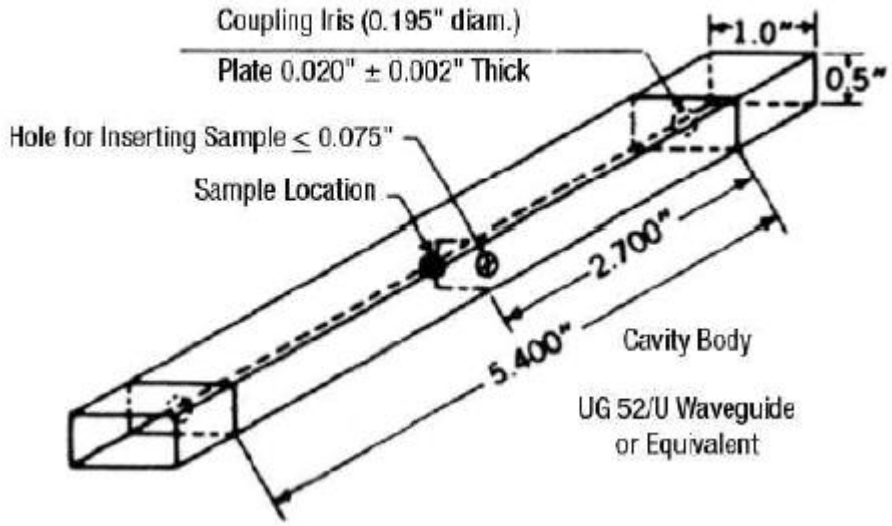

Figure C.2 TE_{106} cavity resonant at 9.4 GHz [43]

Firstly, the attenuation value of the empty resonator is measured which is named as α_o. Then, the sphere sample with a diameter 0.040" is placed in the structure and the maximum absorption is measured which is named as α_r . By using of α_o and α_r, the attenuation value for half power points $\alpha_{1/2}$ can be found with the given governing equation below.

$$\alpha_{1/2} = \alpha_o + 20\log 2 - 20\log\ (10^{((\alpha_o - \alpha_r)/20)} + 1)$$

In order to measure the *resonance linewidth* accurately, a test set-up as below can be used.

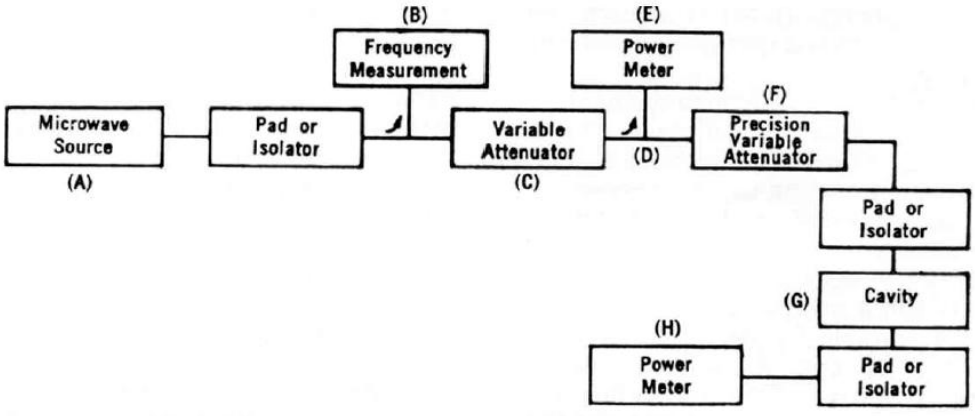

Figure C.3 *Resonance linewidth* measurement set-up [43]

Firstly, without specimen the α_o is found with the help of input power at (E) and output power at (H) given in Figure C.3. Then, the sphere sample is placed in the cavity and the static magnetic field is varied until the maximum absorption is reached. Now, microwave frequency and magnetic field (H_i) can be determined with a wavemeter (B) and rotating coil fluxmeter.With the governing equation and found α_o and α_r values,attenuation for half power absorbtion ($\alpha_{1/2}$) is found. The $\alpha_{1/2}$ value is inserted to the variable attenuator (B), and two different magnetic field values are searched which give the same output power with the maximum absorption case. The separation between the two static fields gives the *resonance linewidth* (**ΔH**) of the ferrite material.

C.3 Test For Saturation Magnetization ($4\Pi M_s$)

In Chapter 2, it is shown that the *saturation magnetization* of the ferrite is one of the main factors that determines the frequency band of the circulator operation. In this part of the appendix, it is aimed to explain the measurement method for the *saturation magnetization* of a ferrite material.

Although different methods exist, vibrating sample method (VSM) has been gaining general acceptance for measuring the *saturation magnetization* of microwave ferrimagnetic materials [44]. In the figure below, a diagram of a typical vibrating sample magnetometer is shown. With the help of an electro-mechanical transducer (A) and tube (B), the sample is vibrated vertically between pick-up coils (C) in a horizontal static magnetic field (C). A suitable frequency of vibration is 100 cycle per second (cps). For a reference saturation value, a calibration sphere (D) is located outside the static magnetic field and situated between another set of coils (G). A suitable permanent magnet for reference material is pure nickel, which has a saturation magnetization of 6070 G.

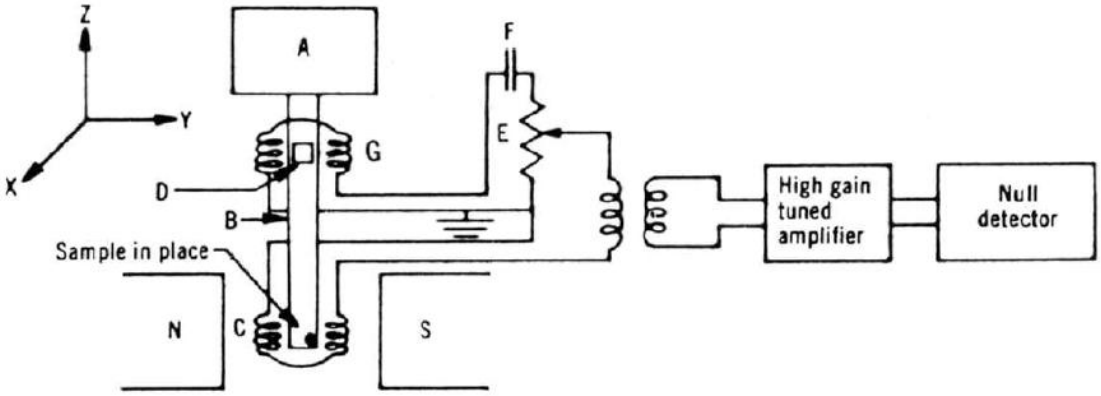

Figure C.4 VSM set-up [44]

With the help of precision potentiometer, the reading R gives the M_s value of the unknown sample in terms of the known sample with the equation below. R_{ref} and R_{sample} are voltage readings of reference magnet and sample,respectively. M_{ref} and M_s are the *saturation magnetization* of reference magnet and measured sample;and V_{ref} and V_{sample} are volumes of the reference magnet and measured sample.

$$\frac{R_{ref}}{R_{sample}} = \frac{M_{ref}V_{ref}}{M_sV_{sample}}$$

To measure the M_s, the measured sample should be saturated. A rule of thumb for saturation is that a decrease in the applied static magnetic field by 25 percent shall result in no more than 1 percent decrease in the indication, R_{sample}. As all the values except M_s is known, the only thing remained is to take M_s out from the equation.